Polymer Composites Based on Functionalized Metal Analogues Incorporated with Ionic Liquids for Electrochemical Applications

Hemshankar Saha Roy

December 2016

Polymer Composites Based on Functionalized Metal Analogues Incorporated with Ionic Liquids for Electrochemical Applications

A dissertation Submitted to University of Dhaka for the Partial Fulfillment of the Requirements of the Degree of Doctor of Philosophy in Chemistry

Submitted by

Hemshankar Saha Roy

Registration No. 169

Session : 2011-2012

DEPARTMENT OF CHEMISTRY

PHYSICAL CHEMISTRY RESEARCH LABORATORY

University of Dhaka

Dhaka-1000, Bangladesh

December 2016

Acknowledgments

This thesis is the one of the most important events in my journey of life in which I have not travelled alone, there are many people who supported and encouraged me for the successful completion of this high academic degree. Furthermore, I would like to thank all those people who made my journey successful and fulfill my long cherished dream. Truly, words are not enough to express my appreciation to all of them.

First, I would like to express my sincere gratitude and appreciation to my respected supervisor, **Prof. Dr. Md. Abu Bin Hasan Susan**, Department of Chemistry, University of Dhaka for his scholastic supervision, keen interest, constructive suggestions and criticisms throughout this research work without which the present research work might not have been completed. Thanks for giving me freedom to develop my research ideas, showing me different ways to solve research problems and being available in time. I gratefully acknowledge my respected supervisors, **Dr. Md. Mominul Islam**, Associate Professor, Department of Chemistry, University of Dhaka and **Prof. Dr. M. Yousuf Ali Mollah**, member, University Grants Commission of Bangladesh for their scholastic supervision, thoughtful guidance, invaluable suggestions at all stages of this research work. Their patience, guidance, encouragement were like a tonic and inspiration throughout this journey.

I am indebted to **Prof. Dr. M. Muhibur Rahman,** University Grants Commission of Bangladesh for his valuable comments and invaluable criticisms throughout this research work. I sincerely express my gratitude to **Dr. Muhammed Shah Miran,** Associate Professor for his prompt response, friendly suggestion and collaboration to overcome the experimental problems in time. Special thank goes to **Dr. Saika Ahmed,** Lecturer, Department of Chemistry, University of Dhaka for her vivid and friendly helpful attitude to my research work.

I sincerely acknowledge friendly and invaluable helps of the members of Material Chemistry Research laboratory. My efforts would have been fruitless without their relentless help and cooperation. I wish to express my heartfelt thanks to all the teachers and researchers of the Department of Chemistry, University of Dhaka. I am also thankful to Chairperson, Department of Chemistry, University of Dhaka for her kind administrative help and cooperation.

I gratefully acknowledge partial financial support from the sub project (CP-231) of the Higher Education Quality Enhancement Project (HEQEP) of the University Grants Commission of Bangladesh financed by World Bank and the Government of Bangladesh. I express my sincere thank to Bose Centre for Advanced Study and Research in natural Sciences, University of Dhaka.

Finally, I am deeply indebted to my dear parents and other family members for their good wishes and support during my difficult time of Ph.D. studies. Most importantly, I am indebted to relentless encouragement, appreciation of my beloved spouse, Chandana Saha without the moral support of whom this great work would not have been possible.

Hemshankar Saha Roy

Abstract

A series of polymer composites have been prepared by using both conducting and non-conducting polymer as matrix phases and different metal oxides as dispersed phases. Conducting polymer, polyaniline (PAni) was prepared by chemical oxidative polymerization as well as electrochemical polymerization while simple solution casting method was used for commercially available non-conducting polymer, poly(vinyl alcohol) (PVA). PAni based MnO_2 and NiO composites and PVA based MnO_2 composites were prepared with a view to achieving novel functionalities as well as for their electrochemical application in supercapacitors. Compatible ionic liquids (ILs) were also incorporated into the polymer composites to monitor influence on the capacitive properties. For instance, hydrophobic IL, 1-ethyl-3-methylimidazolium bis(trifluoromethylsulphonyl) imide, $[C_2mim][TFSI]$ and hydrophilic IL, 1-ethyl-3-methylimidazolium tetrafluoroborate, $[C_2mim][BF_4]$ were incorporated into the chemically prepared PAni-MnO_2 and PVA-MnO_2 composites, respectively and their capacitive behavior were critically examined.

PAni-MnO_2 composites with varying wt.% of MnO_2 were prepared by *in situ* chemical oxidative polymerization using $MnSO_4$ dissolved in aqueous acidic solution of aniline monomer followed by the addition of $KMnO_4$ in which MnO_2 was formed and simultaneously acted as an oxidant to initiate the polymerization. For optical, structural and morphological characterization of the composites UV-visible absorption and specular reflectance spectra, Fourier transform infrared (FT-IR) spectra, X-ray diffraction (XRD) and scanning electron microscopic (SEM) images were used. Thermogravimetric analysis (TGA) was carried out to study the thermal stability and verification of wt.% ratio of PAni and MnO_2 of the composites. X-ray diffraction analysis was performed to evaluate the crystallinity and phase purity and BET surface analysis was carried out to find out the specific surface area and porosity of the composites. Graphite electrodes were modified with the prepared composites by solvent casting method using dimethylsulfoxide and ethanol as solvents. $[C_2mim][TFSI$ was also incorporated into the composites. The electrochemical properties of the modified electrodes were analyzed by cyclic voltammetry, chronopotentiometry, and electrochemical impedance spectroscopic (EIS) techniques. The specific capacitance was determined from the data obtained from

chronopotentiometric measurements of the prepared composites and the results were analyzed for their applications in supercapacitors.

PAni-NiO nanocomposites with wt.% variation of NiO NPs were prepared by *in situ* chemical oxidative polymerization using aniline monomer and pre-formed NiO NPs served as the dispersed phase. Composites prepared were characterized to identify the properties and interaction among the components of the composites. TGA showed that thermal stability of PAni-NiO nanocomposites was higher than that of PAni. AC electrochemical impedance spectroscopic technique was employed and the data obtained were fitted to equivalent circuits. The resistance of the composites from the corresponding equivalent circuits was used to determine the conductivity of the composites. The band gap energy (E_g) of the composites was determined from the specular reflectance spectroscopic data by Kubelka-Munk method using Tauc equation. Dielectric constant and dielectric loss factor were determined from the impedance spectroscopic data. The value of dielectric constant and dielectric loss factor was evaluated for their applications as dielectrics. PAni and PAni-NiO composites were also prepared by electrochemical oxidative polymerization by cyclic voltammetry using aniline monomer and Ni^{2+} salt solution in acidic medium. The electrochemical performance of the electrochemically modified graphite electrodes with PAni and PAni-NiO composites was determined by cyclic voltammetry, chronopotentiometry and electrochemical impedance spectroscopic techniques. The specific capacitance was determined from the data obtained from chronopotentiometric measurements of the prepared composites and the results were analyzed for their applications in supercapacitors.

PVA-MnO_2 nanocomposites were prepared from by adding pre-formed MnO_2 NPs in aqueous solution previously prepared by the reduction of $MnSO_4$ with $Na_2S_2O_3$ in aqueous medium to the aqueous solution of PVA. The composites were then solution casted and dried in an oven to obtain PVA-MNO_2 nanocomposite film.

Thermal behavior of PVA-MnO_2 nanocomposite films changes with variation of MnO_2 NPs loading. The degradation of PVA-MnO_2 nanocomposite has been found to occur at lower temperature than that of PVA on addition of certain wt.% MnO_2 NPs. The degradation temperature then remains constant up to a certain loading followed by lowering of degradation temperature with further addition of MnO_2 into PVA. A complete shielding of UV radiation takes place in PVA-MnO_2 nanocomposite films

containing greater than 1.0 wt.% of MnO_2 NPs. Supercapacitive performance of PVA-MnO_2 nanocomposites modified graphite electrode with incorporation of a hydrophilic ionic liquid, $[C_2mim][BF_4]$, in 0.5 M aqueous Na_2SO_4 solution was investigated. The results of specific capacitance of PVA-MnO_2 and $[C_2mim][BF_4]$ incorporated PVA-MnO_2 nanocomposites are indicative of their feasibility for application in supercapacitors.

PAni-NiO nanocomposites and PVA-MnO_2 nanocomposite films exhibited novel functional properties. The dielectric constant and dielectric loss factor of PAni-NiO determined were significant to be used as dielectric materials. UV-visible spectra of PVA-MnO_2 nanocomposite films in transmittance mode showed almost hundred percent absorption of UV radiation at very low loading of MnO_2 NPs to indicate that PVA-MnO_2 nanocomposite films have potential to be used as UV-shielding materials.

Capacitive properties of MnO_2 embedded conducting PAni and non-conducting PVA based composites have been compared to reveal the influence of the nature of polymer matrix and variation of MnO_2 content of the composites. An attempt has also been made to evaluate the comparative capacitive properties upon incorporation of ILs into these polymer composites.

Thus, a systematic and comprehensive analysis of the composites has been performed to assess various aspects of polymer composites with both conducting and non-conducting matrix phases for desirable chemistry which eventually open up new routes for applications of the composites as materials for UV-shielding and supercapacitors.

Title of the thesis:

Polymer Composites Based on Functionalized Metal Analogues Incorporated with Ionic Liquids for Electrochemical Applications

Submitted by:

Hemshankar Saha Roy, Ph.D. Student, Department of Chemistry, University of Dhaka

Chapter 1: ***General Introduction***

Chapter 1 gives a brief introduction of background research and addresses the necessity and objective of the present research.

Chapter 2: ***Polyaniline Based MnO_2 Composites with Ionic Iiquid Additive for Electrochemical Capacitor***

Chapter 2 describes the preparation of polyaniline (PAni) by chemical oxidative polymerization of aniline monomer in aqueous acidic solution by ammonium peroxy disulfate as an oxidant. Preparation of PAni-MnO_2 composites with varying MnO_2 content by *in situ* chemical oxidative polymerization method using $MnSO_4$ dissolved in aniline monomer in aqueous acidic solution followed by addition of $KMnO_4$ was also described. The successful application of the techniques such as, UV-visible specular reflectance spectroscopy, FT-IR spectroscopy, SEM images, BET surface and thermogravimetric analysis (TGA) for structural characterization, spectroscopic characterization, morphological analysis, thermal analysis, surface area analysis have been mentioned in detail. The Chapter also mentioned the use of a hydrophobic ionic liquid, 1-ethyl-3-methylimidazolium bis(trifluoromethylsulfonyl) imide, [C_2mim][TFSI] for incorporation into PAni and PAni-NiO composites. Finally, to explore the possibility of the composite materials for super capacitor applications, the analyses of the electrochemical results using modified graphite electrodes with the prepared composites by cyclic voltammetry, chronopotentiometry and electrochemical impedance spectroscopic (EIS) techniques have been reported.

Chapter 3: ***Polyaniline Based NiO Nanocomposites as Dielectric Materials for Application in Electrochemical Capacitor***

In Chapter 3, preparation of PAni and PAni-NiO nanocomposites by chemical oxidative polymerization and electrochemical oxidative polymerization methods have been reported. Preparation of PAni-NiO nanocomposites with varying wt.% of NiO NPs and their characterizations have been discussed. Thermal degradation behavior of the composites has been discussed and the enhancement of the thermal stability of PAni-NiO nanocomposites than that of PAni has been corroborated. The band gap energy *(E_g)* and conductivity of PAni and PAni-NiO from specular reflectance spectroscopic

measurement and electrochemical impedance spectroscopic (EIS) techniques have been reported . Dielectric constant, and dielectric loss of the materials determined from EIS data were used to assess the promise as dielectric materials. Electrochemically prepared PAni and PAni-NiO composites were reported for study of the electrochemical performance as supercapacitor materials.

Chapter 4: ***Poly(vinyl alcohol) Based MnO_2 Nanocomposites for Application as UV-Shielding Material and in Electrochemical Capacitors***

Chapter 4 describes the preparation of PVA-MnO_2 nanocomposite films with variation of the content of MnO_2 NPs by simple chemical processing technique. The morphology, structure and thermal behavior of the nanocomposites were discussed in detail. The UV-shielding property of PVA-MnO_2 nanocomposite containing greater than 1.0 wt.% MnO_2 was established. Supercapacitive performance of PVA-MnO_2 nanocomposites with incorporation of an ionic liquid [C_2mim][BF_4] has also been reported. Electrochemical capacitive performance of PVA PVA-MnO_2 and PVA-MnO_2 nanocomposite incorporated with [C_2mim][BF_4] electrodes has been discussed in detail. The analysis of electrochemical results of the modified electrodes by cyclic voltammetry, chronopotentiometry and electrochemical impedance spectroscopic (EIS) techniques were discussed to check the feasibility of PVA, PVA-MnO_2 nanocomposites and PVA-MnO_2 incorporated with [C_2mim][BF_4] for supercapacitors.

Chapter 5: ***Comparative Study on Capacitive Properties of Conducting and Non-conducting Polymer Based Composites with and without Incorporation of Ionic Liquids***

Chapter 5 compares capacitive properties of conducting PAni and non-conducting PVA and their composites with MnO_2 with and without incorporation of ionic liquids by different electrochemical measurements. Electrochemical studies of a conducting polymer, PAni and a non-conducting polymer, PVA based composites as supercapacitor applications have been compared with cyclic voltammetric and chronopotentiometric studies. The specific capacitances of PAni and PAni-MnO_2 composites with those of PVA and PVA-MnO_2 nanocomposites have been compared at different scan rates and current densities. The specific capacitances of PAni-MnO_2 composites with incorporation of an ionic liquid [C_2mim][TFSI] with those of PVA and PVA-MnO_2 nanocomposites with incorporation of another ionic liquid [C_2mim][BF_4] have also been compared at different scan rates and current densities under identical experimental conditions. Finally, the difference in the cyclic voltammetric behaviors and charge-discharge curves have been compared and contrasted to explore the potential of the composites for application in supercapacitors.

Chapter 6: ***General conclusions and outlook***

Chapter 6 makes general conclusions based on the experimental findings on polymer nanocomposites and discusses the future prospect of polymer composites for exploitation of the novel functionalities for manifold applications.

Contents

LIST OF FIGURES

LIST OF TABLES

1.1. Background

Polymer composites have attracted a great deal of attention as excellent materials designed for modern applications such as super- or semi-conductor in electronic devices, catalyst in fuel cells, solar cells, sensors of biological molecules and pollutants, capacitors as energy storage devices *etc.* Composites materials consist of two or more chemically and physically different phases separated by a distinct interface and are combined brilliantly to achieve a system with more useful structural or functional properties that are not attainable by any of the constituent alone. They are a unique class of materials having multi-phase system comprising matrix l and reinforcing materials. Polymer composites are thus materials in which one or more dispersed phases are embedded in a polymer matrix phase/continuous phase/primary phase. In case of nanocomposites, dispersed phases with nanoscale dimensions *i.e.* ≤ 100 nm are embedded in a polymer matrix. Polymer composites have been made for task-specific applications by choosing an appropriate combination of reinforcing and polymer matrix materials of different nature and size that offer better strength and stiffness with light-weight which is a pre-requisite for the use of composite materials [1]. In dispersed or secondary or discontinuous phases, metals, metal oxides, fiber-like or other compounds are held together by different types of interactions in the polymer matrix. Matrix phase which is usually more ductile and less hard than the dispersed phase holds the dispersed phase or reinforcing phase is stronger than the matrix phase sharing a load with it.

Polymer composites may be conducting or non-conducting depending on either the matrix polymer or the reinforcing material is conducting and *vice-versa.* Composite materials of conducting and non-conducting polymers with metals or metal oxide particles have been developed to improve processability, mechanical performance, electrical conductivity, and biocompatibility of the matrix phase. The presence of conjugated double bonds along the backbone gives rise to the conductivity in conducting polymers such as polyaniline (PAni), polypyrrole (PPy) *etc.* Conducting polymers exhibit electrical and optical properties similar to those of metals and semiconductors [2]. Non-conducting polymers possess comparatively low density, low weight, high mechanical characteristics, and of course are low-cost. Due to their synergistic and hybrid properties, nanocomposites based on polymers offer ease of processability combined with the better mechanical and optical properties.

Semiconducting metal oxides can be particles/nanoparticles (NPs), nanowires, *etc.* These have been widely used as sensing materials in chemical sensors. The advantages offered by wide-band-gap semiconductor oxides include their stability in air, relative inexpensiveness, and ease of preparation in the ultradispersed state. Since porous metal oxides have attractive properties such as simplicity in preparation, tunable porosity, good chemical stability, low-temperature encapsulation, negligible swelling, mechanical and biodegradable stability, and high sensitivity at lower operating temperature for detection of reducing and oxidizing gases, they have been used for the fabrication of chemical sensors and biosensors. Non-conducting polymer based composites namely poly(vinyl alcohol) (PVA), incorporated with metal oxides such as PVA-ZnO, PVA-In_2O_3 nanocomposite films have also been prepared and applied as barrier or passivation materials for moisture and oxygen sensitive devices as well as food/pharmaceutical packaging industries [3]. Incorporation of metal oxides or other inorganic UV absorbents to transparent polymer can enhance UV light resistance *via* UV light shielding. Thus, polymer composites can be used as UV-shielding materials in optical and organic electronic devices, food and pharmaceutical packaging industries *etc.*

Ionic liquids (ILs), on the other hand, are composed of entirely bulky asymmetric cations and/or giant organic/inorganic anions which melt at relatively low temperature about up to 100 ^{o}C. ILS can be regarded as one of the versatile compounds that have shown an upsurge of research interest as the excellent media due to, not only their advantageous properties in applications, but also to the diversity of their tailoring according to the desired applications [4, 5]. Among various advantages of ILs, they possess unique properties such as negligible vapor pressure, high ionic conductivity, reasonable thermal stability, ability to dissolve organic, inorganic, and polymeric materials, and large potential window. These fantastic properties specially offer them the superiority over the conventional molecular solvents. ILs have been regarded as 'designers solvent' as their physical and chemical properties can be tailored by switching proper combinations of different cations and anions and changing the alkyl chain of the cations from different compounds for designing specific functionalities. ILs have been prominently used as the media for many electrochemical purposes, such as, batteries [6, 7], electrosynthesis [8, 9], electrodeposition [10] and

electrochemical capacitors [11-14]. Incorporation of ILs into the polymer or polymer composites may show new and fascinating properties that might be useful in the field of practical applications. Such an incorporation of ILs in non-conducting polymer based composites would introduce the conductivity of the composites required for their practical uses in the field of electronic devices, fuel cell as solid electrolyte or other purposes where conductivity is crucial. Ions of ILs hold the various groups of polymer chains by different types of interactions such as dipole-dipole interactions, ion-dipole interactions, van der Waals forces, H-bonding *etc.* By changing the wt.% of ILs, tunable properties of the polymer composites may be obtained for applications in various fields.

Polymer composites have attracted a great deal of attentions as materials for applications in supercapacitors. Electrochemical capacitors or supercapacitors are simple energy storage devices based on electrochemical double layers resulting from the electrostatic adsorption of ionic species at the electrode-solution interface and fast and reversible Faradaic reactions resulting pseudocapacitance. Electrosorption of ionic species can be facilitated if the electrolytic medium containing IL possesses mobile ions and thus ILs are considered to be an promising electrolyte for electrochemical supercapacitors [13, 15].

In this work, a conducting polymer, PAni based composites with MnO_2 and NiO as dispersed phases were prepared by *in situ* chemical oxidative polymerization method. PAni-NiO was also prepared by electrochemical polymerization. A non-conducting polymer, PVA based composite with MnO_2 was prepared by chemical method. Various studies were performed to characterize the composites for their possible use as functional materials. The effect of MnO_2 and NiO on the structural and functional properties of these composites was also elucidated. The capacitive behavior of PAni-MnO_2 and PVA-MnO_2 composites with variation of MnO_2 with or without incorporation of compatible ILs was investigated. A hydrophobic ionic liquid, (1-ethyl-3-methylimidazolium bis(trifluoromethanesulfonyl)-imide), [C_2mim][TFSI] was used for incorporation into PAni-MnO_2 composites while a hydrophilic ionic liquid, 1-ethyl-3-methylimidazolium tetrafluoroborate, [C_2mim][BF_4] was incorporated into PVA-MnO_2 composites. Capacitive property was also investigated for electrochemically prepared PAni-NiO composite. Comparative study on specific

capacitance of PAni-MnO_2 and PVA-MnO_2 composites with and without incorporation of ILs was also performed for their application in supercapacitors.

1.2. Composite Materials

Composites are multi-component, multi-phase systems isolated by a distinct interface; the resulting system has greater utility due to enhanced structural or functional properties that the constituents could not impart alone. They are a unique class of materials having multi-phase systems consisting of matrix and reinforcing materials. Composite materials have three basic phases: the continuous matrix phase, the dispersed reinforcement phase, and the interface phase which is surrounded by the matrix and exists in between the reinforcement and matrix phases. Matrix materials hold the dispersed phase and share a load with it. Dispersed phase is embedded in the matrix in a discontinuous form and is secondary in nature. The dispersed phase is usually stronger than the matrix, hence, it is sometimes referred to as the reinforcing phase. Dispersed phases are usually a range of materials such as organic fibers, metals, and metal oxides. Composite materials can be classified according to their source or reinforcing materials as natural and synthetic or particle reinforced, fiber reinforced and structural composites, respectively.

In composite materials, the different components are held together by different types of interactions involving different groups of atoms held together by covalent bonds and various types of intermolecular forces. Composites can be functional, multifunctional, smart, and intelligent materials depending on their component phases and individual properties. The performance of composite materials depends on the structure, configuration, interaction, and the relative contents of the constituent phases. Composite materials may be divided broadly as natural and synthetic and their components can be physically identified because they form interfaces between the matrix and dispersed phases. They are microscopically non-homogeneous, have a distinct interface; their performances are much better than those of the constituent materials. Composite materials not only maintain the principal characteristics of the original components but also exhibit the best combination of properties called synergistic properties derived from the original components. They can be called designable materials with excellent performance by proper choice of constituent components.

The demand for utilization of composite materials has been increasing progressively for better scientific innovation and standards of living for the human civilization as a whole, which will ultimately lead to national and global development.

1.2.1. Polymer Composites and Nanocomposites

Polymer composites are composed of a matrix or continuous phase with dispersed phases. They are multiphase materials in which one or more dispersed phases are embedded in a polymer matrix (Figure 1.1). In resemblance to polymer composites, polymer nanocomposites are also multiphase materials; however one or more phases has filler of dimension<100 nm incorporated in the polymer matrix. Both of these show improved properties such as enhancement of chemical and thermal stabilities emerging from the combination of components. Furthermore, in polymer nanocomposites, prevention of agglomeration occurs due to interactions of dispersed phase with the polymer matrix phase.

Figure 1.1. Polymer Composite.

Large varieties of polymer composites have been designed for performance based requirements, which are of high specific strength, high specific modulus, excellent chemical corrosion resistance, special optical, electrical, and magnetic properties. Composites comprising electrically conductive metal particles *e.g.* Ni, Cu, Ag, Al and Fe, dispersed in insulating polymer matrix have been prepared and the electrical, optical and antibacterial properties of these composites have been studied for decades. During the preparation of metal-polymer composites, metal ions may be dispersed, resulting in the presence of mobile ionic species in the polymer matrix [16]. Polymer based metal oxide composites such as PAni-MnO_2, PVA-ZnO, PPy-MnO_2 *etc.* have been prepared and investigations have been carried out to assess their electrical, electrochemical, and catalytic activities.

Ternary polymer composites with metal or metal oxide and another component have been reported for enhanced supercapacitive properties [17]. The optimal mechanical properties of such composites are achieved when the interaction between the polymer matrix and filler particle is maximized. Surface to volume ratio significantly increases with one-dimension in the nanometer scale than that of micron-scale particles, maintaining more of the inherent polymer processing properties and appearances [18].

Ionic liquids can also be incorporated as additives into the polymers composites for preparation of ion-gels, membranes *etc.* for various applications.

Fillers play important roles in modifying the desirable properties of polymers and reducing the cost of their composites to make them light-weight and enhance the mechanical properties of the polymers. Such properties can indeed be tailored by changing the volume fraction, shape, and size of the filler particles [19-23]. The dispersion of fillers with dimensions in the nanometer level having very large aspect ratio in a polymer matrix may bring enhanced mechanical performances in the prepared nanocomposites [24, 25]. Rigid inorganic NPs with a smaller aspect ratio are also promising reinforcing and/or toughening materials for the polymers. The nanocomposites belong to an emerging class of organic-inorganic hybrid materials that exhibit improved mechanical properties at very low loading levels compared with conventional microcomposites [26-39].

Polymer based metal oxide nanocomposites have many applications due to their superior electron transport, mechanical and optical properties, good transparency in short-wavelength ligght emitting diodes (LEDs), transparent conductors, organic photovoltaic cells, piezo and pyro electric materials, humidity detector, toxic gas sensors, and thin film transistors [40, 41]. Polymer nanocomposites have a wide range of applications due to their unique electrochemical, mechanical and magnetic properties, especially in conductive polymer nanocomposites [42-44].

The research and development of nanocomposites and nanotechnology fields have been greatly improved by the fabrication of nanodevices with these nanocomposites for task-specific applications.

1.2.2. Polymers: Conducting and Non-conducting

Polymer composites may comprise of conducting and non-conducting polymers as the matrix phase. Conducting polymers are polymers in which the double bonds appear with alternating single bonds known as conjugated bonds in their backbone. Most conducting polymers possess conductivity like that of a metal or semiconductor materials which can be altered by doping. They exhibit different oxidation states in the composites which are accompanied by applying potential and make them promising materials in sensors and biosensors, light emitting diodes and electrochromic display devices, electronic devices, supercapacitors *etc.*

Inherently conducting polymers are generally regarded as synthetic metals since their electrical, optical, electronic and magnetic properties resemble those of metals while possessing the mechanical and physical properties as well as the processability of conventional polymers. Addition of electron donors or acceptors as dopants in the conducting polymer ultimately results in rapid changes in electronic and magnetic properties that increase the conductivity, which nearly approaches to values in the metallic regime. Doping is reversible and produces the original low-conducting or semiconducting polymer, usually without degradation of the polymeric backbone.

Conducting polymer composites can be prepared with a range of combinations of matrix polymer and conductive particulate matter, provided enough filler is used to form an electrically conductive network. Too much filler may block the conductive networks or channels of the composite, making it poorly conducting or even insulating. Incompatibilities between matrix polymer and particulate fillers can prevent the formation of a well dispersed, stable conductive network. The polymer matrix should not oxidize the surface of the filler particles so that conductivity should not alter significantly [45]. Although non-conducting polymers do not conduct electricity they owe their importance due to their structural features which render their manifold applications. Non-conducting polymers possess comparatively low density, low weight, superior mechanical properties, and low cost. Non-conducting polymer based composites with metal oxide NPs as dispersed phases offer ease of processability combined with the enhanced mechanical and optical properties of metals or metal oxide NPs.

1.2.3. Metal Analogue Based Polymer Composites

From time immemorial, the course of development of human civilization is altering perpetually through the transformation of materials, more specifically composite materials. Probably the most famous and widely used synthetic polymer composite is "Bakelite", which is a clay reinforced resin that was developed in the early 20^{th} century. Nevertheless, the true importance of polymer composites was not fully realized until the end of the 20^{th} century [46-48].Metal analogues such as metals, metal ions and metal oxides may be incorporated into polymer matrix to form polymer composites that have multifarious applications in different fields.

With the growing attention towards metal or metal oxide NPs, the investigations towards possible applications of these materials in polymer composites have also become popular. Addition of metal or metal oxide NPs to the polymer matrix enables the modification of polymer properties and even the addition of new properties to the polymers.

PAni, one of the versatile conducting polymers, is an attractive material for use as a matrix material to prepare composites and nanocomposites with metals and metal oxides. Han *et al.* worked on PAni-MnO_2 nanocomposites and showed that the electrical conductivity of the nanocomposites increased due to incorporation of MnO_2 NPs into the conducting polymer and the mechanical stability as well as flexibility of PAni-MnO_2 nanocomposites electrode materials was also enhanced [49]. PVA based nanocomposites with metal oxide NPs in powder and film forms for various applications have also been reported. Gupta *et al.* synthesized PVA-ZnO hybrid nanocomposite films as interactive gas barrier layers for passivation of electronic devices [50]. Ghanipour *et al.* investigated the effect of Ag-Nanoparticles doped PVA *i.e.* Ag-PVA nanocomposite on the structural and optical properties of PVA films [51]. Singhal *et al.* reported the *ex situ* synthesis, characterization and gas-sensing properties of PVA-In_2O_3 nanocomposite films [52].

Composite and nanocomposites of PAni/Zn [53] and PAni/Pd [54] were designed as rechargeable battery assembles and as selective methanol sensors, respectively. Ferromagnetic material incorporated PAni-PVA composite was used as a dielectric material [55]. PAni nanowire modified electrode and PAni nanofiber doped with transition metal salts were used for supercapacitors [56]. Ionic liquid incorporated

PAni film was reported to show enhanced electrochromic property [57]. Ionic liquid-assisted PAni/Au nanocomposite has been synthesized for biocatalytic application [58] as well as the electrosensing of arsenic [59] in water. High sensitivity in amperometric sensing of phenols has been achieved with PAni/IL/carbon nanofiber composite [60].

Recently, polymer composites and nanocomposites of materials such as PPy-CuO, PPy-SiO_2, PAni-Si, prepared by *in situ* polymerization methods are being used for conductive polymer framework for various applications as anode materials, which exhibit much better performances, due to the fast electronic and ionic transfer channels and further maintain mechanical integrity resulting from synergism among the components of the nanocomposites [61].

Due to applications in multi-disciplinary fields, polymer composites and nanocomposites based on metals or metal oxides are therefore very fascinating. The task-specific composites with advantageous properties can be designed through the proper choice of combinations of polymer matrix and metal analogues such as metal and/or metal oxide particles or NPs, as well as ILs.

1.2.4. Versatility of Polymer as Matrix in Composite Materials

Polymers are one of the most important matrix materials due to their ease of preparation, light weight, low-cost, easy processability, high stability in air *etc.* Conducting polymer such as PAni exhibits remarkable changes in its electronic structure and physical properties at its protonated state [62]. They exhibit excellent electrical properties depending on the oxidation state of the main chain through oxidation or reduction. The redox reaction of the conducting polymer and interactions of electron donor or acceptor with them occur spontaneously so that both selectivity and sensitivity decline. Conducting polymers can be composited with metals, metal oxides, and with other polymeric materials due to the similarities in their inherent properties. So, incorporation of secondary components such as metals, metal oxides, organic molecules or other compounds into the polymer matrix to prepare polymer composites are often considered. The compatibility of polymers due to their structural orientations to combine with range of materials such as metals, metal or non-metal oxides, metal salts and even with polymers made them possible for manifold

applications. The mutual influence of the individual components and synergism of their properties make polymer composites promising.

Polymeric matrix can prevent aggregation to stabilize various types of nanostructured materials in the nanocomposites. Biodegradable non-conducting polymers can be used to prepare polymer nanocomposites with metal NPs having antibacterial properties for biomedical devices and hospital equipments. Metal NPs dispersed into or on the surface of polymer matrix may prevent the formation of large aggregates and protect high chances of their undesirable transfer into the environment keeping high efficiency with controlled release in biomedical applications. In fact, discovery of polymer composites using polymers as versatile matrices has opened up a new dimension of high performance composite materials [63].

1.2.5. Metal Analogues as Dispersed Phase

Metal analogues can be described as metal particles or NPs, metal ions, and metal oxide particles or NPs and can be used as dispersed phases in preparing polymer composites. Polymer composites are formed by the combination of polymer as matrix or continuous phase and dispersed phase. Metal analogues can be incorporated into polymer matrix to form polymer composites. Polymer composites are very interesting materials to which certain properties can be introduced by adjusting the ingredients as well as modifying the matrix and dispersed phases and using different techniques for their processing. Dispersed phases or fillers play important roles in modifying the desirable properties of polymers and reducing the cost of their composites. In conventional polymer composites, many inorganic fillers with dimensions in the micrometer range, *e.g.* metal oxides, calcium carbonate, talc, carbon particles *etc.* have been used extensively to make them light-weight and enhance the mechanical properties of polymers.Metal and metal oxide NPs based polymer nanocomposites have been investigated extensively for their manifold applications including separation, catalysis, environmental remediation, sensing, biomedical applications and others. Metal or metal oxide NPs can be stabilized into the polymeric matrix during or after the formation of nanocomposites [64].

1.3. Metal Oxide Nanoparticles

Metal oxides play a very important role in many scientific inventions such as in the fabrication of microelectronic circuits, semiconductor devices, computer chips,

sensors, fuel cells, coatings for the passivation of surfaces against corrosion, and as catalysts. Almost all catalysts in industrial applications involve an oxide as active phase or promoter. Metal oxide NPs show unique physical and chemical properties with respect to their bulk or single-particle species due to their limited size and high surface-to-volume ratio or higher edge surface sites. Low surface-free energy makes the metal oxide NPs of high mechanical or structural stability. Phases that have a low stability in bulk materials can become very stable in nanostructures. This structural phenomenon has been detected in MnO_2 TiO_2, Al_2O_3 *etc.*

Metal oxide based polymer composites and nanocomposites have been prepared with polymer as matrix phase and metal oxide as dispersed phase. Metal oxide particles or NPs may be prepared in aqueous phase from a precursor containing metal and oxygen atoms. Porous metal oxides have attractive properties such as simplicity of preparation, tunable porosity, good chemical stability, low-temperature encapsulation, negligible swelling, mechanical and biodegradable stability, and high sensitivity at lower operating temperatures for detection of reducing and oxidizing gases. They have been used for the fabrication of chemical sensors and biosensors. In technological applications, metal oxides are used in the fabrication of microelectronic circuits, sensors, piezoelectric devices, fuel cells, coatings for the passivation of surfaces against corrosion and as catalysts.

Metal oxide particles or nanostructures can be prepared by a variety of solution based methods such as precipitation method, sol-gel method, hydrothermal method, solvothermal method, electrochemical deposition, microemulsion method *etc.* These methods synthesize metal oxide particles or nanostructures in the form of stable colloid, solid powder, and film depending on experimental conditions. Different types of metal oxides nanostructures such as particles, wires, rods, spiral, flower etc. are observed in both physical as well as chemical routes. The quality of the product obtained by all of these methods depends on the condition for precipitation, purity of the initial reagents and nature of impurities, the values of the concentrations of the solutions used as reagents, the pH, the rate of reagents added, temperature, stirring regime, maturation time, temperature and so on.

There are some advantages and shortcomings of each of the routes. Among the solution based methods, hydrothermal, solvothermal, and precipitation routes have

several advantages such as they can be processed at a low temperature (<100 °C), one-step process, cheap, environment-friendly and give a high yield of particles or NPs of various shapes [65, 66]. These methods deal with the reaction of one solution containing precursors with metal atoms containing acetate, nitrate, chloride *etc.* with the other solution containing some reducing agent such as sodium or ammonium hydroxide/nitrates/carbonates in the presence or absence of stabilizing agents. Particular routes are employed for the synthesis of metal oxide particles or nanostructures for specific applications.

1.4. Methods Used for Synthesis of Polymer Composites

Polymer composites can be prepared by either chemical or electrochemical method depending on the type of monomer and nature of composites, and their applications. Chemical preparation of polymer composites employs chemical oxidative polymerization, template polymerization, self assembly, microemulsion assisted polymerization, mechanical blending, photochemically initiated polymerization, interfacial polymerization *etc.* whereas electrochemical polymerization includes electrochemical deposition polymerization, electrospinning *etc.* [67].

The most commonly used method to prepare conducing polymers and their composites such as PAni, PPy, polythiophene (PTh) *etc.* is carried out by chemical oxidative polymerization in different acidic media. The prepared polymers and their composites differ in solubility, conductivity and mechanical stability. Peroxydisulfate is the most commonly used oxidant in the preparation of conducting polymers and their composites. Depending on the nature of polymer composite materials and their applications, different polymerization methods are carried out to prepare polymer composites for task-specific objectives. Chemical polymerization route is recommended when large amount of polymer are needed.

Electrochemical polymerization can be carried out typically by galvanostatic, potentiostatic or potentiodynamic methods on carbon based electrode materials or inert metal electrodes. Active metals such as aluminum, iron, copper can also be employed as substrates for the electrodeposition of conducting polymers. Other electrodes may include gold, silver, nickel, platinum, carbon cloth, nickel foam, *etc.* Polymerization by electrospinning process is also possible. The choice of the supporting electrolyte is important not only with respect to properties of the polymer,

in several cases the formation and deposition of the polymer can only be achieved using special electrolytes.

Conducting polymers can be synthesized either chemically or electrochemically. Chemical methods of synthesis are followed through use of either condensation polymerization or addition polymerization route in case of non-conducting polymers. Chemical synthesis offers many different possible routes to synthesize a variety of conducting polymers such as PPy, PAni, PTh *etc.* and non-conducting polymers and also permits the bulk quantity of these materials. Whatever may be the synthetic procedure, the main goal of the procedure depends on the specific applications of the prepared polymer composites.

1.4.1. Chemical Polymerization *vs.* Electrochemical Polymerization

Preparation of polymers or their composites can be done by either chemical or electrochemical means. Chemical preparation of polymer composites employ chemical oxidative polymerization, template polymerization, self assembly, microemulsion assisted polymerization, mechanical blending, photochemically initiated polymerization, interfacial polymerization *etc.* whereas electrochemical polymerization includes electrochemical deposition polymerization, electrospinning *etc.* The most commonly used method to prepare conducing polymers such as PAni, PPy, PTh *etc.* and their composites can be carried out efficiently by chemical oxidative polymerization in acidic media. The prepared polymers and their composites differ in solubility, conductivity mechanical stability *etc.* Peroxydisulfate is the most commonly used oxidant in the preparation of conducting polymers and their composites.

Preparation of polymer composites by chemical polymerization can be carried out by simple solution mixing method in which the fabrication process are very simple as the preparation method involves by the addition of preformed inorganic components is mixed with the polymer solution under stirring or ultrasonication. *In situ* chemical oxidative polymerization involves a monomer solution containing an inorganic component upon addition of an oxidant.

Chemical polymerization route is recommended when large amount of polymers or their composites are needed. It has some shortcomings such as complex procedure,

time consuming and instability of the prepared composites. Morphology and size the prepared polymer or their composites can't be controlled due to bulk polymerization.

Electrochemical polymerization can be carried out typically by galvanostatic, potentiostatic or potentiodynamic methods on carbon based electrode materials or metal electrodes. Active metals such as aluminum, iron and copper can also be employed for the electrodeposition of conducting polymers. Polymerization by electrospinning process is also possible.

Electropolymerization of conducting polymers offers the advantage of being able to control the physical and chemical properties by changing the electrochemical parameters such as electrode potential, monomer concentrations, electrolytic solution, electrode materials *etc.* The oxidation state of the prepared polymer can be changed easily by electrochemical polymerization, *e.g.* by potential cycling between the oxidized, conducting state and the neutral and insulating state and by using suitable redox compounds. By proper design of the electrochemical experiment, polymer thickness and conductivity can be easily controlled. It is possible to modify the deposited conducting polymer in order to change its electrical, optical, and other properties. *In situ* electropolymerization does not need an oxidant, and has the advantages of short reaction time, controlled morphology of the composites, operational simplicity [67] *etc.*

Conducting polymers can be synthesized either chemically or electrochemically. Chemical methods of synthesis involve use of either condensation polymerization or addition polymerization route in case of non-conducting polymers. Chemical synthesis offers many different possible routes to synthesize a variety of conducting polymers such as PPy, PAni, PTh *etc.* and non-conducting polymers also permit the bulk quantity of these materials.

Electrochemical synthesis is relatively straightforward for small scale synthesis in a controlled manner and hence, is most commonly used method for preparing conducting polymers and their composites [68]. All of the conducting polymer based composites can be synthesized chemically but electrochemical syntheses of conducting polymers are limited to those systems in which the monomer can be oxidized in a certain potential to form reactive radical cation intermediate for polymerization. The most significant difference between electrochemical and

chemical methods of conducting polymer synthesis is that very thin conducting polymer films in the order of nanometer range can be produced using the electrochemical technique whereas powders or very thick films are typically produced with chemical polymerization.

Each of the polymerization has its own advantages and disadvantages. Chemical oxidative polymerization has several advantages such as, the reactions are fast and simple using relatively mild conditions, polymers could presumably be produced fast at a reasonable cost and large scale productions are achieved. However, possible side reactions may occur during polymerization and strong oxidation conditions affect over oxidation and decomposition. Electrochemical polymerization has some advantages also and these include rapidity of polymerization, absence of catalyst, control of film thickness by deposition charge, direct obtainment of the polymer in the oxidized conducting form *etc.*

1.4.2. Factors Influencing Chemical and Electrochemical Polymerization

Electrochemical preparation provides a simple, versatile, and facile way for preparing electroactive or conducting thin films of polymer or their composites. Different parameters such as electrode potential, current density, monomer, nature of solvents and electrolytes greatly affects the electrochemical polymerization in a controlled way [69, 70]. However, the thickness or morphology of resulting thin films can be influenced by simply varying different parameters such as nature and concentration of monomer, counter ion, solvent, cell conditions (*e.g.* electrode and applied potential), temperature, and pH of the polymerization media [71].

The effects of specific parameters on the electrochemical synthesis of polymer composites depend on doping ions, thickness of the polymer films, applied potential or current density, solvent, electrode substrate *etc.* The most common technique used for electrochemical polymerization is cyclic voltammetry which falls into the potentiodynamic, potetntiostatic and galvanostatic techniques. Various factors such as electrode material, electrolyte composition, type of monomer, and pH of electrolytic solution have been proven to exhibit influence in the electropolymerization and properties of the desired polymer. In case of conducting polymer such as PAni, dopant anions play a significant role in electrochemical polymerization.

Electrochemical polymerization can be performed at various types of inert electrodes,

such as platinum, gold, graphite, glassy carbon or indium-tin-oxide glasses, active metal electrodes like iron, aluminum and steel. The structure and properties of the conducting polymers through radical ion polymerization depend strongly on the solvent in which growth of conducting polymers is carried out. Electrochemical polymerization is commonly carried out in a medium that consists of solvent containing a supporting electrolyte. The supporting electrolyte in the solvent system is dictated primarily by the solubility of the analyte, its redox activity, and by solvent properties, such as the electrical conductivity, electrochemical activity, and chemical reactivity. The solvent should not react with the electrode and should not undergo electrochemical reactions over a wide potential range.

Generally, electropolymerization of electroactive monomers is initiated by the formation of a monomer radical cation and its coupling reactions as a fast step [69]. The structure and properties of the conducting polymers grown by anodic oxidation depend very strongly on the solvent in which the growth of polymerization is carried out. The solvent-supporting electrolyte couples are actually among the most important experimental variables affecting the behavior of the resulting conducting polymers.

1.4.3. Incorporation of Metal Oxides into Polymer: *In Situ* and *Ex Situ* Polymerization Process

The polymer composites or nanocomposites are formed with polymer as matrix phase and generally with inorganic component as dispersed phase. The synthetic strategy of the polymer composites and nanocomposites are categorized whether the polymer matrix or inorganic component based dispersed phase are formed *in situ* or *ex situ*. Four types of synthetic strategies may be described: (i) *ex situ* formation of both the polymer and inorganic components or the commercially available polymer in aqueous solution and inorganic components are prepared and subsequent attachment or integration is either by covalent bonding or non-covalent interactions. The attachment between polymer matrix and inorganic NPs can be achieved by covalent bonding such as in PVA-MnO_2 nanocomposites where O-atom in MnO_2 NPs may form H-bonds with pendants -O-H groups of PVA which is more stable than electrostatic (ii) *in situ* polymerization in the presence of *ex situ* formed inorganic NPs. In this process, preformed inorganic component is added to aqueous monomer solution and polymerization is carried out with addition of oxidant to polymerize forming the

composites or nanocomposites, (iii) *in situ* precipitation of the inorganic components on or in polymer structures. The polymerization is carried out in water in oil microemulsion system by the addition of appropriate ratio of surfactant, non-polar phase and water to form a confined region in which an inorganic precursor and a reductant is added forming the inorganic component to form the polymer composite or nanocomposite, and (iv) strategies in which both polymer and inorganic component are simultaneously formed *in situ.* The monomer and the inorganic precursor solution are dissolved in aqueous or aqueous acidic media followed by addition of an oxidant whereby inorganic component is formed through the oxidation or reduction of precursor solution and the formed inorganic component acts as an oxidant to polymerize the monomer forming the polymer-inorganic component composites or nanocomposites. Preformed NPs are dispersed in a liquid monomer in aqueous solution. When a homogeneous mixture is formed, initiator is added and it is exposed to appropriate source of heat, light, oxidant etc. The polymerization performed *in-situ* results in the formation of composite/nanocomposite. *In situ* approaches are currently getting much attention because of their obvious technological advantages over *ex situ* method [72]. *In situ* and *ex situ* methods have their own advantages and disadvantages. *Ex situ* method is advantageous for large-scale industrial applications than the *in situ* method but in this process the dispersion of the NPs are rather difficult than micro or larger particles in polymer matrix due to more dispersibility of micro particles into the polymer matrix. In *in situ* method, inorganic particles or NPs retains good spatial distribution in the polymer matrix and prevent agglomeration but the un-reacted products of the *in situ* reaction might pose a problem of purity due to difficulty of purifying of the final product [73].

The chemical and electrochemical methods of synthesis described above have their own merits and demerits. Choosing an appropriate method depends on the application of the materials. The final properties of the composites or nanocomposites are derived not from a simple addition of the properties of the individual component but a unique result from synergistic effects of both the components.

1.5. Ionic Liquids

ILs have been widely considered as “green solvents”. The hydrophilicity/lipophilicity are adjustable by varying the combination of cations and anions, therefore, they are

able to dissolve a range of organic, inorganic and organometallic compounds. They are therefore, called "designer solvents" [78]. They are supposed to be replaced by harmful volatile molecular solvents for their ease of handling and potential for recycling from the operating system.

ILs, a material with remarkable properties, have been one of the most fascinating materials in the realm of modern science and technology. ILs are water-free salts which melt at relatively low temperatures, about up to 100 ^{o}C. They are solely composed of bulky and asymmetrical cations in combination with a large variety of inorganic and organic anions (Figure 1.2). Comprising only large weakly coordinating ions, it amazingly possesses both liquidity and purely ionic character near or below room temperature.

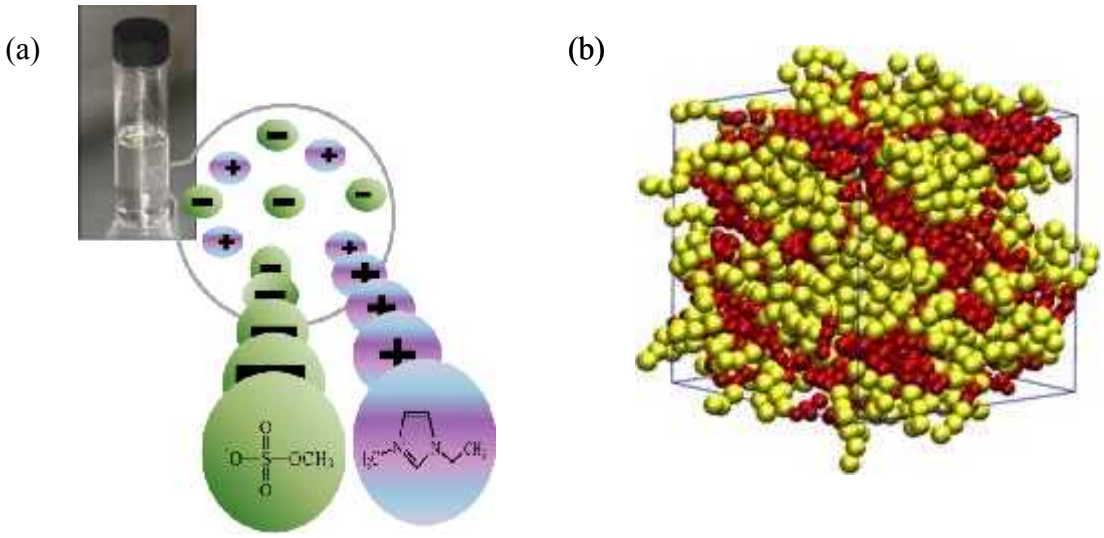

Figure 1.2. (a) Schematic representation of ionic liquid (IL) and (b) model of an ionic liquid [74].

In a broad sense, any salt in molten or liquid state, for instance, NaCl above its melting point (800 ^{o}C), may be termed as an ionic liquid. Now-a-days however, the term "IL" is used to define salts with melting point below 100 ^{o}C and sometimes as low as -96 ^{o}C (Figure 1.3) [75]. Owing to the inherent unique chemical structures, ILs are bestowed with the intriguing features of negligible vapor pressure, high ion conductivity, excellent chemical, electrochemical and thermal stability, wide liquid region (considerable gap between melting point and temperature of decomposition), outstanding dissolving capability for broad range of materials, high heat capacity, environmental compatibility, ability to be recycled and reused, multiple functionality, and task specificity [76]. These magnificent characteristics of ILs enable them to

excel over the traditional volatile molecular solvents and foster their use as green and advanced functional material in multifarious domains.

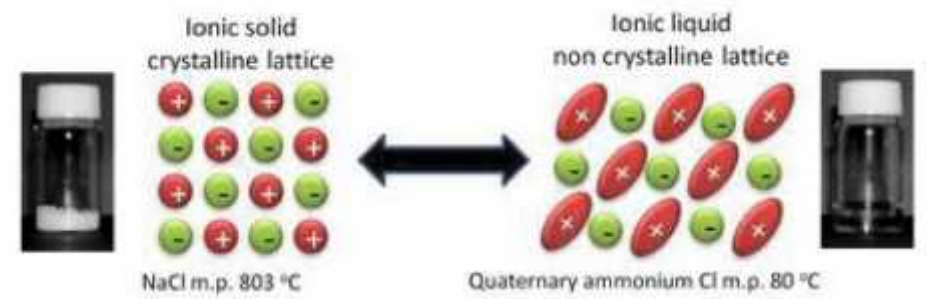

Figure 1.3. Representation of physical state of classical ionic compound NaCl and IL, $N(CH_3)_4Cl$ at ambient condition.

There have been upsurge of interest to exploit the option of fine-tuning the properties of polymers and polymer composites by an appropriate choice of cations and anions of ILs. Interactions of ILs on the basis of the nature of their ions and intermolecular interactions and exploring their fullest potential in polymer system are essential to promote the efficient utilization of ILs [77]. To understand the influence of ILs on polymer composites, it is important to acquire a comprehensive understanding about their basic and characteristic exclusive features. In this work, three ILs 1-ethyl-3-methylimidazolium bis(trifluoromethane) sulfonylimide, [C_2mim][TFSI] and 1-ethyl-3-methylimidazolium tetrafluoroborate, [C_2mim][BF_4] and 1-ethyl-3-methyl imidazolium methane sulfonate, [C_2mim][MS] (Figure 1.4) have been used to study the different properties associated with the interactions among the components of ILs and polymer composites.

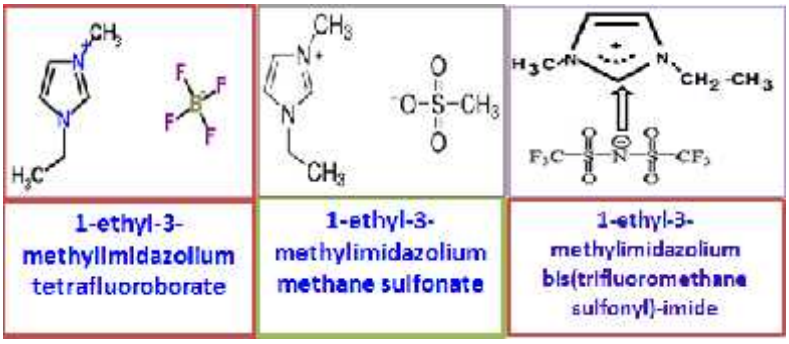

Figure 1.4. Ionic liquids used in this work.

1.5.1. Incorporation of Ionic Liquids in Polymer and Polymer Composites

The incorporation of IL [79, 80-82] in the polymer networks can significantly change the conducting property of a polymer, *i.e.,* a non-conducting polymeric matrix can be tuned to be conducting one. By adding IL into polymer, the properties of the polymer may be changed due to some sort of interactions between the polymer chains and ions of ILs. These interactions include van der Waals attraction, hydrogen bonding, π-π interactions *etc.* In polymer composites inorganic fillers such as metals, metal oxides or other compounds are incorporated into the polymer matrix. Besides, interactions existing between polymer and ILs, other types of interactions such as dipole-dipole interaction, ion-dipole interactions may exist between ILs and polymer composites though both cations and anions may have their own distinct interactions in ILs. In recent years, ILs have been used in polymer science, mainly as polymerization media in several types of polymerization processes, including conventional free radical polymerization [83], as well as in ionic and coordination polymerizations [84, 85].
ILs have been used for highly conductive IL-based ion gels in the form of flexible and transparent films. The most striking result obtained [86] was that the total carrier number in the ion gel at certain compositions exceeded the value obtained for the IL itself. This surprising finding highlights the importance of developing a detailed understanding of the specific physical interactions between ILs and the supporting polymer matrices in which the ILs are compatible. Finally, the main advantage of ILs is the endless number of cation/anion combinations, necessary to synthesize task-specific ionic liquids for polymers.

The combination of polymers with ILs has emerged as a hot topic in the field of polymer science in general and in the field of polymer electrolytes in particular. Some advantages of this interesting combination stem from the fact that ILs can serve both as ion suppliers to the polymer and also as solvents but avoid flammability or evaporation problems commonly observed in the case of molecular organic solvents. Polymer electrolytes containing ILs present higher ionic conductivity, higher thermal stability and improved electrochemical stability than other polymer electrolytes. ILs can be used as plasticizer for various types of polymers without assistance of common plasticizers [87]. Generally, in the polymer composite systems, the existing low compatibility of fillers with polymer systems is due to the different hydrophobicity between the fillers and polymers. Ding *et al.* [88] opined that ionic liquids could be

utilized in the systems for compatibilizing hydrophilic fillers with hydrophobic polymers.

1.6. Applications of Polymer Composites and Nanocomposites

Polymer composites have a number of applications that surpass other materials as a whole due to the unprecedented varieties and forms for shaping up the modern society and civilization. The utility of polymer composites depends on the specific field and type of diversified matter to which they are composed of (Figure 1.6). Composites must meet the certain criteria to possess superior structural or functional properties for specific applications.

Polymer nanocomposites have been developed to meet the requirements of various applications, such as optics, electronics, mechanics, energy, environment, biology, and medicine because they can possess various properties depending on nanofillers (Figure 1.5) [89-94]. Therefore, polymer nanocomposites have been used in membranes and separation devices, functional smart coatings as passivation materials, in fuel and solar cells, as catalysts, sensors, military equipment and aerospace, paints, automobiles, drug carriers, energy storage and in tissue engineering [95]. Polymer nanocomposites made up of polymers and transition metal oxides are being used for gas sensing applications as transition metal oxides act as semiconductor materials and fast change of conductivity occurs due to oxygen vacancies in presence of an oxidizing and reducing gas [96]. These materials are characterized for their applications as barrier materials for moisture and oxygen sensitive organic devices.

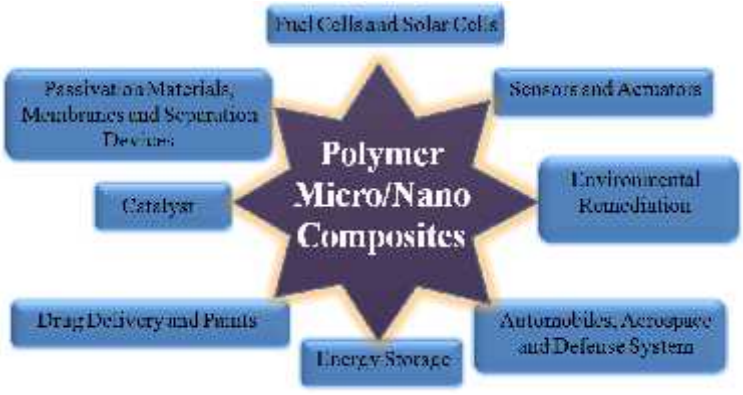

Figure 1.5. Applications of polymer composites and nanocomposites.

The preparation of composites needs special care so that, well-dispersed fillers in the polymer matrix is maintained properly, since properties of the composites strongly depend on the uniform distribution of the fillers to impart strength and other desired for specific applications [97, 98]. Potential applications of polymer-metal oxide nanocomposites in automotives include strengthened light-weight components such as exterior parts of cars and window glasses coated with composite thin films [99]. These materials are characterized for their applications as barrier materials for moisture and oxygen sensitive organic devices. In future, the applications of polymer composites and nanocomposites will surpass as a whole all of the materials to shape up the modern world and civilization.

1.6.1. Electrochemical Applications- Electrochemical Capacitors for Storing Energy

Polymer nanocomposites play a vital role in the field of electrochemistry such as in electrochemical capacitor applications. The nanodimension with a highly defined geometry and morphology along with high surface area and well defined pore structures are essential in designing electrochemical capacitors in which fast ion movements can take place due to the electroactive nature of materials and Faradaic reactions are promoted as well.

One of the most important electrochemical applications of polymer composites or nanocomposites is in electrochemical capacitors. Supercapacitors store energy as charge on the electrode surface or sub-surface layer. Therefore, they can provide high power due to their ability to release energy more easily from surface or sub-surface layer than from the bulk as in batteries. Since charging-discharging does not induce drastic structural changes on electroactive materials, supercapacitors possess excellent cycling ability. There are two types of supercapacitors: electrochemical double layer capacitors (EDLCs) and pseudocapacitors (Figure 1.6). In EDLCs, the energy is stored electrostatically at the electrode-electrolyte interface in the double layer, while in pseudocapacitors charge storage occurs *via* fast redox reactions on the electrode. However, EDLCs have lower energy density values than pseudocapacitors since pseudocapacitors involve redox active materials to store charge both on the surface as well as in sub-surface layer.

Although carbon-based materials, metal oxides and conducting polymers are the most common electroactive materials for supercapacitor, each type of material has its own unique advantages and disadvantages. Carbon-based materials can provide high power density and long life cycle but its small specific capacitance (mainly double layer capacitance) limits its application for high energy density devices. Metal oxides possess pseudocapacitance in additional to double layer capacitance and have wide charge-discharge potential range. However, they have relatively small surface area and poor cycle life. On the other hand, conducting polymers have the advantages of high capacitance, good conductivity, low cost and ease of fabrication but they have relatively low mechanical stability and cycle life. Coupling the unique advantages of these dissimilar capacitive materials is an important approach to control, develop and optimize the structures and properties of electrode material for enhancing their performance as supercapacitors. Recently, considerable efforts have been made to develop conducting polymer based on metal oxides composites or nanocomposites because these materials play a vital role in the field of electrochemical capacitor applications. Design and fabrication of polymer nanocomposite based electroactive materials for supercapacitor applications needs the consideration of many factors, such as material selection, synthesis methods, fabrication process parameters, electrical conductivity, size, surface area, porosity *etc.* [100]. Although significant progress has been made to develop nanocomposite electroactive materials for supercapacitor applications, there are still a lot of challenges to be overcome.

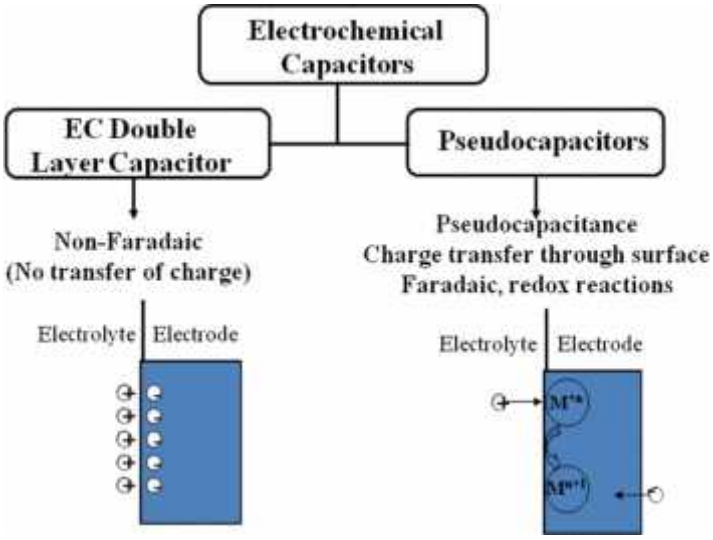

Figure 1.6. Capacitive storage systems.

1.7. Objectives of the Work

The present work was aimed to accomplish the following objectives:

- to prepare polymer composites based on metal oxides incorporated with ionic liquids with a view to achieving novel functionality for task-specific applications,
- to explore electrochemical applications of the composites as supercapacitors, and
- to study comparative capacitive properties of conducting and non-conducting polymer based composites with an without incorporation of ionic liquids.

1.8. Present Work

Modern applications of polymer composites have made these materials inevitable for diversified research activities as they can be prepared by changing their compositions and components. Furthermore, the addition of ILs as additives makes this system really fascinating to fabricate task-specific composites for multidisciplinary fields. Therefore, this work aims at studying different properties associated with multi-components of polymer composites.

This research work was initiated with the preparation of a conducting polymer, PAni and a non-conducting polymer PVA -based composites with MnO_2 and NiO as dispersed phases. *In situ* chemical oxidative polymerization method was followed for the preparation of PAni-MnO_2, PAni-NiO composites and simple chemical processing method was followed for the preparation of PVA-MnO_2 composite. The prepared composites were characterized for their structural and functional properties for specific applications. PVA-MnO_2 nanocomposites at different compositions were tested for hundred percent absorption of UV radiation and thus for application as UV-shielding materials. PAni-NiO nanocomposites prepared by chemical method were investigated as dielectric materials.

The main focus of this research has been centered on electrochemical application of the prepared polymer composites as supercapacitor materials. For this, modified electrode was fabricated with PAni-MnO_2 composites by solvent casting technique with and without incorporation of [C_2mim][TFSI]. Modified graphite electrode was

also prepared with PVA-MnO_2 nanocomposites by the same technique with and without incorporation of $[C_2mim][BF_4]$. Investigation of the performance of the modified electrodes was carried out by different electrochemical techniques includin cyclic voltammetry, chronopotentiometry and electrochemical impedance spectroscopy. The results of specific capacitance obtained were evaluated for the supercapacitor application of the composite electrodes. PAni-NiO composite was prepared by electrochemical polymerization method onto graphite electrode and electrochemical performance of the modified electrodes was also assessed for application as supercapacitor materials by the same way.

Finally, comparative capacitive properties of conducting PAni-MnO_2 with incorporation of $[C_2mim][TFSI]$ and non-conducting PVA-MnO_2 with incorporation of $[C_2mim][BF_4]$ were analyzed for their application in supercapacitors.

References

[1] T. Oshaka, A-N Chowdhury, M. A. Rahman and M. M. Islam, Trends in polyaniline research, Nova Science Publishers, Inc., New York, USA, 2003, 7, 151.

[2] G. Kaur, R. Adhikari , P. Cass , M. Bown and P. Gunatillake, *Electrically conductive polymers and composites for biomedical applications,* RSC Adv.**,** 2015, 5, 37553-37567.

[3] S. Gupta, S. Sindhu, K. Arul Varman, P. C. Ramamurthy and G. Madras, *Hybrid nanocomposite films of polyvinyl alcohol and ZnO as interactive gas barrier layers for electronics device passivation,* RSC Adv., 2012, 2, 11536–11543.

[4] T. Welton, *Room-Temperature ionic liquids. Solvents for synthesis and catalysis,* Chem. Rev.*,* 1999, 99, 2071–2084.

[5] M. Galinski, A. Lewandowski and I. Stepniak, *Ionic liquids as electrolytes,* Electrochim. Acta, 2006, 51, 5567-5580.

[6] H. Nakagawa, Y. Fujino, S. Kozono, Y. Katayama, T. Nukuda, H.Sakaebe, H. Matsumoto and K. Tatsumi, *Application of nonflammable electrolyte with room temperature ionic liquids (RTILs) for lithium-ion cells,* J. Power Sources, 2007, 174, 1021-1026.

[7] H. Sakaebe, H. Matsumoto and K. Tatsumi, *Application of room temperature ionic liquids to Li batteries,*Electrochim. Acta, 2007, 53, 1048-1054.

[8] D. Zane, A. Raffaele, A. Curulli, G. B. Appetecchi and S. Passerini, *Electrosynthesis of poly(*o*-phenylenediamine) in a room temperature ionic liquid,* Electrochem. Commun., 2007, 9, 2037-2040.

[9] P. S. Murray, S. F.Ralph, C. O. Too and G. G.Wallace, *Electrosynthesis of novel photochemically active inherently conducting polymers using an ionic liquid electrolyte*, Electrochim. Acta, 2006, 51, 2471-2476.

[10] A. P. Abbott and K. J. McKenzie, *Application of ionic liquids to the electrodeposition of metals,*Phys. Chem. Chem. Phys., 2006, 8, 4265–4279.

[11] M. Lazzari, M. Mastragostino and F. Soavi, *Capacitance response of carbons in solvent-free ionic liquid electrolytes,* Electrochem. Commun., 2007, 9, 1567-1572.

[12] A. Lewandowski and M. Galinski, *Carbon–ionic liquid double-layer capacitors,* J. Phys. Chem. Solids, 2004, 65, 281-286.

[13] T. Sato, G. Masuda and K.Takagi, *Electrochemical properties of novel ionic liquids for electric double layer capacitor applications,* Electrochim. Acta, 2004, 49, 3603-3611.

[14] Q. Zhu, Y. Song, X. Zhu and X. Wang, *Ionic liquid-based electrolytes for capacitor applications,* J. Electroanal. Chem., 2007, 601, 229-236.

[15] A. B. McEwen, S. F. McDevitt and V. R. Koch, *Nonaqueous electrolytes for electrochemical capacitors: Imidazolium cations and inorganic fluorides with organic carbonates,* J. Electrochem. Soc., 1997, 144, L84-L86.

[16] E. T. Thostenson, C. Li and T.-W. Chou, *Nanocomposites in context*, Compos. Sci. Technol., 2005, 65, 491-516.

[17] Y. Hou, Y. Cheng, T. Hobson and J. Liu,*Design and synthesis of hierarchical MnO_2 nanospheres/carbon nanotubes/conducting polymer ternary composite for High performance electrochemical electrodes,* Nano Lett., 2010, 10, 2727–2733.

[18] A. C. Balazs, T. Emrick and T. P. Russell, *Nanoparticle polymer composites: where two small worlds meet,* Science, 2006, 314, 1107-1110.

[19] Z. Bartczak, A. S. Argon, R. E. Cohen and M. Weinberg, *Toughness mechanism in semi-crystalline polymer blends: II. High-density polyethylene toughened with calcium carbonate filler particles,* Polymer, 1999, 40, 2347-2365.

[20] R. K. D. Misra, P. Nerikar, K. Bertrand and D. Murphy, *Some aspects of surface deformation and fracture of 5–20% calcium carbonate-reinforced polyethylene composites,* Mater. Sci. Eng. A, 2004, 384, 284-298.

[21] H. Unal, A. Mimaroglu and M. Alkan*, Mechanical properties and morphology of nylon-6 hybrid composites,* Polym. Int., 2004, 53, 56–60.

[22] A. Takahara, T. Magome and T. Kajiyama, *Effect of glass fiber-matrix polymer interaction on fatigue characteristics of short glass fiber-reinforced poly(butylene terephthalate) based on dynamic viscoelastic measurement during the fatigue process,* J. Polym. Sci. Part B: Polym. Phys., 1994, 32, 839-849.

[23] A. T. Dibenedetto, *Tailoring of interfaces in glass fiber reinforced polymer composites: a review,* Mater. Sci. Eng., 2001, A302, 74-82.

[24] M. F. Yu, O. Lourie, M. J. Dryer, K. Molor, T. F. Kelly and R.S. Ruoff,*Strength and breaking mechanism of multiwalled carbon nanotubes under tensile load,* Science, 2000, 287, 637-640.

[25] M. F. Yu, B. S. Files, S. Arepalli and R. S. Ruoff, *Tensile loading of ropes of single wall carbon nanotubes and their mechanical properties,* Phys. Rev. Lett., 2000, 84, 5552-5555.

[26] M. Alexandre, P. Dubois, M. Alexandre and P. Dubois,*Polymer-layered silicate nanocomposites: preparation, properties and uses of a new class of materials,* Mater. Sci. Eng., 2000, 28, 1-63.

[27] S. C. Tjong, Y. Z. Meng and A.S. Hay, *Novel preparation and properties of polypropylene−vermiculite nanocomposites,* Chem. Mater., 2002, 14, 44–51.

[28] S. C. Tjong, Y. Z. Meng and Y. Xu, *Structure and properties of polyamide-6/vermiculite nanocomposites prepared by direct melt compounding,* J. Polym. Sci.: Part B: Polym. Phys., 2002, 40, 2860-2870.

[29] S. C. Tjong and Y. Z. Meng, *Preparation and characterization of melt-compounded polyethylene/vermiculite nanocomposites,* J. Polym. Sci. Part B: Polym. Phys., 2003, 41, 1476-1484.

[30] S. C. Tjong and Y. Z. Meng, *Impact-modified polypropylene/vermiculite nanocomposites*, J. Polym. Sci. Part B: Polym. Phys., 2003, 41, 2332-2341.

[31] S. C. Tjong and S. P. Bao, *Preparation and nonisothermal crystallization behavior of polyamide 6/montmorillonite nanocomposites,* J. Polym. Sci. Part B: Polym. Phys., 2004, 42, 2878-2891.

[32] S. C. Tjong and S.P. Bao, *Crystallization regime characteristics of exfoliated polyethylene/vermiculite nanocomposites,* J. Polym. Sci. Part B: Polym. Phys., 2005, 43, 253-263.

[33] H. Fischer, *Polymer nanocomposites: from fundamental research to specific applications,* Mater. Sci. Eng. C, 2003, 23, 763-772.

[34] K. P. Pramoda and T. Liu, *Effect of moisture on the dynamic mechanical relaxation of polyamide-6/clay nanocomposites,* J. Polym. Sci. Part B: Polym. Phys., 2004, 42, 1823–1830.

[35] J. Kotek, V. Kelnar, M. Studenovsky and J. Baldrian, *Chlorosulfonated polypropylene: preparation and its application as a coupling agent in polypropylene-clay nanocomposites,* Polymer, 2005, 46, 4876-1481.

[36] K. E. Strawhecker and E. Manias, *Structure and properties of poly(vinyl alcohol)/Na^+ montmorillonite nanocomposites, Chem. Mater.*, 2000, 12, 2943–2949.

[37] Z. Wang and T. J. Pinnavaia, *Nanolayer reinforcement of elastomeric polyurethane,* Chem. Mater.,1998, 10, 3769–3771.

[38] E. P. Giannelis, R. Krishnamorti and E. Manias, *Polymer-silicate nanocomposites: model systems for confined polymers and polymer brushes*, Adv. Polym. Sci., 1999, 138, 107-147.

[39] H. Wang, C. Zeng, M. Elkovitch, L. J. Lee and K.W. Koelling, *Processing and properties of polymeric nano-composites,* Polym. Eng. Sci., 2001, 41, 2036-2046**.**

[40] M. Kokabi, M. Sirousazar and Z. M. Hassan**,** *PVA-clay nanocomposite hydrogels for wound dressing,* Eur. Polym. J., 2007, 43, 773–781.

[41] A. Chrissanthopoulos, S. Baskoutas, N. Bouropoulos, V. Dracopoulos, D. Tasis, and S. N. Yannopoulos,*Novel ZnO nanostructures grown on carbon nanotubes by thermal evaporation,*Thin Solid Films, 2007, 515, 8524–8528.

[42] J. Zhu, S. Wei, L. Zhang, Y. Mao, J. Ryu, P. Mavinakuli, A. B. Karki, D. P. Young, and Z. Guo, *Conductive polypyrrole/tungsten oxide metacomposites with negative permittivity,* J. Phys. Chem. C, 2010, 114, 16335–16342.

[43] R. Gangopadhyay and A. De, *Conducting Polymer Nanocomposites: A Brief Overview,* Chem. Mater., 2000, 12, 608-622.

[44] W. Wang, S. P. Gumfekar, Q. Jia and B. Zhao, *Ferrite-grafted polyaniline nanofibers as electromagnetic shielding materials,* J. Mater. Chem. C, 2013, 1, 2851-2859.

[45] P. Ghosh, Polymer Science and Technology, Plastics, Rubbers, Blends and Composites, Tata McGraw Hill Education Private Limited, Third Edition, India, Polymer Blends and Composites, 2011, 502-521.

[46] C. Sanchez, P. Belleville, *M. Popall and L. Nicole, Applications of advanced hybrid organic–inorganic nanomaterials: from laboratory to market,* Chem. Soc. Rev.**,** 2011, 40**,** 696-753.

[47] P. Gómez-Romero and C. Sanchez*, Hybrid materials. Functional properties. From Maya Blue to 21st century materials,* New J. Chem.**,** 2005**,** 29**,** 57-58.

[48] P. Gomez-Romero and C. Sanchez, *Functional hybrid materials,* Wiley-VCH, Weinheim, Germany, 2004, 1-6.

[49] J. Han, L. Li, P. Fang, and R. Guo, *Ultrathin MnO_2 nanorods on conducting polymer nanofibers as a new class of hierarchical nanostructures for high performance supercapacitors,* J. Phys. Chem. C*,* 2012, 116, 15900–15907.

[50] S. Gupta, S. Sindhu, K. A. Varman, P. C. Ramamurthy and G. Madras*, Hybrid nanocomposite films of polyvinyl alcohol and ZnO as interactive gas barrier layers for electronics device passivation*, RSC Adv.**,** 2012, 2, 11536-11543.

[51] Z. H. Esfahani, M. Ghanipour and D. Dorranian,*Effect of dye concentration on the optical properties of red-BS dye-doped PVA film,* J. Theor. Appl. Phys., 2014, 8, 117–121.

[52] A. Singhal, M. Kaur, K. A. Dubey, Y. K. Bhardwaj, D. Jain, C. G. S. Pillaia and A. K. Tyagi, *Polyvinyl alcohol–In_2O_3 nanocomposite films: synthesis, characterization and gas sensing properties,* RSC Adv., 2012, 2, 7180–7189.

[53] B. C. Dalui and I. N. Basumallick, *Zinc-poly(aniline) rechargeable battery assembled with aqueous electrolyte*, Indian J. Chem. Tech., 2008, 15, 576-580.

[54] A. A. Athawale, S. V. Bhagwat and P. P. Katre, *Nanocomposite of Pd–polyaniline as a selective methanol sensor,* Sens. Actuators B, 2006, 114, 263-267.

[55] V. Gupta, N. Miura, *Electrochemically deposited polyaniline nanowire's network a high-performance electrode material for redox supercapacitor*, Electrochem. Solid-State Lett., 2005, 8, A630-A632.

[56] N. Bıc¸, B. F. Senkal and E. Sezer, *Preparation of organo-soluble polyanilines in ionic liquid,* Synth. Met., 2005, 155, 105-109.

[57] R. Asami, M. Atobe and T. Fuchigami, *Electropolymerization of an immiscible monomer in aqueous electrolytes using acoustic emulsification,* J. Am. Chem. Soc*.,* 2005, 127, 13160–13161.

[58] W. Yang, J. Liu, R. Zheng, Z. Liu, Y. Dai, G. Chen, S. Ringer and F. Braet, *Ionic liquid-assisted synthesis of polyaniline/gold nanocomposite and its biocatalytic application,* Nanoscale Res. Lett., 2008, 3, 468–472.

[59] A.-N. Chowdhury, S. Ferdousi, M. M. Islam, T. Okajima and T. Ohsaka, *Arsenic detection by nanogold/conducting-polymer-modified glassy carbon electrodes,* J. App. Poly. Sci., 2007, 104, 1306-1311.

[60] J. Zhang, J. Lei, Y. Liu, J. Zhao and H. Ju, *Highly sensitive amperometric biosensors for phenols based on polyaniline–ionic liquid–carbon nanofiber composite,* Biosen. Bioelectron., 2009, 24, 1858-1863.

[61] C. Yang, H. Wei, L. Guan, J. Guo, Y. Wang, X. Yan, X. Zhang, S. Wei, and Z. Guo, *Polymer nanocomposites for energy storage, energy saving, and anticorrosion,* J. Mater. Chem. A**,** 2015, 3**,** 14929-14941.

[62] U. Lange, N. V. Roznyatovskaya1, and V. M. Mirsky, *Conducting polymers in chemical sensors and arrays, Anal. Chim. Acta,* 2008, 614, 1-26.

[63] M. Agarwala, T. Barman, D. Gogoi, B. Choudhury, A. R. Pal and R. N. S. Yadav, *Highly effective antibiofilm coating of silver–polymer nanocomposite on polymeric medical devices deposited by one step plasma process,* J. Biomed. Mater. Res. Part B, 2014, 102, 1223-1235.

[64] S. Sarkar, E. Guibal, F. Quignard and A. K. SenGupta**,** *Polymer-supported metals and metal oxide nanoparticles: synthesis, characterization, and applications,* J. Nanopart. Res., 2012, 14, 1-24.

[65] S. Xu and Z. L. Wang, *One-dimensional ZnO nanostructures: Solution growth and functional properties,* Nano Res., 2011, 4, 1013–1098.

[66] S. Kishwar, M. H. Asif, O. Nur, M. Willander and P. O. Larsson, *Intracellular ZnO nanorods conjugated with protoporphyrin for local mediated photochemistry and efficient treatment of single cancer cell,* Nanoscale Res. Lett., 2010, 5, 1669-1674.

[67] X. Zang, X. Li, M. Zhu, X. Li, Z. Zhen, Y. He, K. Wang, J. Wei, F. Kang and H. Zhu, *Graphene/polyaniline woven fabric composite films as flexible supercapacitor electrodes,* Nanoscale, 2015, 7, 7318-7322.

[68] G. Kaur, R. Adhikari, P. Cass, M. Bown and P. Gunatillake, *Electrically conductive polymers and composites for biomedical applications,* RSC Adv., 2015, 5, 37553–37567.

[69] A. S. Sarac, S. Sezgin, M. Ates and M. C. Turhan, *Monomer concentration effect on electrochemically modified carbon fiber with poly[1-(4-methoxyphenyl)-1H-pyrrole] as microcapacitor electrode,* Adv. Polym. Tech., 2009, 28, 120–130.

[70] A. Sezai Sarac, S. Sezgin, M. Ates and M. C. Turhan, *Monomer concentration effect on electrochemically modified carbon fiber with poly[1-(4-methoxyphenyl)-1*H-*pyrrole] as microcapacitor electrode,* Adv. Polym. Tech., 2009, 28, 120–130.

[71] R. Ansari, *Polypyrrole Conducting Electroactive Polymers: Synthesis and Stability Studies,* Eur. J. Chem., 2006, 3, 186-201.

[72] M. A. Hood, M. Mari and R. Muñoz-Espí, *Synthetic strategies in the preparation of polymer/inorganic hybrid nanoparticles,* Materials, 2014, 7, 4057-4087.

[73] J. C. Boyer, N. J. J. Johnson and F. C. J. M. van Veggel, *Upconverting lanthanide-doped NaYF4-PMMA polymer composites prepared by in Situ polymerization*, Chem. Mater., 2009, 21, 2010–2012.

[74] K. R. Seddon, A. Stark and M. J. Torres, *Influence of chloride, water, and organic solvents on the physical properties of ionic liquids,* J. Pure Appl. Chem., 2000,72, 2275-2287.

[75] M. Galinski, A. Lewandowski and I. Stepniak, *Ionic liquids as electrolytes,* Electrochim. Acta, 2006, 51, 5567-5580.

[76] M. Freemantle, *An Introduction to Ionic Liquids,* RSC Publishing, Cambridge, UK, 2010, 1-10.

[77] K. A. Fletcher, I. A. Storey, A. S. Pandey and S. Pandey, *Behavior of the solvatochromic probes Reichardt's dye, pyrene, dansylamide, Nile Red and 1-*

pyrenecarbaldehyde within the room-temperature ionic liquid bmim$PF_{6,}$ Green. Chem., 2001, 3, 210-215.

[78] C. S. Brazel and R. D. Rogers, *Ionic Liquids in polymer systems,* American Chemical Society, Washington DC, 2005, 2.

[79] R. Asami, M. Atobe and T. Fuchigami, *Electropolymerization of an immiscible monomer in aqueous electrolytes using acoustic emulsification,* J. Am. Chem. Soc., 2005, 127, 13160-13161.

[80] S. Xiong, F. Yang, G. Ding, K. Y. Mya, J. Ma and X. Lu, *Covalently bonded polyaniline/fullerene hybrids with coral-like morphology for high-performance supercapacitor,* Electrochim. Acta, 2012, 85, 235-242.

[81] J. Zhang, J. Lei, Y. Liu, J. Zhao and H. Ju, *Highly sensitive amperometric biosensors for phenols based on polyaniline-ionic liquid-carbon nanofiber composite,* Biosen. Bioelectron., 2009, 24, 1858-1863.

[82] P. Kubisa*, Ionic liquids in the synthesis and modification of polymers,* J. Polym. Sci., Part A: Polym. Chem., 2005, 43, 4675–4683.

[83] H. Zhang, K. Hong, J. W. Mays, *Synthesis of block copolymers of styrene and methyl methacrylate by conventional free radical polymerization in room temperature ionic liquids,* Macromolecules, 2002, 35, 5738–5741.

[84] J. Chiefari, Y. K Chong, F. Ercole, J. Krstina, L. Jeffery and R. T. A. Mayadune, *Living free-radical polymerization by reversible addition fragmentation chain transfer: the RAFT process,* Macromolecules, 1998, 31, 5559–5562.

[85] R. Vijayaraghavan and D. R. Macfarlane, *Living cationic polymerization of styrene in an*

ionic liquid, Chem Commun., 2004, 6, 700–701.

[86] M. A. B. H Susan, T. Kaneko, A. Noda and M. Watanabe, *Ion gels prepared by in situ radical polymerization of vinyl monomers in an ionic liquid and their characterization as polymer electrolytes,* J. Am. Chem. Soc., 2005, 127, 4976-4979.

[87] A. A. Shamsuri, and R. Daik, *Applications of ionic liquids and their mixtures for preparation of advanced polymer blends and composites: a short review,* Rev. Adv. Mater. Sci., 2015, 40, 45-59.

[88] Y. Ding, P. Wang, Z. Wang, L. Chen, H. Xu and S. Chen, *Magnesium hydroxide modified by 1-n-tetradecyl-3-carboxymethyl imidazolium chloride and its effects on the properties of LLDPE,* Polym. Eng. Sci., 2011, 51, 1519-1524.

[89] J. Jordan, K. Jacob, R. Tannenbaum, M. A. Sharaf and I. Jasiuk, *Experimental trends in polymer nanocomposites-A review,* Mater. Sci. Eng. A, 2005, 393, 1-11.

[90] I. Jeon and J. Baek, *Nanocomposites derived from polymers and inorganic nanoparticles,* Materials, 2010, 3, 3654-3674.

[91] G. Schmidt and M. M. Malwitz, *Properties of polymer-nanoparticle composites,* Curr. Opin. Colloid Interface Sci., 2003, 8, 103-108.

[92] P. H. C. Camargo, K. G. Satyanarayana and F. Wypych, *Nanocomposites: synthesis, structure, properties and new application opportunities,* Mater. Res., 2009, 12, 1-39.

[93] K. Fukushima, M.-H. Wu, S. Bocchini, A. Rasyida and M.-C. Yang, *PBAT based nanocomposites for medical and industrial applications,* Mat. Sci. Eng. C, 2012, 32, 1331–1351.

[94] S. Kango, S. Kalia, A. Celli, J. Njuguna, Y. Habibi and R. Kumar, *Surface modification of inorganic nanoparticles for development of organic-inorganic nanocomposites-A review,* Prog. Polym. Sci., 2013, 38, 1232-1261.

[95] A. Singhal, M. Kaur, K. A. Dubey, Y. K. Bhardwaj, D. Jain, C. G. S. Pillai and A. K. Tyagi, *Polyvinyl alcohol–In_2O_3 nanocomposite films:synthesis, characterization and gas sensing properties,* RSC Adv., 2012, 2, 7180-7189.

[96] N. G. Sahoo, S. Rana, J. W. Cho, L. Lin, and S. H. Chan, *Polymer nanocomposites based on functionalized carbon nanotubes,* Prog. Polym. Sci., 2010, 35, 837–867.

[97] T. D. Fornes, D.L. Hunter and D. R. Paul, *Nylon-6 nanocomposites from alkylammonium-modified clay: the role of alkyl tails on exfoliation,* Macromolecules, 2004, 37, 1793–1798.

[98] F. Li, K. Hu, J. Li and B. Zhao, *The friction and wear characteristics of nanometer ZnO filled polytetrafluoroethylene,* Wear, 2001, 249,877–882.

[99] J. Bravo, L. Zhai, Z. Wu, R. E. Cohen and M. F. Rubner, *Transparent superhydrophobic films based on silica nanoparticles,* Langmuir, 2007, 23, 7293-7298.

[100] B. E. Conway, *Electrochemical supercapacitors: scientific fundamentals and technological applications*, Kluwer Academic/Plenum, New York, USA, 1999.

Abstract

Polyaniline-manganese dioxide (PAni-MnO_2) composites of varying compositions were prepared by *in situ* chemical oxidative polymerization of aniline monomer in aqueous acidic medium in the presence of different amount of MnO_2 formed *in situ* by the reaction of $MnSO_4$ with $KMnO_4$ PAni was also synthesized from aniline in acidic solution using ammonium peroxy disulfate as an oxidant for use as a reference material. PAni and PAni-MnO_2 composites were characterized by UV-visible specular reflectance and FT-IR spectroscopy, XRD measurements, Brunauer-Emmett-Teller (BET) surface analysis, scanning electron microscopy (SEM) and thermogravimetric analysis (TGA). Both UV-vis and FT-IR spectra revealed the formation of PAni and PAni-MnO_2 composites. SEM images showed different morphologies of PAni and PAni-MnO_2 composites. Spherical MnO_2 particles were distributed in the PAni matrix. Modified graphite electrode was prepared with PAni and PAni-MnO_2 composites using solvent casting technique. Supercapacitive performance of PAni, PAni-MnO_2 and PAni-MnO_2 composites with incorporation of an hydrophobic ionic liquid, 1-ethyl-3-methylimidazolium bis(trifluoromethylsulfonyl) imide, [C_2mim][TFSI] in 0.5 M aqueous Na_2SO_4 electrolytic solution was investigated using cyclic voltammetry, chronoptentiometry and electrochemical impedance spectroscopic techniques. The specific capacitance (C_s) of PAni-MnO_2 composites as high as 242 F g^{-1} could be obtained which was stable up to 1000 cycles at a current density of 0.25 A g^{-1}. Electrochemical capacitors were developed by fabricating graphite electrodes modified with PAni, PAni-MnO_2 and [C_2mim][TFSI] incorporated PAni, PAni-MnO_2 composites electrodes in the range of 0.0–0.8 V. The C_s of the materials was found to be 99 to 242 F g^{-1} at a current density of 0.10 A g^{-1} in the potential range of 0.0 to 0.8 V. These results indicate that PAni, PAni-MnO_2 and [C_2mim][TFSI] incorporated PAni-MnO_2 composites have potential for application in supercapacitors.

2.1. Introduction

Synthetic polymer composites such as polymer-metal and polymer-metal oxide based composites have attracted a great deal of attention as excellent materials designed for modern applications as super-conductor in electronic devices, catalyst in fuel and solar cells, catalyst for degradation or removal of organic pollutants from aquatic environment, sensors of biological molecules, capacitors in energy storage devices, [1-10] *etc.* The use of polymers for preparation of composites has been increasing day by day due to the ability of polymers to hold the components of composites such as metal or metal oxides particles by its networks through various interactions. In addition, millions of polymer matrix-based composites with tunable properties can be

fabricated by changing their compositions and components [11-20]. The fabrication of task-specific composites could also be achieved by modifying functional sites of polymers.

Intrinsically conducting polymers have been used as a versatile candidate for applications in various domains such as photonics, optoelectronics, electrochromics, electrocatalysis, supercapacitors, waste water treatment, sensors *etc.* On the other hand, transition metal oxides have been used as catalysts, magnetic materials, supercapacitors, electrochromics, gas sensors, dye sensitized solar cells, [14] *etc.* Conducting polymers have high electrical conductivity and low cost but their poor cycle life and low mechanical stability restrict their widespread use for applications such as supercapacitor. On the other hand, most of the transition-metal oxides, which are promising for their low cost and high abundance suffer from poor electrical conductivity, instability and higher electrolyte resistance in acidic medium [12]. Therefore, incorporation of MnO_2 to an electrically conducting polymer, PAni may reduce the chance to alleviate the poor electrical conductivity of MnO_2 and enhance cyclability and mechanical stability.

With a view to having best possible properties or property synergism among the components, a conducting polymer, PAni based on MnO_2 composites with varying amount of MnO_2 were prepared and their properties related to their application as supercapacitor have been investifated in detail. PAni and PAni-MnO_2 composites with different compositions were synthesized by *in situ* chemical oxidative polymerization method. The formation of PAni-MnO_2 composites and their morphology, structure and thermal stability were characterized. Graphite electrode was modified with PAni, PAni-MnO_2 and [C_2mim][TFSI] incorporated PAni-MnO_2 by solvent casting method using a mixed solvent of dimethyl sulfoxide and ethanol and poly(vinyl alcohol) as a binder. The electrochemical properties related to specific capacitance C_s of PAni and PAni-MnO_2 composites were analyzed by cyclic voltammetry, chronopotentiometry and electrochemical impedance spectroscopic techniques. Finally, the propspect of the composites use in supercapacitors has been explored.

2.2. Experimental

2.2.1. Materials and Methods

Manganese(II) sulphate monohydrate (BDH, England), potassium permanganate (Merck, India) sulphuric acid (Merck, Germany) and ammonium peroxydisulfate (Merck, India) were used as received without further purification. Aniline (Merck, India) was distilled under reduced pressure prior to use. All solutions were prepared and all experiments were carried out with de-ionized water (conductivity: 0.055 μScm^{-1} at 25.0 °C) from HPLC grade water purification systems (BOECO, BOE 8082060, Germany).

The morphology, structure, and thermal stability were studied by scanning electron microscopy (JSM-6490LA, JEOL, USA), energy dispersive X-ray spectroscopy (JSM-6490LA, JEOL, USA), specular reflectance spectroscopy (UV-1800, Shimadzu, Japan), Fourier transform infrared spectroscopy (Frontier FT-NIR/MIR, Perkin Elmer, USA) and thermogravimetric analysis (TG/DTA 7200 EXSTAR, Hitachi, Japan) techniques. FT-IR spectra of PAni and PAni-MnO_2 composites were recorded using KBr pellets in the range of 4000-400 cm^{-1} with 4 cm^{-1} resolution. Phase analysis and chemical characterization of the samples were carried out using x-ray diffractometer (Philips PW 1724) x-ray generator using XDC-700 Guinier-Hagg focusing camera with strictly monochromatized Cu Kα radiation (λ=1.540598). Specular reflectance spectra (disk type sample with thickness of 1 mm and area of 0.78 cm^2) were recorded using a double beam Shimadzu UV-visible spectrophotometer (UV-1800, Shimadzu, Japan) with an integrating sphere attachment DRA-CA-30I.

2.2.2. BET Surface Analyzer

The specific surface area of the samples were measured by nitrogen gas adsorption-desorption through Brunauer-Emmett-Teller (BET) method using BET surface analyzer by Belsorp miniII, BEL, Japan and the pore volume, average pore diameter and the pore size distribution were determined by analyzing the BET data with Barrett-Joyner-Halenda (BJH) method with a surface area of 0.01 m^2g^{-1} and above.

The linear form of the BET equation for the adsorption of gas on a solid surface is given by:

$$\frac{1}{\mathrm{V}[(p_0/p)-1]} = \frac{c-1}{v_m c}\left(\frac{p}{p_0}\right) + \frac{1}{v_m c}$$

where, V_a= volume of gas adsorbed per gram of sample, P and P_0= equilibrium and saturation pressures of adsorbate at adsorption temperature, respectively, c= BET constant, υ_m= volume of gas adsorbed for monolayer formation.

If the value of the slope of BET plot is "A" and that of the y-intercept is "I", then the volume of gas adsorbed for monolayer formation and BET constant can be determined by the following equations:

$$\begin{aligned} v_m &= \frac{1}{A+I} \\ c &= 1+\frac{A}{I} \\ S_{\text{total}} &= \frac{(v_m N s)}{V} \\ S_{\text{BET}} &= \frac{S_{\text{total}}}{a} \end{aligned} \qquad (2.1)$$

where, S_{total} = total surface area, S_{BET}= specific surface area, N= Avogadro's constant, s= adsorption cross-section of adsorbing species, V= molar volume of adsorbate gas, and a= mass of the adsorbent.

Pore size distributions and pore volume can be derived from Barrett, Joyner and Halenda (BJH) plots using the following equations:

$$\begin{aligned} V_p &= V/22414 \times M_g/\rho_a \\ d_p &= \frac{4\times V_p}{a_{S,BET}} \times 10^3 \end{aligned} \qquad 2.1\text{A}$$

M_g, ρ_a =Molecular weight and density of adsorptive (N_2) respectively and V_p= Total pore volume.

2.2.3. Cell and Electrodes Used for Electrochemical Measurements

A single compartment three-electrode glass cell was used for various electrochemical measurements. A computer-controlled electrochemical analyzer (Model: 760E, CH Instruments, USA) with working electrode was employed for the electrochemical measurements. The schematic diagram of the instrumental setup of the computerized electrochemical analyzer system is shown in Figure 2.1. The measurements were conducted by using a graphite electrode from Bioanalytical Systems (BAS, USA, surface area: surface area: 0.009 cm^2). A coiled platinum wire and an Ag/AgCl (Sat. KCl) electrodes were used as the counter and reference electrodes, respectively using 0.5 M aqueous Na_2SO_4 solution as the electrolyte.

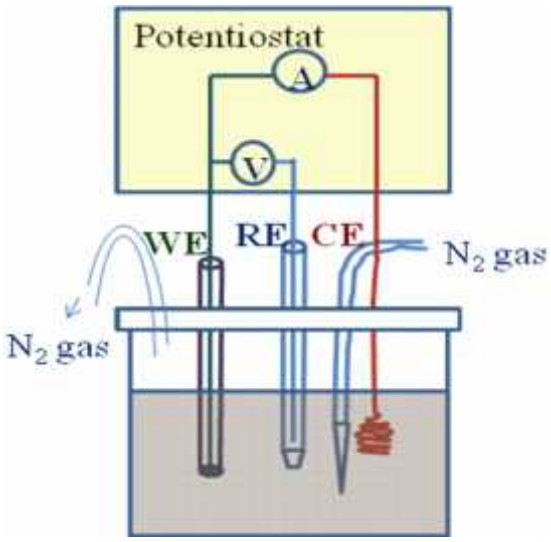

Figure 2.1. Scheme of a single compartment three-electrode electrochemical cell: WE, RE, and CE represent the working, reference and counter electrodes, respectively.

The electrochemical characterization of the graphite electrode fabricated with the active materials was carried out by cyclic voltammetry, chronopotentiometry and electrochemical impedance spectroscopy using the aforementioned electrochemical analyzer to investigate the electrochemical performance of the modified electrods as supercapacitors. Cyclic voltammetry was used to determine maximum cell voltage or potential window in which redox process occurs and galvanostatic charge-discharge was used to assess the performance of the modified electrode to be used as supercapacitors. Cyclic voltammetries were performed in the potential range of -0.20 to 1.2 V *vs.* Ag/AgCl (Sat. KCl) reference electrode under scan rate of 0.01-0.10 V s^{-1}. Galvanostatic charge-discharge experiments were carried out by cycling the voltage

from 0 to 0.80 V at different current densities (0.10-0.25 A g^{-1}).

Electrochemical impedance spectroscopic measurements were performed in an AC frequency range from 10^5 to 0.01 Hz with an excitation signal of 5 mV. All electrochemical experiments were carried out at ambient conditions.

Typical cyclic voltammogram, galvanostatic charge-discharge cycles and electrochemical impedance are measured using three-electrode systems in which the modified graphite electrode is considered to be the working electrode. The specific capacitance was calculated from cyclic voltammograms of the supercapacitor electrode at different scan rates using the equation: [21]

$$C_s = \frac{IdV}{m \times \nu} \quad (2.2)$$

where, C_s= specific capacitance, $I \times dV$ = area under the cyclic voltammogram, m = mass of electroactive material on the electrode in grams, v = scan rate in Vs^{-1}.
The specific capacitance of the graphite electrode modified by the materials could be calculated from galvanostatic charge-discharge cycles or chronopotentiometry at different current densities using the equation: [22]

$$C_s = \frac{i \times \Delta t}{\Delta V \times m} \quad (2.3)$$

Here, $\boldsymbol{C}_s$ is the specific capacitance from galvanostatic charge-discharge curves in F g^{-1}, i = current in ampere, Δt = the discharge time in second, ΔV= potential difference in volt and m = mass of active materials in gram which was casted on graphite electrode.

The cycling performance of the supercapacitor electrode was justified by a chronopotentiometry by applying a controlled current between the working and counter electrodes from a current source or galvanostat and recording the potential between the working and reference electrodes. The current flowing through the electrode was controlled while the potential changed as a function of time within a certain number of charge-discharge cycles. Charge-discharge cycles were carried out in the potential window from cyclic voltammograms where Faradaic process and electrical double layer charging process occur.

2.2.3.1. Modification of Graphite Electrodes

For electrochemical measurements, graphite electrodes were modified. 95 wt.% electroactive materials (*i.e.* pristine PAni, PAni-MnO_2 and [C_2mim][TFSI] incorporated PAni and PAni-MnO_2 composites) were mixed with 5 wt.% poly(vinyl alcohol) (PVA) in a mixed solvents of dimethyl sulfoxide (DMSO) and ethanol to form a thick paste. 10.0 μL of the paste was then casted into graphite electrode surface. The prepared electrodes were dried at 60 ^oC for 6 h under vacuum. The total weight of the active material in the electrode was usually ~0.5 mg.

2.2.4. Preparation of PAni-MnO_2 Composites

PAni was prepared by chemical oxidative polymerization from aniline monomer using ammonium peroxydisulfate as an oxidant and initiator. The efficient polymerization of aniline was carried out in aqueous sulphuric acid solution, where aniline exists as an anilinium cation and equimolar proportion of aniline and acid were used. The freshly prepared ammonium peroxydisulfate $(NH_4)_2S_2O_8$, initiator was then mixed under constant stirring at 0-5 ^oC. The reaction mixture was kept overnight with continuous stirring for complete polymerization. The precipitate of greenish PAni matrix was filtered by successive washing with double distilled water and finally dried in an electric oven at 60 °C till constant weight of PAni was achieved.

PAni-MnO_2 composites were prepared by *in situ* chemical oxidative polymerization of aniline in the presence of manganese(II) sulphate in acidic solution. The weight ratio of aniline to manganese(II) sulphate were varied as 93.3:6.7, 52.4:47.6, 18.1:81.9, 13.6:86.4, 10.9:89.1 as summarized in Table 2.2. Typically, 0.1056 g of manganese(II) sulphate monohydrate was taken in a 500 mL beaker containing 0.1 M aniline in 0.2 M sulphuric acid and the reaction mixture was kept in an ice bath at 0-5 °C with continuous stirring. 0.0553g of $KMnO_4$ was added drop wise at 0-5 ^oC. MnO_2 was formed instantly and initiated the polymerization. After about 5 min of addition, the aniline was found to undergo polymerization as was traced by observing the change of color from colorless to green. The mixture was then stirred at around 25 ^oC for 15 h. PAni-MnO_2 composite formed was collected by filtration and repetitively washed with double distilled water and acetone until the filtrate became colorless and then dried in an oven at 60 ^oC until the weight of product became constant.

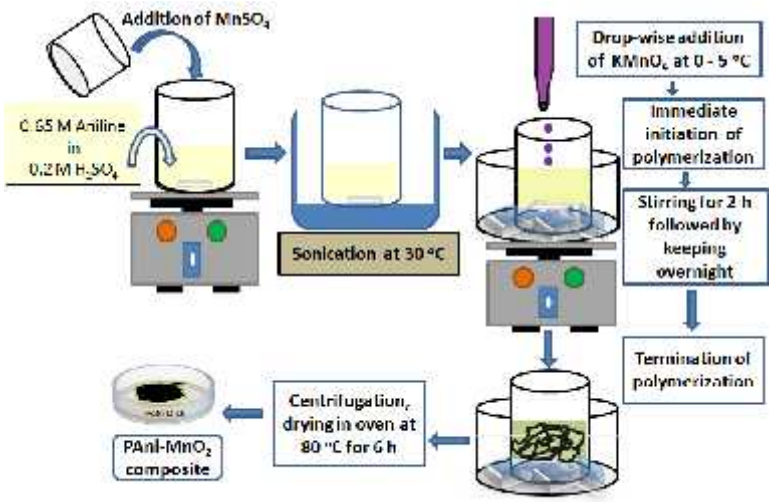

Figure 2.2. Schematic representation of synthesis of PAni-MnO_2 composites.

The compositions of PAni-MnO_2 composites as well as their thermal stability were evaluated with TGA in the presence of O_2 (air) under isothermal condition with the samples held at at 450 ^oC for 4 h, where no residual mass retained for PAni (data are not shown here). The compositions were named as PM1 (PAni-2% MnO_2), PM2 (PAni-7% MnO_2), PM3 (PAni-20% MnO_2), PM4 (PAni-20% MnO_2) and PM5 (PAni-35% MnO_2).

2.3. Results and Discussion

2.3.1. Specular Reflectance Spectral Analysis

Specular reflectance spectra of PAni and PAni-MnO_2 composites (Figure 2.3) were recorded in solid state to characterize them concerning their electronic properties. The spectra of PAni indicate the π-π* transition at 270 nm for benzenoid ring, polaron-π* transition at 435 nm indicating that PAni emaraldine salt is in the doped state. The spectrum of PAni also shows a band at 800 nm extending to the near-infrared region indicating a free carrier tail that implies the presence of protonated PAni in expanded coil conformation [23]. The spectra of PAni-MnO_2 composites show similar transitions with the shifting of bands of PAni, for example, the bands for π-π* and polaron-π* occurred at 270 and 435 nm in PAni shifted to 280 and 430 nm, respectively, in PAni-MnO_2 composites. Similar results are observed for all of the PAni-MnO_2 composites prepared by varying the composition of PAni and MnO_2. Incorporation of [C_2mim][TFSI] in PAni and PAni-MnO_2 composites show similar shifting of bands from those without incorporation of [C_2mim][TFSI].

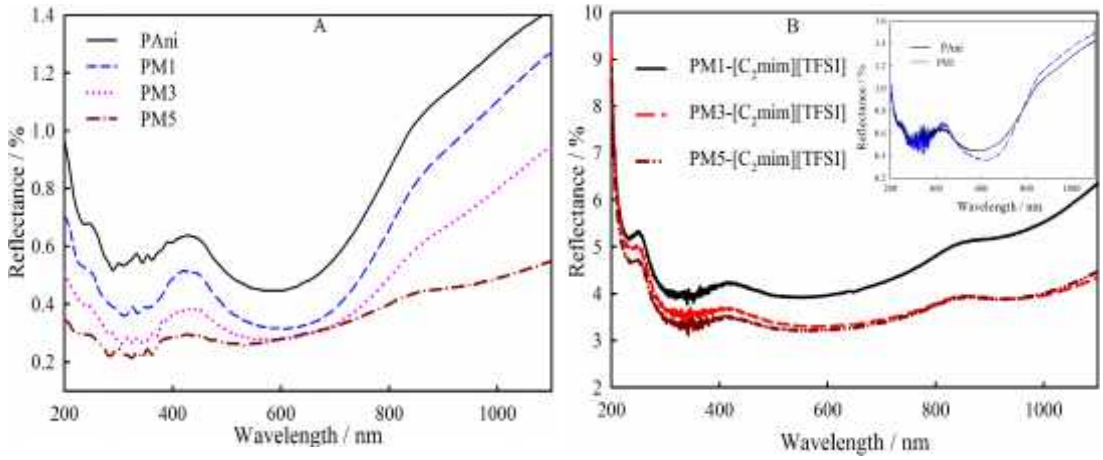

Figure 2.3. Specular reflectance spectra of PAni, PM1, PM3 and PM5-(A) and PM1, PM3 and PM5 with incorporation of $[C_2mim][TFSI]$-(B), Inset is spectra of PAni and PM1.

2.3.2. Molecular characterization by FT–IR Spectral Analysis

FT-IR spectra of pure PAni and PAni-MnO_2 composites are shown in Figure 2.4. The assignment of the major bands with corresponding wavenumbers is summarized in Table 2.1. FT-IR spectra of PAni and PAni-MnO_2 composites are similar except for the observation of characteristic band shifting to higher wavenumbers in the case of the composites. The bands of PAni observed at 1569, 1479, 1294, 1128 and 803 cm^{-1} correspond to the C-C stretching mode of quinoid ring, C-C stretching mode of benzenoid ring, C-N stretching mode of aromatic amine, N=Q=N (Q represents the quinoid ring) stretching of the quinoid rings and the C-H out-plane bending of benzene rings, respectively. The N=Q=N stretching band at 1128 cm^{-1} is the characteristic band of PAni in emeraldine form. This was described by Macdiarmid *et al.* as the "electron-like band" and is considered to be a measure of delocalisation of electrons and, thus, it is a characteristic peak for the conductivity of PAni [24]. All of the PAni-MnO_2 composites also show the similar characteristic peaks except for the shifting of some characteristic bands of PAni. The bands of pure PAni at 1569, 1479, 1294, 1128 and 803 cm^{-1} were shifted to 1554, 1494, 1299, 1169 and 854 cm^{-1}, respectively in the PM1 (PAni-2% MnO_2) composite. In addition, a new peak at 587 cm^{-1} was observed in the case of composites. This peak may be attributed to the Mn-O stretching vibration for MnO_2. Thus, FT-IR spectra of the PAni-MnO_2 composites exhibit both the characteristic bands of PAni and MnO_2 which confirms the presence of both components in the composite. In addition, the peak shifting observed in this case may be ascribed to be due to the formation of hydrogen bonding between MnO_2

and the N-H group of PAni on the surface of MnO_2 particles [25]. Similar shifting was marked for all of the PAni-MnO_2 composites (Table 2.1). In case of composites containing more than 20% of MnO_2 the -O-H stretching bands are absent due to total loss of absorbed moisture.

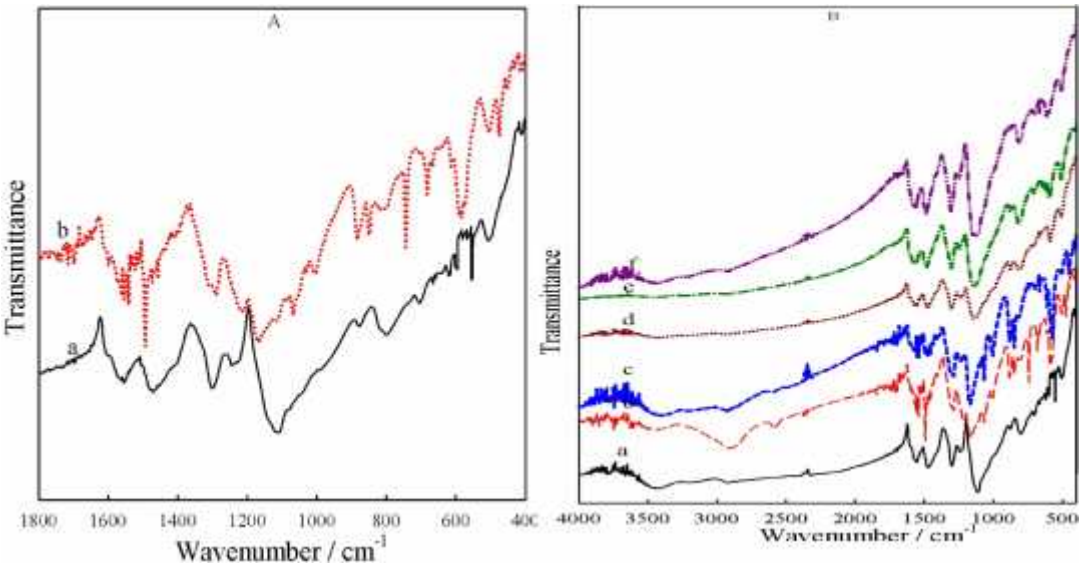

Figure 2.4. FT-IR spectra of (a) PAni and (b) PM1 (A) and (a) PAni, (b) PM1, (c) PM2, (d) PM3, (e) PM4 and (f) PM5 (B).

Table 2.1. Assignments of FT-IR bands of PAni and PAni-MnO_2 composites

Sample	N=Q=N str. (cm^{-1}) Q=Quinoid ring	C-N str. (Aromatic amine) (cm^{-1})	C-C Str. of benzenoid ring (cm^{-1})	C-C Str. of quinoid ring (cm^{-1})	N-H Str. of benzenoid ring (cm^{-1})	O-H str. (cm^{-1})	Mn-O str. (cm^{-1})
PAni	1128	1294	1479	1569	2919	3444	-
PM1	1169	1299	1494	1554	2919	3413	587
PM2	1194	1298	1464	1569	2919	3413	587
PM3	1134	1299	1479	1569	2919	-	587
PM4	1149	1315	1495	1570	2919	-	587
PM5	1135	1315	1480	1570	2919	-	587

In [C_2mim][TFSI] the C-H stretching bands between 2950-3200 cm^{-1} were observed for [C_2mim] cation. Generally, the aliphatic C-H modes of the methyl and ethyl moieties are observed between 2800 and 3050 cm^{-1}. The bands at 3129 and 3151 cm^{-1} may be ascribed to the terminal CH_3-symmetric stretching and alkyl chain asymmetric stretching respectively. The aromatic C-H stretching may also be assigned to this region. The spectral bands at 1359, 1202 and 1059 cm^{-1} appeared for C-F stretching of $–CF_3$, asymmetric stretching of S-O and symmetric stretching of S-O in [TFSI] anion, respectively. The bands of pristine PAni at 1569, 1479, 1294, 1128 and 803 cm^{-1} were

shifted to 1554, 1494, 1299, 1169 and 854 cm^{-1}, respectively in the PM1 (PAni-2% MnO_2) composite. After the incorporation of [C_2mim][TFSI], few bands of PAni and PM1 composite were shifted. The bands of PAni-[C_2mim][TFSI] shifted to 1577, 1487, 1307, 1142 and 812 $cm^{-1}$and the bands of PM1-[C_2mim][TFSI] were shifted to 1562, 1494, 1329, 1134 and 872 cm^{-1}. The shifting may be due to electrostatic interactions among the polarons and bipolarons in the PAni chain and [C_2mim] cations and [TFSI] anions in the IL. H-bonding may also become feasible among the different species of PAni, PM1 composite and [C_2mim][TFSI].

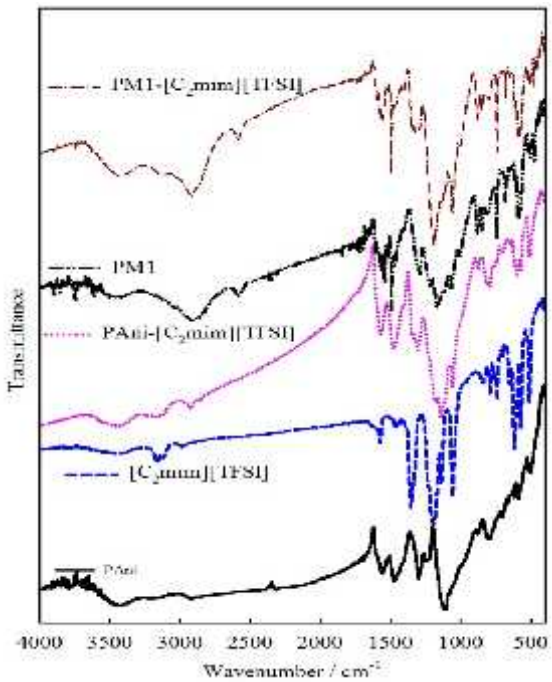

Figure 2.5. FT-IR spectra of PAni, [C_2mim][TFSI], PAni-[C_2mim][TFSI] and PM1-[C_2mim][TFSI].

2.3.3. X-ray Diffraction Analysis

XRD pattern analysis was performed to check phase purity and to assess the crystalline nature of the synthesized samples. XRD patterns of the pristine PAni and PAni-MnO_2 composites are shown in Figure 2.6. The XRD pattern of pristine PAni shows three broad peaks from 2θ *ca.* 17.6, 25 and 27º indicating semicrystalline morphology. The broad peaks observed at 17.6º and 25º are similar to those observed by king *et al.* [26]. The additional peaks at 2θ = 20°, 24° and 30º can be identified as α-MnO_2 phase (Joint Committee on Powder Diffraction Standards (JCPDS no. 44-0141) of MnO_2 with diffracting planes (200), (220) and (310), respectively [27]. So, it can be concluded that in PAni-MnO_2 composites, MnO_2 particles were successfully

incorporated into the PAni matrix. With higher percentage of MnO_2, the intensities of these peaks became weak and broad, indicating the transitions from semicrystalline to amorphous nature of the composites.

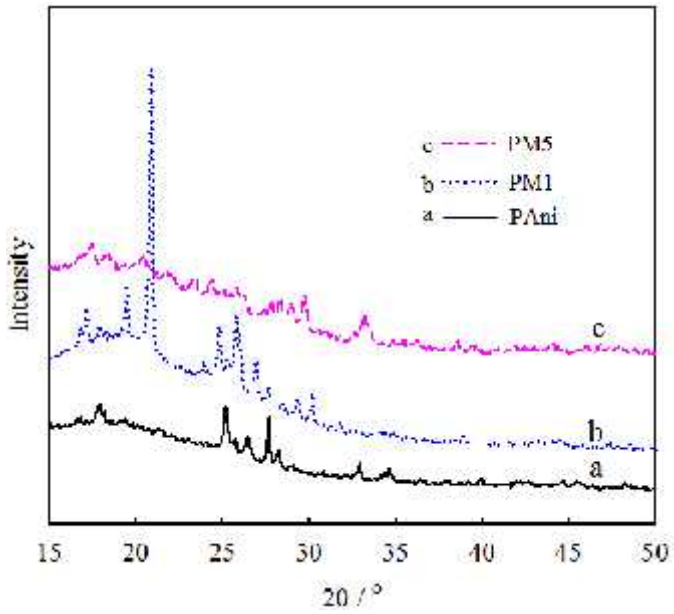

Figure 2.6. X-ray diffraction pattern of (a) PAni, (b) PM1 and (c) PM5 composites.

2.3.4. Size and Morphology Analysis

Scanning Electron Microscopy (SEM)

Figure 2.7 shows the SEM images of the PAni and PAni-MnO_2 composites.

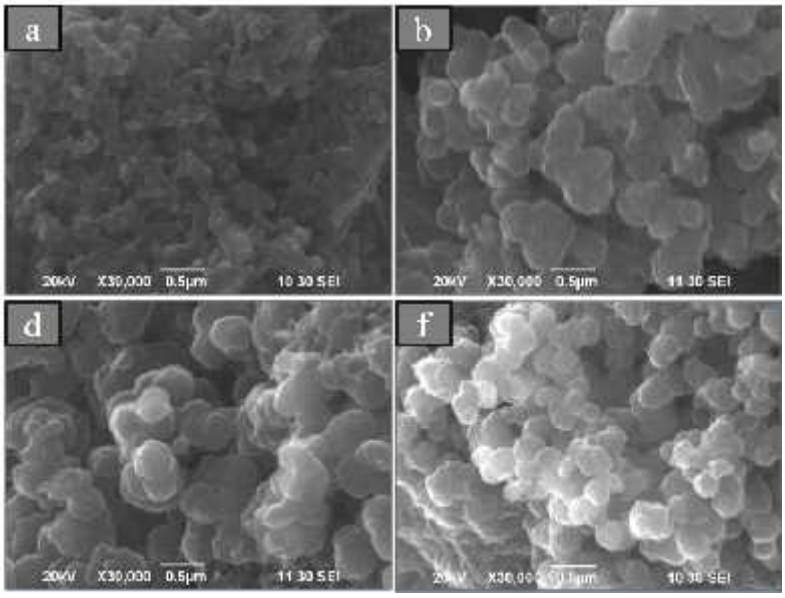

Figure 2.7. SEM images of (a) PAni, (b) PM1, (d) PM3 and (f) PM5 composites.

PAni shows morphology different from PAni-MnO_2 composites. While PAni shows interconnected network like morphology, compact granular morphology was

noticeable for PAni-MnO_2 composites which becomes more prominent as the wt.% MnO_2 loading increases. The average radius of PAni-MnO_2 composites was about 200 nm.

2.3.5. Thermogravimetric Analysis

Figure 2.8 depicts the TGA curves of PAni, MnO_2 and different PAni-MnO_2 composites . Three-steps weight loss of PAni and PAni-MnO_2 composites were found to take place. The first weight loss up to 115 ^oC is attributed to the loss of absorbed moisture and the second weight loss ranging from 115 to 230 ^oC is due to the removal of low molecular weight oligomers [28]. A slow and somewhat gradual weight loss profile tarting from 230 ^oC presents degradation of the skeletal PAni chain structure [29].

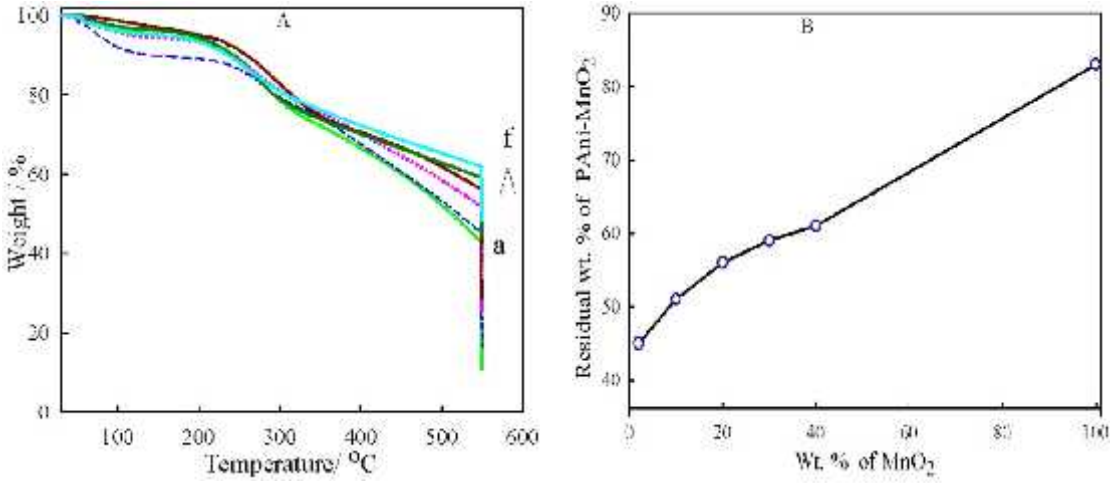

Figure 2.8. TGA curves of (a) PAni, (b) PM1, (c) PM2, (d) PM3, (e) PM4 and (f) PM5 under N_2 atmosphere (A) and residual weight of PAni-MnO_2 (PM1 to PM5) composites upon variation wt.% of MnO_2 (B).

Thermal degradation of PAni-MnO_2 composites with varying MnO_2 loading was almost the same with a slight variation of onset degradation temperature compared to PAni. This may be associated with some sort of interactions between the skeleton of PAni and MnO_2. It may be worth noting that some percent of mass (*ca.* 12%) was found to retain for PAni even when the temperature was hold at 550 ^oC for 30 min in N_2 gas environment. For a complete combustion, similar measurements were carried out in the presence of O_2 (air) under isothermal condition at 450 ^oC hold for 4 h, where no residual mass was observed (data are not shown here). The residual mass of MnO_2 retained in the composites is summarized in Table 2.2. The amount of MnO_2 retained in the composite increases as the amount of $MnSO_4$ used was increased during the polymerization.

Table 2.2. Composition of PAni-MnO_2 composites

Sample Name	Compositions	Weight ratio of aniline to $MnSO_4$ used during polymerization	MnO_2 retained in composites (Wt.%)
PM1	PAni-2 % MnO_2	93.3 : 6.7	2
PM2	PAni-7 % MnO_2	52.4 : 47.6	7
PM3	PAni-20 % MnO_2	18.1 : 81.9	20
PM4	PAni-27 % MnO_2	13.6 : 86.4	27
PM5	PAni-35% MnO_2	10.9 : 89.1	35

Figure 2.9 (A) and 2.9 (B) show the thermal degradation pattern of PAni, PAni with wt.% variation of [C_2mim][TFSI] and PAni-MnO_2 composites with incorporation of [C_2mim][TFSI], respectively under N_2 atmosphere isothermally held at 550 ^oC for 30 min. [C_2mim][TFSI], PAni and PAni-[C_2mim][TFSI] show one step, two steps and three steps weight loss processes, respectively. The degradation of [C_2mim][TFSI] started at 430 ^oC whereas in PAni two main steps weight loss occur that include up to 115 ^oC for loss of absorbed moisture and from 220 ^oC onwards for degradation of PAni chain. All PAni-MnO_2 composites upon incorporation of [C_2mim][TFSI] show three step weight loss in which first two stages weight losses are similar to those of PAni but third weight loss occurs at 407 ^oC due to the incorporation of [C_2mim][TFSI] into PAni chain. This may be ascribed to the H-bonded interaction between hydrogen atom of PAni chain and O atom of S=O in [C_2mim][TFSI] which probably weakens the degradation process of [C_2mim][TFSI] from the PAni chains.

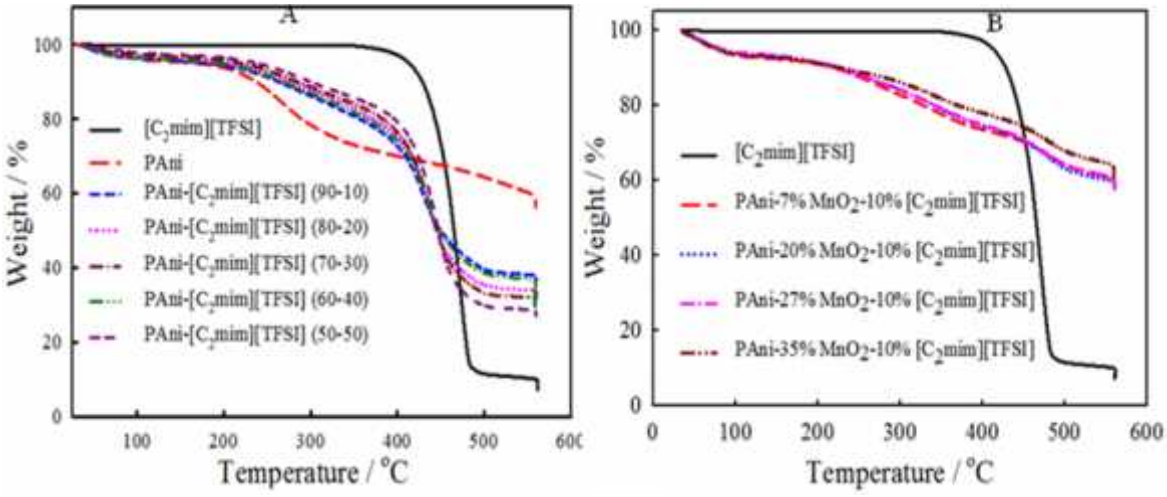

Figure 2.9. TGA curves of pristine PAni and PAni-[C_2mim][TFSI] (A) and PAni-MnO_2 composites with incorporation of [C_2mim][TFSI] (B).

The onset degradation temperature of [C_2mim][TFSI] decreases from 430 ^oC to 407 ^oC. In other words, the thermal stability of PAni increases on addition of

[C_2mim][TFSI] into PAni. This can be further justified from the TG curves that at 407 ^oC weight loss decreases from 77% to 69% in PAni-[C_2mim][TFSI] to PAni. In Figure 2.8 (B) PAni-MnO_2 composites with incorporation of [C_2mim][TFSI] show different degradation pattern under identical conditions to that of Figure 2.8 (A). Incorporation of [C_2mim][TFSI] with all PAni-MnO_2 composites show same degradation pattern of PAni-[C_2mim][TFSI] except slight variation of TGA curves in the third steps. The first step, which corresponds to approximately 5% weight loss from 25 to 115 ^oC, is due to the evaporation of moisture from all of the samples. The major weight loss at above 235 ^oC is attributed to the degradation of PAni chain. After that weight loss occurs almost linearly. The third weight loss which corresponds to degradation of [C_2mim][TFSI] from the PAni chain increases from 407 ^oC to nearly 450 ^oC due to hindrance of the degradation process by MnO_2 in all PAni-MnO_2 composites with incorporation of [C_2mim][TFSI]. The incorporation of [C_2mim][TFSI] thus enhances thermal stability of the composites and thermal stability has a definite improvement over PAni or PAni-MnO_2 composite.

2.3.6. BET Analysis

Surface area and pore size distribution were determined from adsorption-desorption of N_2 gas at different relative pressures and a constant temperature of -196 ^oC for PAni and PAni-MnO_2 composites after pre-treatment. Adsorption isotherms, BET and BJH plots were used for this purpose. Brunauer *et al.* and Sing classified six types of isotherms according to the type of surface in 1985. The IUPAC Commission on Colloid and Surface Chemistry proposed a modification of this classification; in addition to the original five types of Brunauer *et al.* they added a sixth type, the stepped isotherm [30]. These six types are shown schematically in Figure 2.10 along with the types of corresponding surfaces. The surface area was calculated from multipoint BET using Equation 2.1 in Section 2.2.2 while the pore size distribution was evaluated by BJH plot using Equation 2.1A from the desorption part of the isotherm.

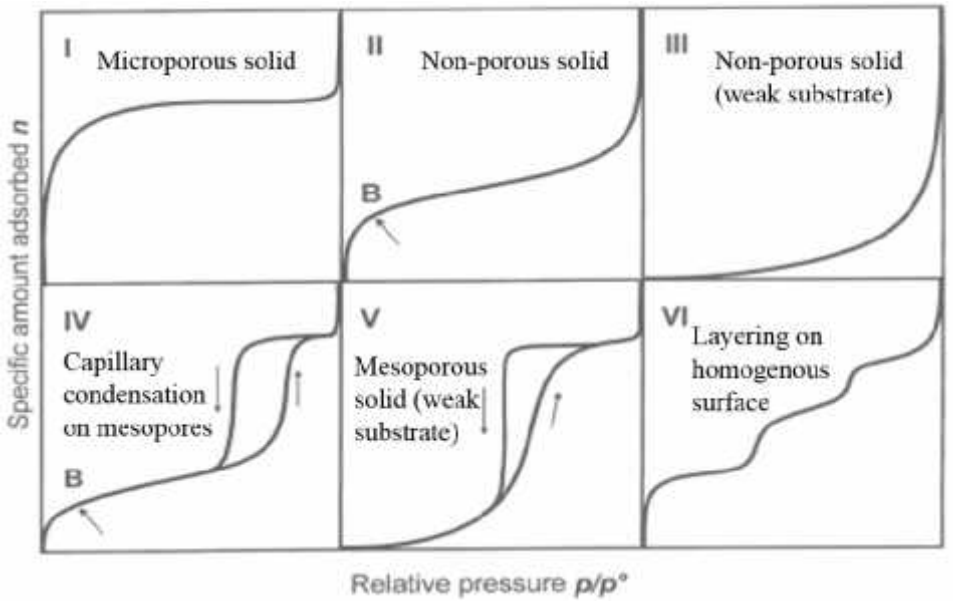

Figure 2.10. Six types of adsorption isotherm according to the 1985 IUPAC classification.

The nitrogen adsorption–desorption isotherms are shown in Figure 2.11. The results suggest that PAni all the PAni-MnO_2 composites show similar typical isotherm for materials with a mixture of meso- and macro-porosity [31]. All the isotherms in Figure 2.11 resemble Type-V (Figure 2.10) of the 1985 IUPAC classification, indicative of mesoporous surface adsorbing the greatest volume of gas [32]. In all the adsorption isotherms a hysteresis loop can be seen from which it can be inferred that the surface is mesoporous and has weak affinity for the adsorbate.

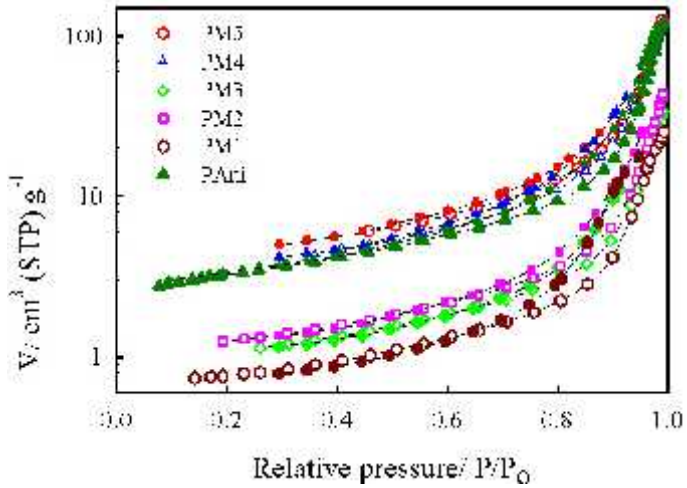

Figure 2.11. Nitrogen adsorption-desorption isotherms of PAni and PAni-MnO_2 composites.

Figure 2.12 shows the mean pore diameter of the composites upon variation of wt.% of MnO_2 and Table 2.3 summarizes pore size and volume, specific surface area and mean particle size of PAni and PAni-MnO_2 composites The pore volume is inversely

proportional to pore size for PAni and all of the PAni-MnO_2 composites. In simultaneous oxidation and incorporation of the formation of PAni-MnO_2 composites MnO_2 is formed *in situ* and simultaneously oxidizes aniline to form PAni. In this case, MnO_2 is incorporated into the PAni surface making the surface unevenly distributed with MnO_2 particles and creates uneven pores. Upon addition of 2 wt.% of MnO_2 particles pore diameter increase and remains constant up to 20 wt.% increment (Figure 2.13). Pore diameter decreases after additional MnO_2 loading into the PAni-MnO_2 composites. This may be attributed to penetration of the additional MnO_2 into the inner surface of the composites that might create partial blockage in the deeper pores. The specific surface area, pore volume and pore size distributions determined using Equation 2.1 and 2.1 A which is summarized as Table 2.3.

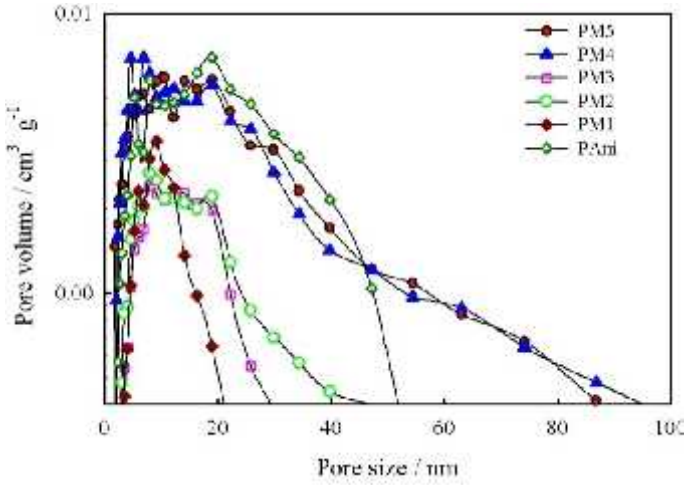

Figure 2.12. Pore size distribution and pore volume of PAni and PAni-MnO_2 composites (PM1 to PM5 composites).

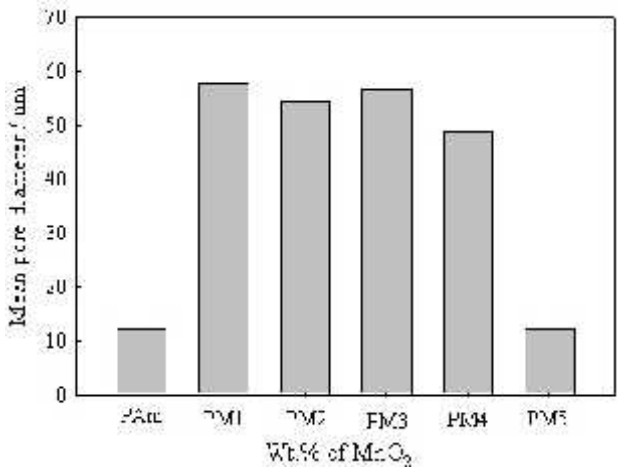

Figure 2.13. Mean pore diameter *vs.* wt.% of the PAni and PAni-MnO_2 (PM1 to PM5) composites.

Table 2.3. Pore size and volume, specific surface area and mean particle size of PAni and PAni-MnO_2 composites

Material	Specific surface area ($m^2\ g^{-1}$)	Total pore volume ($cm^3\ g^{-1}$)	Mean pore diameter (nm)	Mean particle size (nm)
PAni	11.4	0.1804	63.20	386.36
MnO_2	128	0.3906	12.25	9.35
PM1	2.84	0.0363	51.20	-
PM2	4.46	0.0645	57.94	-
PM3	3.84	0.0524	54.58	-
PM4	13.00	0.1847	56.77	-
PM5	15.60	0.1906	49.00	-

2.3.7. Electrochemical Characterization

2.3.7.1. Cyclic Voltammetry

Figure 2.14 shows cyclic voltammograms (CVs) of PAni and PAni-MnO_2 composites modified graphite electrode at different potential scan rates. Within the potential window of -0.2 to 1.2 V, the curves have some humps, indicating the Faradaic reactions within this region. Two pairs of redox peaks can be observed for both the PAni and PAni-MnO_2 composites in the range of 0.15 to 0.65 V that are originated from the transitions from leucoemeraldine form to emeraldine, and emeraldine to pernigraniline forms of PAni [33]. In addition, peak currents observed with pure PAni are generally larger than those with PAni-MnO_2 (PM5) composite. This is indicative of capacitive nature of the active materials with a combination of the double-layer capacitance and pseudocapacitance. The higher current density of CV of PAni than that of PM5 composite indicates the high conductivity and low internal resistance of PAni modified graphite electrode. This is due to the fact that the electrolyte ions can only be accessible to the outer surface of the electrode at high scan rates, and the active material that has the ability to reach only through the deep pores does not actively contribute to the pseudocapacitance as well as total capacitance [34].

From these CVs the specific capacitances of PAni and PAni-MnO_2 (PM5) composite at scan rates of 0.01, 0.02, 0.05 and 0.10 V s^{-1} were determined using equation 2.2. The specific capacitance values are summarized in Table 2.4. It can be observed that the specific capacitance decreases from 242 to 169 F g^{-1} in PM5 composite with the increase in current density from 0.10 to 0.25 F g^{-1}. That is why, high scan rates

provide low specific capacitance of the active material under study. The larger specific capacitance of PAni-MnO_2 composite may be due to larger specific surface area than PAni which might contribute to the larger utililization of electrolytic ions into the active materials. This may also provide better conductive paths for fast electron transportation. In addition to pseudocapacitance of PAni, MnO_2 may contribute to electrochemical double layer capacitive behavior in the PAni-MnO_2 composites.

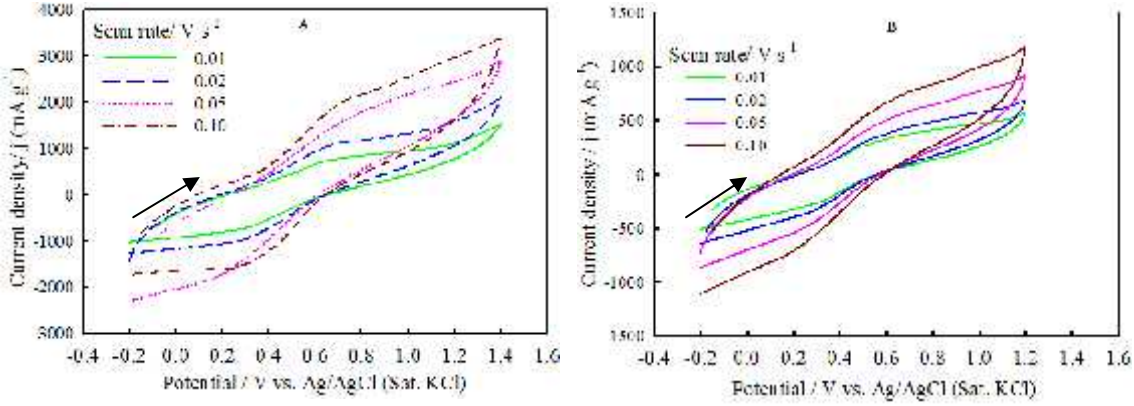

Figure 2.14. CVs of PAni (A) and PM5 composite (B) measured at different potential scan rates.

Table 2.4. Specific capacitance of PAni and PM5 composite

Material	Scan rate (V s^{-1})	Specific capacitance (F g^{-1})	Material	Scan rate (V s^{-1})	Specific capacitance (F g^{-1})
PAni	0.01	109	PM5	0.01	218
	0.02	79		0.02	149
	0.05	61		0.05	64
	0.10	38		0.10	51

2.3.7.2. Chronopotentiometry Analysis

Figure 2.15 illustrates the typical charging-discharging behavior of the graphite electrodes modified with PAni and PAni-MnO_2 composites recorded in aqueous 0.5 M Na_2SO_4 solution. For both electrodes there is a sharp decrease in voltage at the commencement of discharge followed by linear decrease with time of discharge. The sharp change in voltage at the beginning of charge or discharge is attributed to the effect of internal resistance of the capacitor. During charging, initially charge is stored easily but difficulty arises due to place additional charge on the electrode surface for Coulombic repulsion from the charge already deposited on the electrode surface. On the other hand, the discharging involves Coulombic repulsion that pushes out charge

easily as voltage is decreased but as more charge is removed from the electrode, it becomes increasingly difficult to get rid of the small amount of charge remaining from the electrode. Linear variation of voltage during charge or discharge is indicative of the property of a capacitor. C_s values determined from the charge-discharge curves at different current densities using Equation 2.2 2 are summarized in Table 2.5. The C_s decreases from 99 to 19 F g^{-1} and 242 to 169 F g^{-1} for PAni and PM5 (PAni-35% MnO_2) composites, respectively at current densities of 0.10 to 0.25 A g^{-1}.

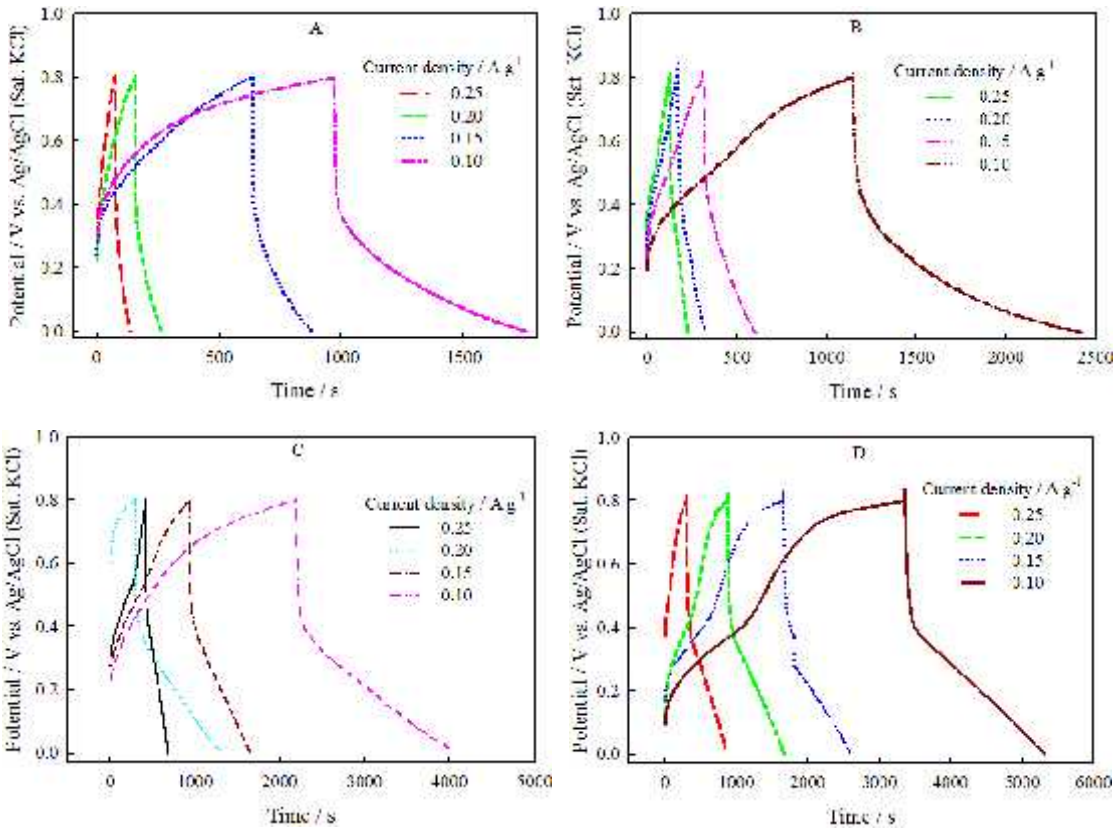

Figure 2.15. Charge-discharge curves of PAni (A), PM1(B), PM3 (C) and PM5(D) at different current densities.

Table 2.5. Determination of specific capacitance from charge-discharge curves of PAni and PM5 composites at different current densities

Material	Current density (A g^{-1})	Specific capacitance (F g^{-1})	Material	Current density (A g^{-1})	Specific capacitance (F g^{-1})
	0.10	99		0.10	242
	0.15	45		0.15	206
PAni	0.20	29	PM5	0.20	177
	0.25	19		0.25	169

This observation can be explained due to the fact that, at lower current density, the active materials on the electrode surface get necessary time for sufficient insertion or release of Na^+ from the electrolytic solution during the charging-discharging process. Charging-discharging process takes longer time which contributes to the higher C_s [35]. The cycling stability of the fabricated electrodes at a current density of 0.25 A g^{-1} in the potential window 0.0-0.8 V was tested by galvanostatic charge-discharge process up to 1000 cycles (Figure 2.16). Both charging and discharging times do not significantly change on cycling, which indicates significant retention of the initial C_s up to 1000 cycles. Moreover, the curves of the latter cycles show some small steps during charging-discharging to indicate that the change of potential was too small to be detected by the instrument, followed by rapid jumps [36].

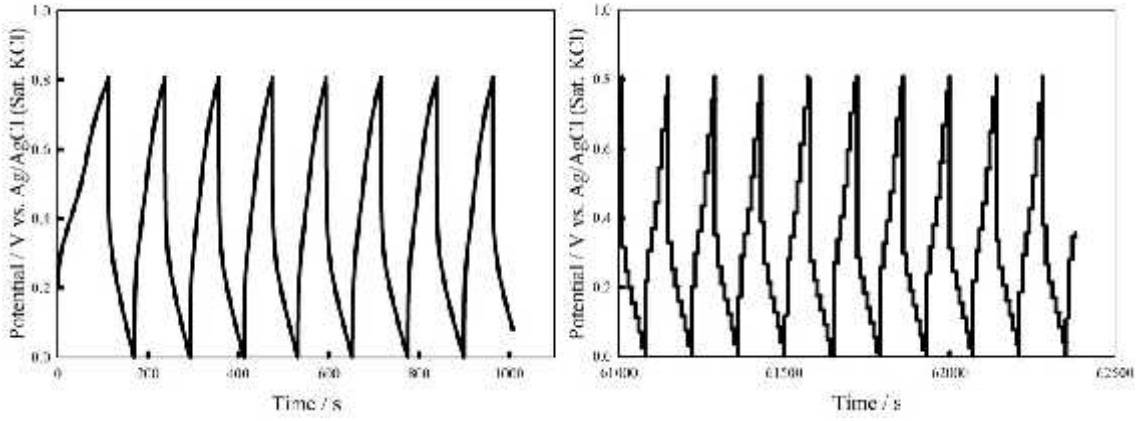

Figure 2.16. Charge-discharge cycling stability of PM5 (PAni-35% MnO_2) composite up to 1000 cycles.

The galvanostatic charge-discharge curves of [C_2mim][TFSI] incorporated PAni and PAni-MnO_2 (PM1, PM3 and PM5) composites are shown in Figure 2.17 at current densities of 0.10 to 0.25 A g^{-1}. The C_s determined from the charge-discharge curves using equation 2.2 are summarized in Table 2.6. The C_s of PAni-[C_2mim][TFSI] (213 F g^{-1}) is about 2 times higher than that of PAni but in PM5-[C_2mim][TFSI] (71 F g^{-1}), it is much lower than that of PM5 (242 F g^{-1}) at a current density of 0.1 A g^{-1}. As the wt.% of MnO_2 increases in the composites incorporation of [C_2mim][TFSI] lowers the C_s. Same trend is observed for all PAni-MnO_2 composites upon incorporation of [C_2mim][TFSI] at a constant current density of 0.10 A g^{-1}.

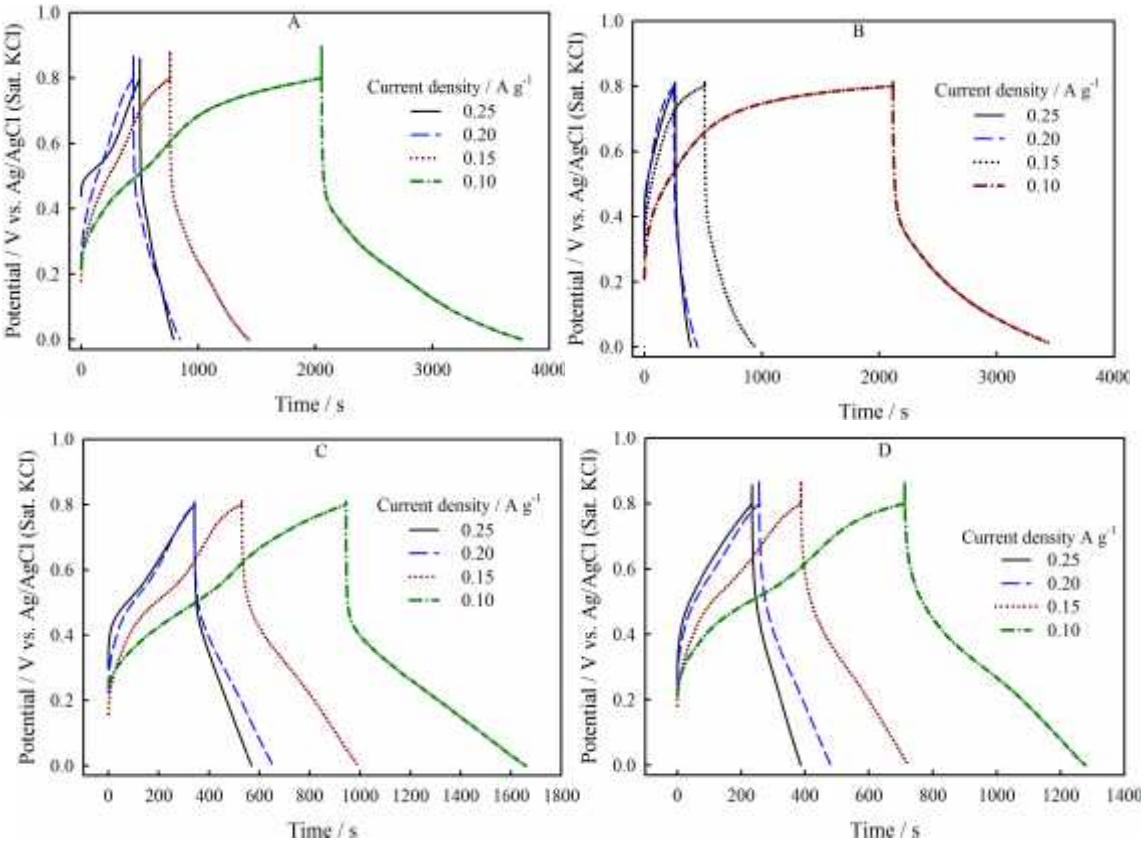

Figure 2.17. Charge-discharge curves of PAni-[C_2mim][TFSI] (A), PM1-[C_2mim][TFSI] (B), PM3-[C_2mim][TFSI] (C) and PM5-[C_2mim][TFSI] at different current densities.

Table 2.6. Determination of specific capacitance from charge-discharge curves of [C_2mim][TFSI] incorporated PAni and PM5 composites at different current densities

Material	Current density (A g^{-1})	Specific capacitance (F g^{-1})
PAni-[C_2mim][TFSI]	0.10	213
	0.15	126
	0.20	94
	0.25	88

Material	Current density (A g^{-1})	Specific capacitance (F g^{-1})
PM5-[C_2mim][TFSI]	0.10	71
	0.15	62
	0.20	56
	0.25	169

Effects of applied current densities on C_s are shown in Figure 2.18 from which it can be seen that the C_s of PAni, PAni-MnO_2 composites and [C_2mim][TFSI] incorporated PAni and PAni-MnO_2 composites decreases with increasing current density. C_s retained 19%, 70%, 38% and 57% for PAni, PM5, PAni-[C_2mim][TFSI] and PM5-[C_2mim][TFSI] composites, respectively when the current density increased from 0.10 A g^{-1} to 0.25 A g^{-1}. PAni has the lowest retention of specific capacitance which

might result from the swelling and shrinking of the material during charging-discharging process indicating lower mechanical strength. Especially, at high current density the active materials may have suffered from deep penetration that can't maintain to keep up changing the voltage instantly and eventually C_s decreases. In case of [C_2mim][TFSI] incorporated PAni and PM5 composite, moderate retention

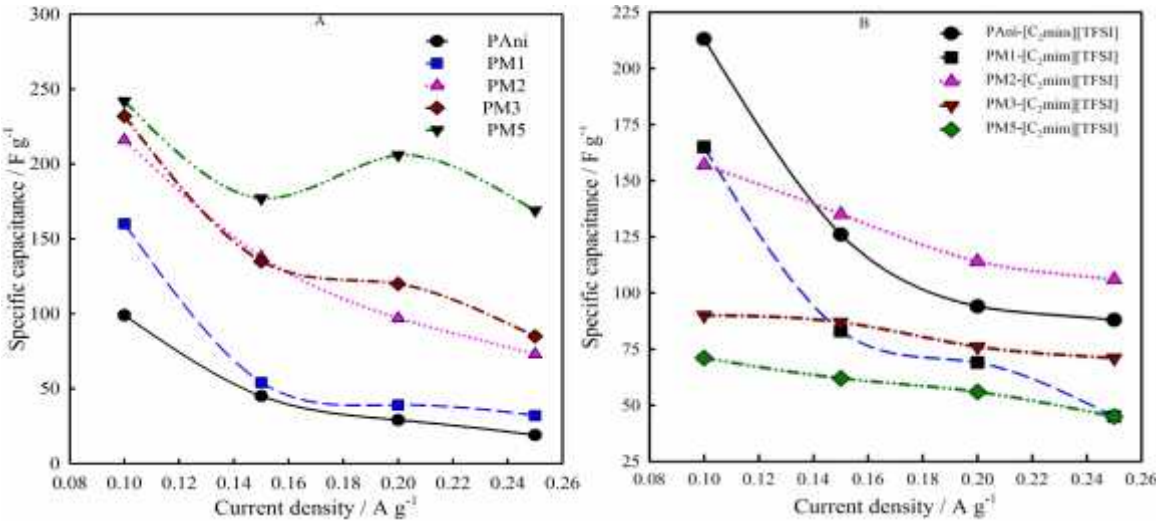

Figure 2.18. Variation of specific capacitance on current densities of PAni, PM1, PM2, PM3 and PM5 composites (A), [C_2mim][TFSI] incorporated PAni, PM1, PM2, PM3 and PM5 composites (B) at current densities from 0.10 to 0.25 A g^{-1}.

2.3.8. Electrochemical Impedance Spectroscopy

The Nyquist plots of PAni and PM5 composites are shown in Figure 2.19. PM5 composite shows almost a semicircle in the high frequency region which is related to the charge-transfer resistance from the interface between the electrode surface and 0.5 M Na_2SO_4 electrolytic solution. The Nyquist plot of PAni modified graphite electrode represents a semicircle at high frequencies; but the PM5 composite electrode has no defined semicircle. The data of impedance were fitted to equivalent model circuits shown in Figure 2.19. PM5 shows a higher internal resistance (18.73 Ohm) compared to PAni (13.57 Ohm) which may be attributed to the lower electrical conductivity of PM5 than that of PAni. This observation is in accordance with the higher current densities of PAni than that of PM5 as shown in Figure 2.14. PAni shows higher charge-transfer resistance (19.84 Ohm) than that of PM5 (0.001 Ohm) composite. Capacitance of PM5 (6.45×10^{-5}) composite is approximately 1.5-fold higher than that of PAni (4.15×10^{-5}). This may be consistent with the value of C_s obtained by chronopotentiometric method.

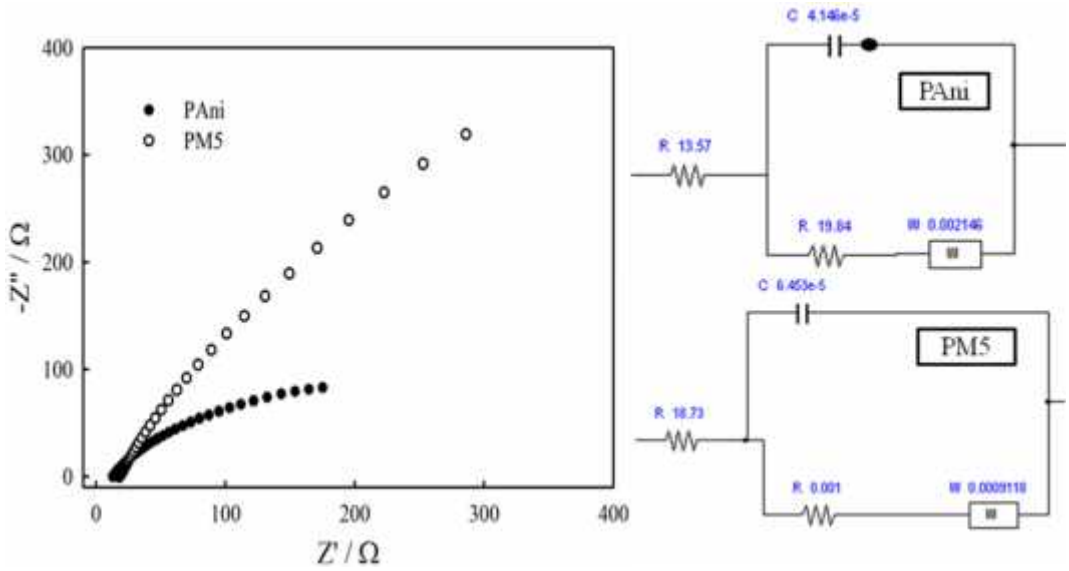

Figure 2.19. Nyquist impedance plot of PAni and PM5 composites and their corresponding equivalent fitting circuits.

2.3.9. Effect of MnO_2 Content on Specific Capacitance in Composites

The C_s of PAni-MnO_2 composite was found to increase with the content of MnO_2 in the composite, as shown in Table 2.7. The C_s of PM5 (242 F g^{-1}) is higher among all the PAni-MnO_2 composites (PM1 to PM5). C_s of PM5 is about 3 times higher than that of PAni (99 F g^{-1}) at a current density of 0.10 A g^{-1}. The increasing trend of C_s may be explained with the contribution of conductive PAni in facilitating charge transport and energy storage. The facile charge transport can be assumed in utilization of full active materials and adsorption of electrolytic ions onto the electrode surface. From the galvanostatic charge-discharge curves it can be seen that the time of discharging increases which also indicates the slow discharge leading to the increase of C_s in the PAni-MnO_2 composites. The results of C_s upon variation of wt.% of MnO_2 are summarized in Table 2.7. As shown in Figure 2.16, the charge-discharge curves of PM5 composite in the last consecutive cycles up to 1000^{th} cycle are identical as the cycles of commencement indicates a good cycling ability of the composites. The MnO_2 particles provide strong deposition support into the surface of PAni and consequently offer strong and enhanced mechanical strength of the composite, resulting in the long charge-discharge ability. The mesoporous structure of the composite may be additionally involved in the good C_s and retention ability or cycling performance of the composite. Moreover, the curves

of the latter cycles show some small steps during charging-discharging, are indicative of the change of potential to be too small to be detected by the instrument, followed by rapid jumps.

Table 2.7. Variation of specific capacitance of PAni and PAni-MnO_2 composites with variation of MnO_2 content and with incorporation of [C_2mim][TFSI] at a current density of 0.10 A g^{-1}

Material	MnO_2 content (%)	Specific capacitance ($F g^{-1}$)	Material	MnO_2 content (%)	Specific capacitance ($F g^{-1}$)
PAni	0	99	PAni-[C_2mim][TFSI]	0	213
PM1	2	160	PM1-[C_2mim][TFSI]	2	165
PM2	7	216	PM2-[C_2mim][TFSI]	7	157
PM3	20	232	PM3-[C_2mim][TFSI]	20	90
PM4	27	236	PM4-[C_2mim][TFSI]	27	76
PM5	35	242	PM5-[C_2mim][TFSI]	35	71

2.3.10. Effect of [C_2mim][TFSI] on Specific Capacitance

As shown in Table 2.5, C_s increases from 99 to 213 F g^{-1} upon incorporation of [C_2mim][TFSI] in PAni at current density of 0.10 F g^{-1} and it decreases in case of PAni-MnO_2 composites (PM1 to PM5) upon incorporation of [C_2mim][TFSI] at the same current density. Pure ionic liquid, [C_2mim][TFSI] exists as ion aggregates in its pure state. When this is incorporated into PAni, these aggregates of ions can impart different types of interactions leading to disaggregation of [C_2mim][TFSI] from PAni. As PAni contains polarons and bipolarons in its chain and [C_2mim][TFSI] contains cations and anions, some conductive channels inside the materials may create leading to more active sites. Insertion and de-insertion of Na^+ ions from electrolytic solution facilitates and C_s increases to a large extent. On the other hand, in [C_2mim][TFSI] incorporated PM1 composite, C_s is higher to some extent but upon increasing wt.% MnO_2 from PM2 to PM5 composites it decreases. This may be due to the blockage of some conductive channels inside the materials which help to lower C_s.

2.4. Conclusions

PAni interacts with MnO_2 in PAni-MnO_2 composites. The nature and strength of interactions vary depending on the loading of MnO_2 in the composites. The incorporation of [C_2mim][TFSI] in the composites enhances the thermal stability significantly and attains thermal stability higher than the individal compontes of the composites. PAni, PAni-MnO_2 and [C_2mim][TFSI] incorporated PAni and PAni-MnO_2 composites exhibit ideal capacitive behavior. C_s increases from PAni to PM5 composite (99 to 242 F g^{-1}) with current density of 0.10 F g^{-1}. C_s also increases in PAni upon incorporation of [C_2mim][TFSI]. But it decreases from PAni to PM5 (213 to 71 F g^{-1}) upon incorporation of [C_2mim][TFSI] at current density of 0.1 A g^{-1}. Thus, PAni, PAni-MnO_2 and [C_2mim][TFSI] incorporated PAni and PAni-MnO_2 composites show excellent electrochemical properties suitable for application in supercapacitors.

References

[1] J. Stejskal and R. G. Gilbert, *Polyaniline: preparation of a conducting polymer*, Pure Appl. Chem., 2002, 74, 857-867.

[2] S. Bhadra, N. K. Singha and D. Khastgir, *Electrochemical synthesis of polyaniline and its comparison with chemically synthesized polyaniline,* J. Appl. Polym. Sci., 2007, 104, 1900-1904.

[3] R. Ansari and M. B. Keivani, *Polyaniline conducting electroactive polymers: Thermal and environmental stability studies,* Eur. J. Chem., 2006, 3, 202-217.

[4] H. Eisazadeh, G. Spinks and G. G. Wallace, *Electrodeposition of polyaniline and polyaniline composites from colloidal dispersions,* Polym. Int., 1995, 37, 87-91.

[5] A.-N. Chowdhury, S. R. Jesmeen, M. M. Hossain, *Removal of dyes from water by conducting polymeric adsorbent,* Polym. Adv. Technol., 2004, 15, 633-638.

[6] A. M. P. Hussain, A Kumar, *Electrochemical synthesis and characterization of chloride doped polyaniline,* Bull. Mater. Sci., 2003, 26, 329-334.

[7] J. Huang, S. Virji, B. H. Weiller, R. B. Kaner, *Nanostructured Polyaniline Sensors,* Chem. Eur. J., 2004, 10, 1314 -1319.

[8] D. D. L. Chung, *Electromagnetic interference shielding effectiveness of carbon materials,* Carbon, 2001, 39, 279-285.

[9] J. Joo and A. J. Epstein, *Electromagnetic radiation shielding by intrinsically conducting polymers,* Appl. Phys. Lett., 1994, 65, 2278-2280.

[10] S. H. Kim, S. H. Jang, S. W. Byun, J. Y. Lee and J. S. Joo, *Electrical properties and EMI shielding characteristics of polypyrrole–nylon 6 composite fabrics,* J. Appl. Polym. Sci., 2003, 87, 1969-1974.

[11] Y. L. Yang, M. C. Gupta, K. L. Dudley, R. W. Lawrence., *Conductive carbon nanofiber-polymer foam structures,* Adv. Mater., 2005, 17, 1999-2003.

[12] N. Sarkar, M. K. Ram, A. Sarkar, R. Narizzano and S. Paddeu, *Nanoassemblies of sulfonated polyaniline multilayers,* Nanotechnology, 2000, 11, 30-36.

[13] W. Yang, J. Liu, R. Zheng, Z. Liu, Y. Dai, G. Chen, S. Ringer and F. Braet, *Ionic liquid-assisted synthesis of polyaniline/gold nanocomposite and its biocatalytic application,* Nanoscale Res. Lett., 2008, 3, 468-472.

[14] V. Gupta and N. Miura, *Electrochemically Deposited Polyaniline Nanowire's Network, A High-Performance Electrode Material for Redox Supercapacitor,* Electrochem. Solid-State Lett., 2005, 8, A630-A632.

[15] S. Mu, *Pronounced effect of the ionic liquid on the electrochromic property of the polyaniline film: Color changes in the wide wavelength range,* Electrochim. Acta, 2007, 52, 7827-7834.

[16] N. Bıc¸, B. Filiz, S. Enkal and E. Sezer, *Preparation of organo-soluble polyanilines in ionic liquid,* Synth. Met., 2005, 155 105-109.

[17] J. P. Saikia, S. Banerjee, B. K. Konwar and A. Kumar, *Biocompatible novel starch/polyaniline composites:Characterization, anti-cytotoxicity and antioxidant activity,* Colloids Surf. B: Biointerfaces, 2010, 81, 158-164.

[18] R. Asami, M. Atobe and T. Fuchigami, *Electropolymerization of an Immiscible Monomer in Aqueous Electrolytes Using Acoustic Emulsification*, J. Am. Chem. Soc., 2005, 127, 13160-13161.

[19] R. Asami, T. Fuchigami and M. Atobe, *Development of a Novel Environmentally Friendly Electropolymerization of Water-Insoluble Monomers in Aqueous Electrolytes Using Acoustic Emulsification,* Langmuir 2006, 22, 10258-10263.

[20] A.-N. Chowdhury, S. Ferdousi, M. M. Islam, T. Okajima and T. Ohsaka, *Arsenic Detection by Nanogold/Conducting-PolymerModified Glassy Carbon Electrodes*, J. App. Poly. Sci., 2007, 104, 1306-1311.

[21] Z. Hu, L. Zu, Y. Jiang, H. Lian, Y. Liu, Z. Li , F. Chen, X. Wang and X. Cui, *High specific capacitance of Polyaniline/Mesoporous manganese dioxide composite using KI-H_2SO_4 electrolyte,* Polymers, 2015, 7, 1939–1953.

[22] Q. Lu, M. W. Lattanzi, Y. Chen, X. Kou, W. Li, X. Fan, K. M. Unruh, J. G. Chen, and J. Q. Xiao, *Supercapacitor Electrodes with High-Energy and Power Densities Prepared from Monolithic NiO/Ni Nanocomposites,* Angew. Chem., 2011, 123, 6979 – 6982.

[23] P. B. Balbuena and K. E. Gubbins, *Theoretical Interpretation of Adsorption Behavior of Simple Fluids in Slit Pores,* Langmuir, 1993, 9, 1801-1814.

[24] J. Laska, J. Widlarz and E. Wozny, *Precipitation polymerization of aniline in the presence of water-soluble organic acids*, J. Polym. Sci.: Part A: Polymer Chemistry, 2002, 40, 3562-3569.

[25] R. C. Y. King, F. Roussel, J.-F. Brun and C. Gors, *Carbon nanotube-polyaniline nanohybrids: Influence of the carbon nanotube characteristics on the morphological, spectroscopic, electrical and thermoelectric properties,* Synth. Met., 2012, 162, 1348–1356.

[26] Jaidev, R. I. Jafri, A. K. Mishra and S. Ramaprabhu, *Polyaniline–MnO_2 nanotube hybrid nanocomposite as supercapacitor electrode material in acidic electrolyte*, J. Mater. Chem., 2011, 21, 17601-17605.

[27] L. Chen, L. J. Sun, F. Luan, Y. Liang, Y. Li, *Synthesis and pseudocapacitive studies of composite films of polyaniline and manganese oxide nanoparticles*, J. Power Sources, 2010, 195, 3742-3747.

[28] M. S. Islam, M. S. Miran, M. M. Rahman, M. Y. A. Mollah and M. A. B. H. Susan, *Polyaniline-silica composite materials: influence of silica content on the thermal and thermodynamic properties*, J. Nanostructured Polym. Nanocomposites, 2013, 9(3), 83-89.

[29] R. K. Sharma, A. Karakotic, S. Seala and L. Zhai, *Multiwall carbon nanotube-poly(4-styrenesulfonic acid) supported polypyrrole/manganese oxide nano-composites for high performance electrochemical electrode,* J. Power Sources, 2010, 195, 1256–1262.

[30] Y. Yu, B. Che, Z. Si, L. Li, W. Chen and G. Xue, *Carbon nanotube/polyaniline core-shell nanowires prepared by in situ inverse microemulsion, Synthetic Met.*, 2005, 150, 271–277.

[31] S. H. kazemi, B. Karimi, S. A. Aghdam and M. A. Kianic, *Polyaniline-Ionic liquid derived ordered mesoporous carbon nanocomposite: synthesis and its supercapacitive behavior,* RSC Adv., 2015, 5, 69032-69041.

[32] G. Han, Y. Liu, L. Zhang, E. Kan, S. Zhang, J. Tang and W. Tang, *MnO_2 Nanorods intercalating Graphene Oxide/Polyaniline ternary composites for robust high-performance supercapacitors,* Scientific Reports, Electronic Properties and Devices, Electronic Materials, 2014, 4, 1-7.

[33] H. Jiang, L. Yang, C. Li, C. Yan, P. S. Lee and J. Ma, *High–rate electrochemical capacitors from highly graphitic carbon–tipped manganese oxide/mesoporous carbon/manganese oxide hybrid nanowires,*Energy Environ. Sci., 201, 4, 1813-1819.

[34] J. Zhang, D. Shu, T. Zhang, H. Chen, H. Zhao, Y. Wang, Z. Sun, S. Tang, X. Fang and X. Cao, *Capacitive properties of PAni/MnO_2 synthesized via simultaneous-oxidation route,* J. Alloys and Comp., 2012, 532, 1-9.

[35] R. K. Sharma and L. Zhai, *Multiwall carbon nanotube supported poly(3,4-ethylenedioxythiophene)/manganese oxide nano-composite electrode for super-capacitors,* Electrochim. Acta, 2009, 54, 7148–7155.

[36] S. R. Sivakkumar, W. J. Kim, J-A. Choi, D. R. MacFarlane, M. Forsyth and D-W. Kim, *Electrochemical performance of polyaniline nanofibres and polyaniline/multi-walled carbon nanotube composite as an electrode material for aqueous redox supercapacitors,* J. Power Sources, 2007, 171, 1062–1068.

Abstract

PAni-NiO nanocomposites with varying amount NiO NPs were prepared by *in situ* chemical oxidative polymerization of aniline with ammonium peroxy disulfate using NiO NPs dispersed in aqueous acidic solution. PAni was also prepared using the same method without NiO for use as a reference material. The structure, size, morphology, band gap energy and thermal stability of the composites were studied in detail by using Fourier transform infrared spectroscopy (FT-IR), dynamic light scattering measurements (DLS), scanning electron microscopy, specular reflectance spectroscopy, and thermogravimetric analysis (TGA).The conductivity, dielectric constant and dielectric loss of PAni and PAni-NiO nanocomposites were also determined from electrochemical impedance spectroscopic data. The hydrodynamic diameter of NiO NPs determined from DLS measurements was *ca.* 178 nm. PAni and PAni-NiO nanocomposites showed same thermal degradation pattern but PAni-NiO exhibited greater thermal stability compared to PAni. The band gap energy *(E_g)* of PAni-NiO was found to decrease with increasing amount of NiO NPs. PAni and PAni-NiO composites were also prepared by oxidative polymerization of aniline in acidic solution by electrochemical method using cyclic voltammetry and chracterized. The specific capacitances of PAni and PAni-NiO composites perepared by electrochemical polymerization were found to be 233 F g^{-1} and 141 F g^{-1}, respectively using chronopotentiometric technique at a constant current density 0.25 F g^{-1}. PAni and PAni-NiO composites show potential for use as dielectrics and for applications in supercapacitors.

3.1. Introduction

The intrinsically conducting polymers are unique materials that have attracted significant interest for their interesting electrical, thermal, optical, magnetic, electrochemical and catalytic properties [1, 2]. By proper choice of inorganic filler materials, hybrid organic-inorganic composites can be formed. Amongst conducting polymers, polyaniline (PAni) is considered one of the most technologically important materials for its ease of preparation, environmental stability and special doping mechanism. Composites of PAni and inorganic NPs such as MnO_2, ZnO *etc.* have been reported to show special combiniatorial properties which could be difficult to attain separately with the individual components [3, 4].

PAni with TiO_2, SnO_2, Fe_3O_4, Co_3O_4, Al_2O_3,V_2O_5, and ZnO show synergistic advantages in transport properties of the polymer [5-15]. Inorganic metal oxide NPs including NiO play the major role in strengthening the proper of the nanocomposites since they offer large interfacial area per volume between the filler and the host polymer matrix. Thus, incorporation of NiO NPs into conducting polymer matrix

provide opportunities to enhance optical, electrical and catalytic properties associated with conventional composite materials through property synergism [16].

Conducting polymers and NiO NPs show dielectric properties which are reflected as the electric charge movement inside the material in response to an external electric field, contributing to the polarization and the phenomenon of dielectric relaxation, which is a frequency dependent process. The interaction of these materials with an electric field results in energy storage and energy loss [17, 18]. Polymer nanocomposites are light-weight and mechanically flexible that can preserve excellent dielectric and capacitive performance after extensive uses and can be used extensively in high-temperature electronics and energy storage devices [19]. Impedance spectroscopic study revealed that dielectric behavior of the nanocomposites is largely influenced by percentage composition of the components and charge transport properties through them. Bora *et al.* investigated electrical, electrochemical, magnetic properties of PAni-NiO nanocomposites [20]. Shambharkar *et al.* studied electrical and magnetic properties at room temperature and Nandapure *et al.* investigated transport and magnetic properties of PAni-NiO nanocomposites [21, 22]. However, the dielectric behavior of PAni-NiO nanocomposites has not so far been available in the literature.

Dielectric behavior of polymer composites depends on the applied frequency due to polarization effect that is influenced by orientation of direction against the applied electric field and composition of the materials under study. In this work, the PAni-NiO nanocomposites with varying amount of NiO NPs were prepared and the dielectric behavior was investigated by AC impedance spectroscopic method. The conductivity has been discussed with variation in frequency and wt.% of NiO NPs in the nanocomposites. The prospect of PAni-NiO composites, prepared by electrochemical polymerization, has also been examined for application as supercapacitor materials.

3.2. Experimental

3.2.1. Materials and Methods

All the chemicals used in our experiments were of analytical reagent grade and were used without further purification. Nickel(II)nitrate hexahydrate (Merck, India),

hydrochloric acid 37% AR (RCI Labscan, Thailand), sodium hydroxide (Merck, Germany), ammonium peroxydisulphate (Merck, India) were used as received without further purification. Aniline (Merck, India) was distilled under reduced pressure prior to use. All solutions were prepared and all experiments were carried out with de-ionized water (conductivity: 0.055 μScm^{-1} at 25.0 °C) from HPLC grade water purification systems (BOECO, BOE 8082060, Germany) throughout the experiments.

The optical absorption spectra for NiO NPs dispersed in ethanol were recorded using a double beam UV-visible spectrophotometer (UVD-3500, Labomed Inc., USA). Rectangular quartz cell of path length 1 cm was used throughout the investigation.

Fourier transform infrared (FT-IR) spectra were recorded using a Perkin Elmer FT-NIR/MIR spectrometer, (Frontier, USA) in the wavenumber range of 4000-400 cm^{-1} of 4 cm^{-1} resolution at transmittance mode. KBr mixed with PAni and PAni-NiO nanocomposite in the pellet form was used for recording FT-IR spectra.

Thermal properties were studied by thermogravimetry/differential thermal analizer, TG/DTA 7200 EXSTAR, Hitachi, Japan in the temperature range 30–550 ^oC at a heating rate of 10 $^oC\ min^{-1}$ at a flow rate of 10 mL min^{-1} in both nitrogen and air atmosphere. In air atmosphere the samples were held in isothermal condition at 550 ^oC for 1 h. In TGA the onset degradation temperature was obtained from the point of intersections of the two tangents drawn on the second inclination point of the TG curves.

Particle size and size distribution of the NiO NPs were measured by using a Zetasizer Nano ZS90 (ZEN3690, Malvern Instruments Ltd., UK) by dynamic light scattering (DLS) method. A He-Ne laser beam of wavelength 632.8 nm was used and the measurements were made at a fixed scattering angle of 90 ^oC. The calcined NiO NPs was dispersed in ethanol by sonication prior to measurement. The particle size detection limit was about 0.3 nm-5 μm (diameter) and accuracy of the average diameter determined has been ±2%. The temperature of the apparatus was controlled automatically within ±0.01K by a built-in Peltier device.

The morphological study was conducted using JEOL analytical SEM (model: JSM-6490LA, USA). The samples were dispersed in acetone and were taken on the carbon coated aluminum stubs for the measurements at an acceleration voltage of 20 kV.

Crystallinity of the sample and crystallite size of NiO NPs and PAni-NiO nanocomposites were determined by X-ray diffraction (XRD) technique. The powder XRD patterns were recorded using Rigaku Ultima IV, Japan diffractometer at 25 ^{o}C employing Cu Kα (λ= 0.15408 nm) radiation generated at 40 kV and 40 mA with a scan rate of 0.05^{o} s^{-1} from 5 to 90^{o}. The crystallite size of the NiO powders were approximated applying the Scherrer equation,

$$D = \frac{k\lambda}{\beta Cos\theta} \qquad (3.1)$$

where, D is the crystallite size for individual peak, k is the spherical shape factor taken as 0.89, λ is the X-ray wavelength, β is the full width at half maximum height (FWHM) of the respective peak measured in radians and θ is the XRD diffraction angle in degrees. the crystallite size of NiO NPs and PAni-NiO nanocomposites was determined. The average crystallite size was obtained from the (111), (200) and (220) peaks.

3.2.2. Specular Reflectance Spectroscopy

Specular reflectance spectra (disk type sample with thickness of 1 mm and area of 0.78 cm^2) were recorded using a double beam Shimadzu UV-visible spectrophotometer (UV-1800, Shimadzu, Japan) with an integrating sphere attachment DRA-CA-30I to determine the optical band gap energy (E_g) of the samples. According to the UV-vis spectra analysis (absorption or reflectance) as well as the type of transition band considered, directly or indirectly, the E_g value differs strongly depending on the method employed. Among the optical methods, UV-vis diffuse reflectance spectroscopy is one of the most employed techniques for the determination of the E_g for solid compounds or thin films. The E_g values were determined from the UV–vis diffuse reflectance spectra by using Kubelka–Munk (K-M or f (R)) method that offers great advantages in estimation of the E_g. The K–M method is based on the following equation.

$$f(R) = \frac{(1-R)^2}{2R} \qquad (3.2)$$

where R is the reflectance, f (R) is proportional to the extinction coefficient (α). This equation is usually applied to highly light scattering materials and absorbing particles in a matrix. A modified Kubelka-Munk function can be obtained by multiplying the

f (R) by hυ using the corresponding coefficient (n) associated with an electronic transition as follows:

$$[f(R)\times h\upsilon] = B(h\upsilon - E_g)^n \qquad (3.3)$$

For direct allowed transition n = ½ and B is an energy-independent constant.

By plotting the equation (3.2) as a function of the energy (E) in eV, the band gap of the samples can be obtained. The modified K-M function plotted $[f(R)\times h\upsilon]^2$ *versus* hυ. Such a representation is known as the Tauc method [23, 24]. The optical band gap was determined by extrapolating the linear portion of the plot to $(\alpha h\upsilon)^2 = 0$.

3.2.3. Electrochemical Impedance Spectroscopy

Electrochemical impedance spectroscopic (EIS) method was used to evaluate conductivity and dielectric behaviors of PAni and PAni-NiO nanocomposites and to explore their potential application as energy storage in dielectrics and supercapacitors. Different electric-dielectric phenomena can be analyzed because of the vast range of frequencies allowed by AC impedance spectroscopy.

The frequency dependent AC conductivity and dielectric permittivity of the chemically prepared PAni and PAni-NiO nanocomposites (disk type sample with thickness of 1 mm and area of 0.78 cm^2) were obtained using a computer-controlled precision impedance analyzer MAC80085, Metrohm Autolab B.V., Switzerland by applying an alternating electric field of amplitude 10 mV with DC potential of 0.20 V across the sample cell in the frequency region of 0.1 Hz to 32 MHz. A parallel plate configuration was used for all the electrical measurements. A high pressure (7.5 Ton) was applied to the solid sample to get hard round-shaped pellets (10.0 mm diameter, 1.0 mm thickness), which were used to measure the electrochemical impedance. The impedance data can be fitted by the response of equivalent model circuits whose elements can be associated with different charge transport behavior and gives their corresponding values within the materials.

The AC conductivity of PAni and PAni-NiO nanocomposites was determined from the impedance data using the following formula:

$$\sigma = \frac{1}{R}\times\frac{L}{A} \qquad (3.4)$$

where R is the resistance which is equivalent to value of real part of impedance, Z' and extracted from the equivalent circuits at high frequency, L is the thickness of the pellets of the sample ~1 mm, A is the surface area of pellets ~0.79 cm^2.

3.2.4. Cell and Electrodes Used for Electrochemical Measurements

A single compartment three-electrode glass cell was used for electrochemical preparation of PAni and PAni-NiO nanocomposites and various electrochemical measurements. A computer-controlled electrochemical analyzer (Model: 660E, CH Instruments, USA) with working electrode was employed for the electrochemical measurements. The schematic diagram of the instrumental setup of the computerized electrochemical analyzer system is shown in Figure 2.1 in chapter 2. The measurements were conducted by using a graphite electrode from Bioanalytical Systems (BAS, USA, surface area: surface area: 0.009 cm^2). A coiled platinum wire and an Ag/AgCl (Sat. KCl) electrode were used as the counter and reference electrodes, respectively.

Electrochemical polymerization of aniline was carried out for preparation of PAni and PAni-NiO composite using cyclic voltammetry and the performance was evaluated by cyclic voltammetry, chronopotentiometry and electrochemical impedance spectroscopy (EIS) using electrochemical analyzer, 660E, CH Instruments, USA.

The details of electrochemical cell have been described in section 2.2.3 of chapter 2.

The electrolyte used was 0.5 M aqueous H_2SO_4 solution. The potential scans were made from 0.0 to 1.00 V at 0.01, 0.02, 0.05 and 0.10 V s^{-1} for recording cyclic voltammetry, Chronopotentiometry or charge–discharge experiments was carried out at different constant current densities with voltages of 0.0 to 1.0 V. EIS measurements for the PAni-NiO nanocomposite modified electrodes were performed in an AC frequency range from 10^5 to 0.01 Hz with an excitation signal of 5 mV. All electrochemical experiments were carried out at ambient conditions. From the chronopotentiometric measurements or galvanostatic charge-discharge curves, the specific capacitance (C_s) of PAni and PAni-NiO modified electrodes can be determined as,

$$C_s = \frac{i \times \Delta t}{\Delta V \times m} \qquad (3.5)$$

where, C_s is the specific capacitance from discharge time of charge-discharge curves in F g^{-1}, i is the current in ampere, Δt is the discharge time in second and ΔV is the potential difference in volt.

3.2.5. Preparation of NiO NPs by Sol-Gel Method

NiO NPs were synthesized from $Ni(NO_3)_2.6H_2O$ and NaOH. Typically, 5.8162 g of $Ni(NO_3)_2.6H_2O$ was dissolved in 100 mL deionized water under continuous magnetic stirring at 25 ^oC for 30 min to ensure that Ni^{2+} ions were dispersed homogeneously in the solution. Then 50 mL NaOH solution (2.40 g) was added drop-wise into the solution containing Ni^{2+} ions. This reaction mixture was stirred constantly to obtain a homogeneous navy blue solution and subsequently transferred into a 500 mL beaker. The solution was then placed in a heater at 70 ºC for 1 h at atmospheric pressure under continuous stirring. A blue fluffy solid was formed indicating the completion of reaction. The product was separated from the solution by centrifugation and washed three-times with de-ionized water and ethanol, respectively. The products were dried under vacuum at 60 ºC for 12 h. The as-prepared products were calcined at 400 ºC for 2 h in a furnace. The resulting NiO NPs were then characterized and used for preparation of PAni-NiO nanocomposites.

3.2.6. Preparation of PAni-NiO Nanocomposites by Chemical Method

PAni-NiO nanocomposites with different weight percentages of NiO to aniline (5.28%, 17.40%, 24.52%, 49.04%) were prepared by *in situ* chemical oxidative polymerization. The preparation is schematically represented in Figure 3.2. 0.4 mL aniline was dissolved in 6.0 mL deionized water containing 0.4 mL hydrochloric acid. It was then sonicated for 30 min for homogeneous mixing and allowed to cool at 0-5 ^oC in an ice bath. Weighed amount of NiO was added in the beaker and kept in the sonication bath for another 30 min for proper dispersion to form a homogeneous mixture. 1.6 mL of 0.92 M ammonium peroxydisulfate as oxidizing agent was added drop wise for 30 min to the well dispersed suspension with continuous stirring for 30 min and kept for 2 h. The reaction mixture was allowed to stand for 12 h for complete polymerization of aniline to PAni. The resultant polymer composite was filtered, washed with de-ionized water several times followed by ethanol and acetone to remove impurities and low molecular weight oligomers. The blackish green precipitate of PAni-NiO nanocomposite was obtained and it was dried in an oven until it showed constant weight at 60 ^oC. Similarly, different wt.% of NiO NPs were added during the polymerization to get PAni-13 % NiO (PN1), PAni-33 % NiO (PN2),

PAni-41 % NiO (PN3) and PAni- 60 % NiO (PN4). PAni was prepared with the same procedure without the addition of NiO NPs.

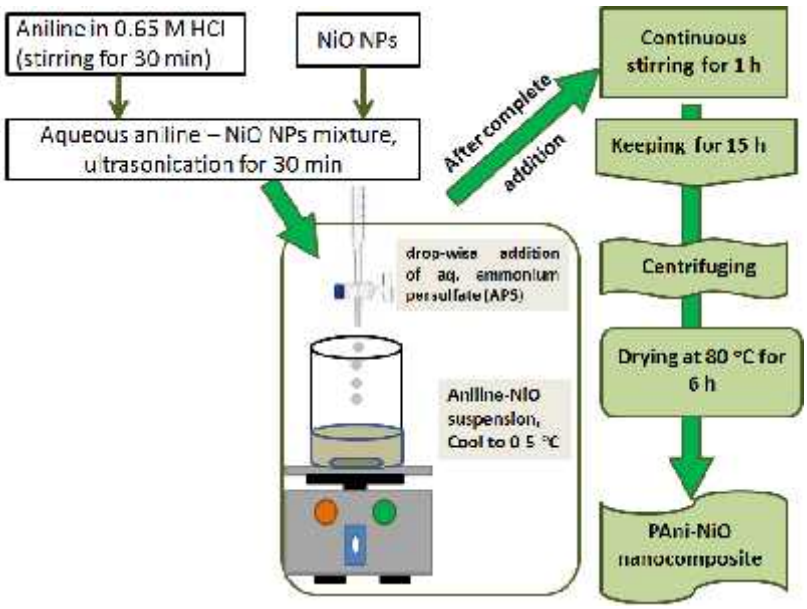

Figure 3.1. Schematic representation for preparation of PAni-NiO nanocomposites.

3.2.7. Electrochemical Preparations of PAni and PAni-NiO Composites

Polymerization of aniline was carried out on graphite electrode. 0.73 M aniline was dissolved in 0.65 M HCl solution. Polymerization was carried out by scanning the potential in the region of -0.2 to 1.2 V at the san rate of 0.05 V s^{-1}. Well adherent coating of PAni was obtained on graphite electrode. The resulting greenish black coating on graphite electrode substrate was washed with deionized water several times to remove impurities and ions originated from reaction medium. The graphite electrode modified with PAni was dried in an oven at 80 ^{o}C for 15 h. The PAni-NiO composite was formed by following the same procedure in the presence of 0.27 M Ni^{2+} in aqueous solution.

3.3. Results and Discussion

3.3.1. Dynamic Light Scattering Measurement

DLS measurement was used to obtain the average size (diameter) and size distribution of the solid particles dispersed in a suitable solvent. Hydrodynamic diameter of the particles distributed in ethanol is measured. Freshly prepared NiO particles was dispersed in ethanol and DLS measurement was recorded to obtain the average diameter of NiO NPs (Figure 3.2 (A)). The average diameter of NiO NPs was *ca.* 178 nm.

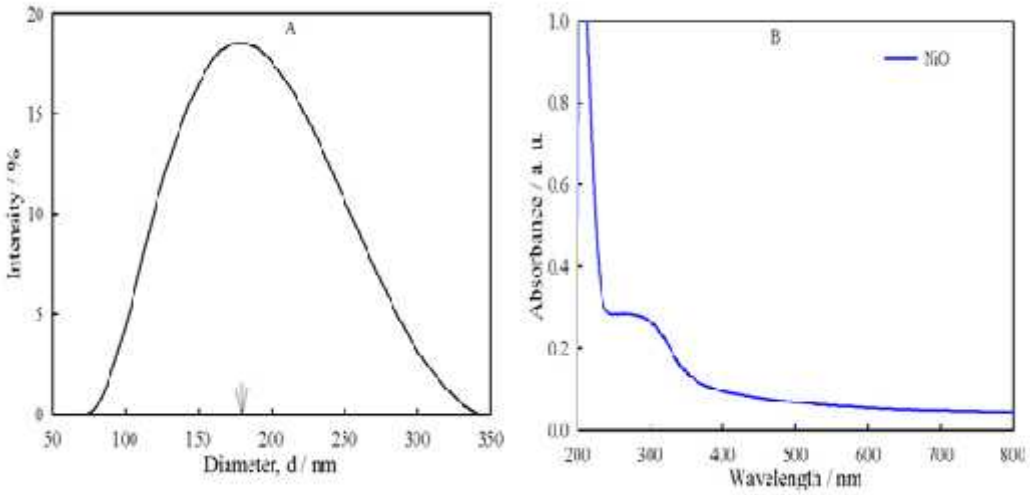

Figure 3.2. Particle size distribution (A) and UV-visible spectrum (B) of NiO NPs.

3.3.2. UV-visible Spectrum of NiO NPs

UV-visible absorption spectrum of the as-synthesized NiO NPs calcined at 400 ^{o}C and then dispersed in absolute ethanol by ultrasonication, was recorded (Figure 3.2 (B)). The broad absorption band in the UV region is observed at λ_{max} = 298 nm. This absorption in the UV region can be attributed to the electronic transition from the valence band to the conduction band in the NiO NPs [25].

3.3.3. Size and Morphology Analysis

Scanning Electron Microscopy (SEM)

The morphologies of the PAni and PAni-NiO nanocomposites were analyzed by SEM images as shown in Figure 3.3.

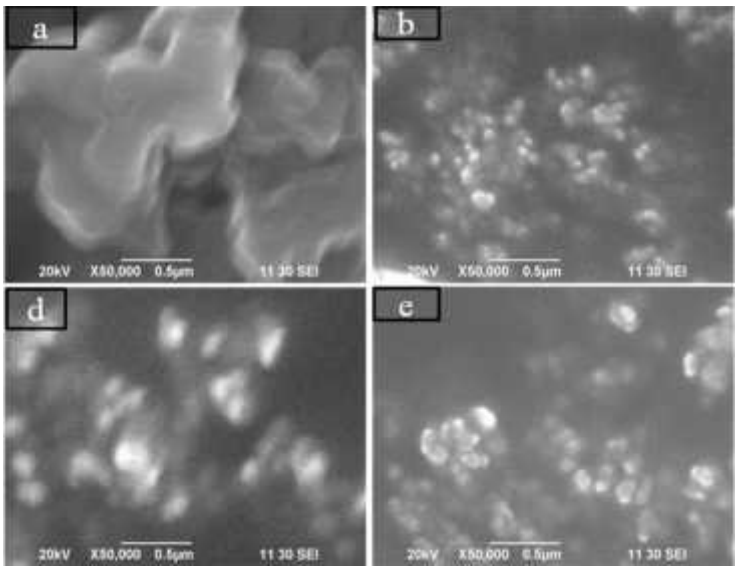

Figure 3.3. SEM images of (a) PAni, (b) PN2, (d) PN3 and (e) PN4.

PAni shows different morphology than those of PAni-NiO nanocomposites. PAni shows connected petals of a flower-like morphology whereas PAni-NiO nanocomposites display spherical bunch-like morphology. This morphological features become more prominent as the wt.% of NiO in the PAni matrix increases. PAni-NiO nanocomposites exhibit particle size (diameter) of about 100 nm.

3.3.4. FT-IR Spectral Analysis

FT-IR spectra were analyzed to identify the presence of stretching or bending vibrations in the synthesized PAni and PAni–NiO nanocomposites and hence to confirm formation of the materials. Figure 3.4 shows the FT-IR spectra of pristine PAni, pure NiO and the PAni-NiO nanocomposites with different NiO NP loading.

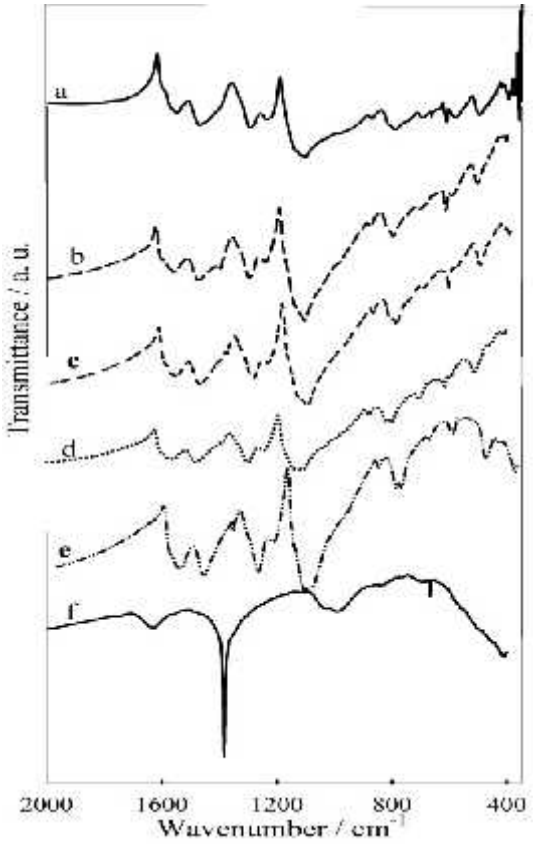

Figure 3.4. FT-IR spectra of (a) PAni, (b) PN1, (c) PN2, (d) PN3, (e) PN4 and (f) NiO NPs.

NiO NPs show Ni-O stretching vibration at 411 cm^{-1} [26]. Bands at 1386 cm^{-1} and 1621 cm^{-1} are attributed to -O-H bending vibrations of adsorbed water on NiO NPs [27]. Pristine PAni shows bands at 1560 cm^{-1}, 1477 cm^{-1}, 1298 cm^{-1}, 1243 cm^{-1}, 1112 cm^{-1} and 803 cm^{-1} corresponding to the C=C stretching mode of quinoid rings, the C= C stretching mode of the benzenoid rings, stretching mode of C–N, the stretching

mode of N=Q=N where Q represents the quinoid ring and C–H bending mode of aromatic rings, respectively [28]. The nanocomposites PN1 (PAni-13 % NiO) also shows the same characteristic bands. However, the corresponding band of pristine PAni at 1560 cm^{-1} shifted to 1573 cm^{-1}, 1477 cm^{-1} shifted to 1483 cm^{-1}, 1298 cm^{-1} shifted to 1312 cm^{-1}, 1243 cm^{-1} shifted to 1257 cm^{-1}, 1112 cm^{-1} shifted to 1119 cm^{-1}, 803 cm^{-1} shifted to 810 cm^{-1} in the PN1 nanocomposites. The similar kinds of shiftinghas been observed for all the prepared nanocomposites. This shift may be ascribed to the H-bonding interactions between the pendant –N-H groups of PAni chain and the O-atom on the surface of the NiO NPs. Such kind of interactions has also been observed by Paul *et al.* [29] in PAni-ZnO composites. Co-ordination bonds between lone pair of nitrogen atoms on the PAni chain and NiO NPs may also be possible for the shifting of bands to higher wavenumber for all of the PAni-NiO nanocompsites.

3.3.5. XRD Analysis

XRD pattern analyses were conducted to carry out phase analysis and to assess the crystalline nature of the synthesized samples. XRD patterns of the pristine PAni, NiO and PAni-NiO nanocomposites are shown in Figure 3.5.

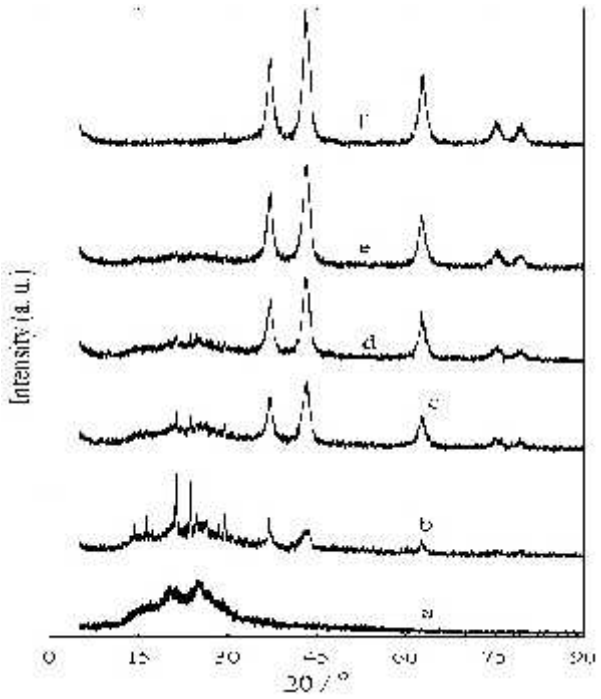

Figure 3.5. XRD patterns for (a) PAni, (b) PN1, (c) PN2, (d) PN3, (e) PN4 and (f) NiO NPs.

The XRD pattern of pristine PAni shows three broad peaks from 2θ ca. 15.6, 20.4 and 24.9º indicating semicrystalline morphology. The broad peaks observed at 20.4^{o} and 24.9^{o} are in agreement with those observed by Gemeay *et al.* [30]. The crystalline peaks at 2θ = 29.3°, 37·2°, 43·2°, 62·5°, 75·3°, 79·2° have been identified as peaks of single phase cubic structure of NiO with diffracting planes (111), (200), (220), (311), (222), respectively of the cubic phase of NiO which is also in agreement with JCPDS file no. 73-1523**.** The XRD pattern of PAni-NiO nanocomposites shows peaks related to both PAni and NiO indicating the presence of both components. However, in the case of PAni-NiO nanocomposites, the peaks become stronger with increased relative peak intensity which implies that the composite has a more ordered arrangement than pure PAni. The crystallite size of NiO NPs and PAni-NiO nanocomposites was determined using Equation (3.1). The most prominent sharp peak is at 24.9^{o} and the size of the crystallite of PAni has been evaluated as *ca.* 16 nm. The size of PAni-NiO nanocomposites has been in the order of 50-56 nm by using the most prominent peak at 43.2^{o}.

3.3.6. Thermogravimetric Analysis

TGA was employed to determine the degradation temperature, absorbed moisture content and composition of PAni and PAni-NiO nanocomposites. The thermal degradation behavior and temperature effect of the pure PAni and PAni-NiO nanocomposites were analyzed by TG measurements in Figure 3.7(A) under a controlled temperature program in N_2 atmosphere.

TGA curves of pure PAni and PAni-NiO nanocomposites undergo three-step weight loss or degradation pattern. Three-step weight loss was observed in PAni and all the PAni-NiO nanocomposites. The first step weight loss starting from 30 ^{o}C up to about 110 ^{o}C correspond to the loss of absorbed water, the second step loss from around 220 to 330^{o}C is associated with a loss of dopant ions from the polymer and low molecular weight oligomers and the third major weight loss from 350−550 ^{o}C is attributed to the degradation and decomposition of the polymeric backbone [31].

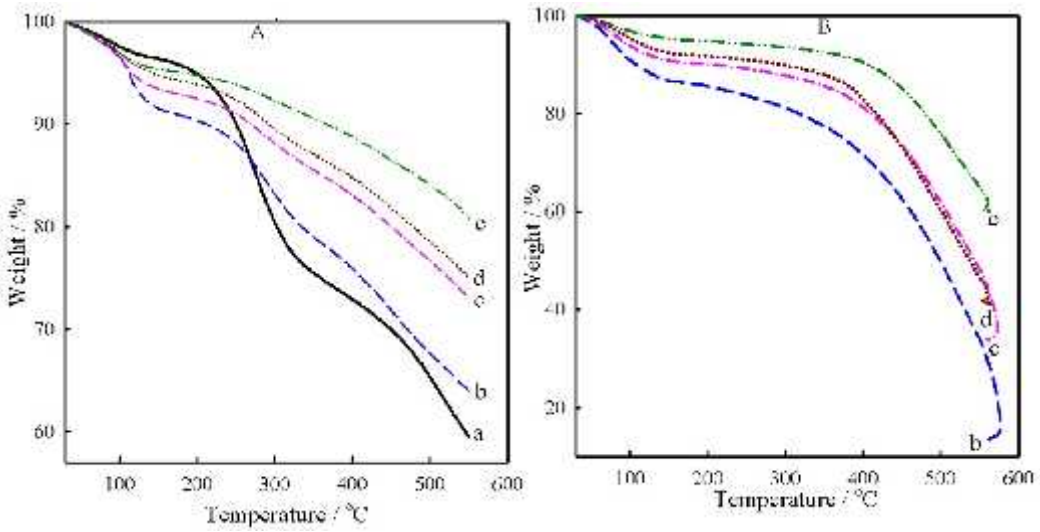

Figure 3.6. TGA curves of (a) PAni, (b) PN1, (c) PN2, (d) PN3 and (e) PN4 in N_2 atmosphere (A) and in O_2 atmosphere (B).

The TG curves of PAni and PAni-NiO nanocomposites with variation of wt.% NiO NPs at N_2 atmosphere are shown in Figure 3.6 (A). It is clearly seen that after the loss of moisture from the materials the first onset degradation temperature (t_{d1}) increases from 226 ^{o}C (PAni) to 245 ^{o}C (PN4 nanocomposite) which is due to the loss of dopant and low molecular weight oligomers from PAni to PN4. Second onset degradation temperature (t_{d2}) also varies from 425 to 453 ^{o}C and residual weight increases from 59 wt.% to 81 wt.% from PAni to PN4 nanocomposite. Moreover, degradation process occurs slowly from PAni to PN4 nanocomposite as clearly depicted from the TG curves. These factors altogether indicate that the thermal stability increases from PAni to all PAni-NiO nanocomposites (PN1 to PN4). The greater thermal stability of the nanocomposites may be due to the interaction between PAni and NiO NPs which hinders the all types of molecular motion of NiO NPs into the network of PAni chain which categorically restricts the thermal motion of PAni chain in the composite and enhance the thermal stability of the nanocomposites [32].

The TGA measurement was also carried out in air (O_2) atmosphere under isothermal condition at 550 ^{o}C for 1 h as shown in panel B in Figure 3.6. In this condition, PAni completely decomposes leaving no residue in the pan. Thus, from the residual weight of NiO the composition of PAni and NiO could be determined for all of the nanocomposites. The amount of NiO retained in different composites is summarized in Table 3.1. The highest weight loss was observed for PAni *ca.* 40%. However, NiO has shown very negligible weight loss in the scanned region.

Table 3.1. Compositions of the prepared PAni-NiO composites

Sample	Weight ratio (aniline : NiO) used during polymerization	NiO retained (% wt.)*
PAni	0.0 : 100	-
PN1	5.2 : 94.8	13
PN2	17.4 : 82.6	33
PN3	24.5 : 75.5	41
PN4	49.0 : 51.0	60

* Data were taken from TGA measurement under O_2 atmosphere

The amount of NiO retained in the composites increases as the amount of NiO NPs used was increased during the polymerization. The increase is in agreement with the feed ratio; although the residual amount differs silghtly differs from calculated amount.

3.3.7. Specular Reflectance Spectral Analysis

Specular reflectance spectra were recorded to characterize the PAni and PAni-NiO nanocomposites concerning their electronic properties. The spectra are shown in Figure 3.7.

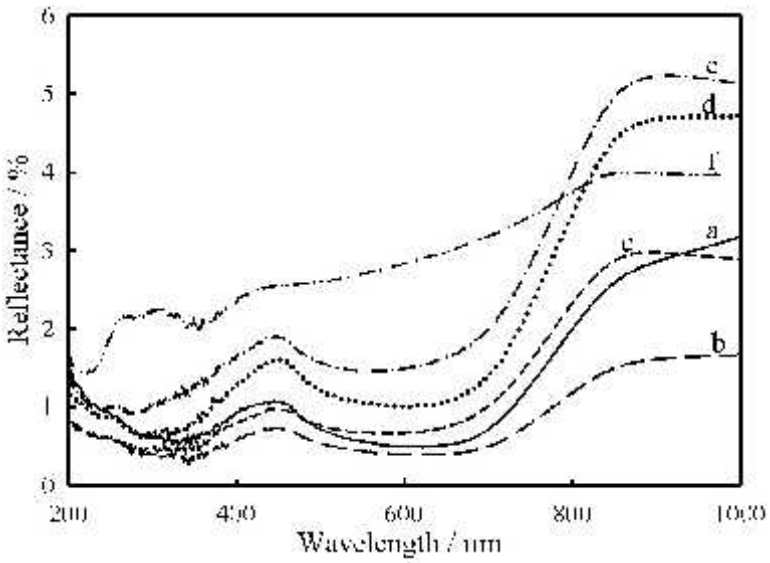

Figure 3.7. Specular reflectance spectra of (a) PAni , (b) PN1, (c) PN2, (d) PN3 (e) PN4 and (f) NiO NPs.

The spectra of PAni display the π-π* transition at 239 nm for benzenoid ring and polaron-π* transition at 447 nm for quinoid ring. These transitions may be interpreted as the doped state of PAni which exists in emaraldine salt form. The spectrum of PAni also show a band at 800 nm which extends to the near-infrared region. These

transitions may be observed due to a free carrier tail that implies protonated PAni is in expanded coil conformation [33]. The spectra of PAni-NiO nanocomposites show similar transitions with the shifting of bands of PAni, for example, the bands for π-π* and polaron-π* noticed at 239 and 447 nm in PAni shifted to 252 and 459 nm, respectively in PN1 nanocomposite. Similar results are observed for all of the PAni-NiO nanocomposites prepared by varying the amount of NiO. These results further support the formation of nanocomposite of PAni with NiO.

3.3.7.1. Determination of Band Gap Energy

The band gap energy of PAni is related to the different oxidation states. The UV-visible reflectance data showed electronic band structures that are linked to one of the oxidation states of PAni, *i.e.*, leucoemeraldine, emeraldine and pernigraniline [33]. The E_g of PAni and PAni-NiO nanocomposites was determined from the UV-vis specular reflectance spectroscopic data using Kubelka–Munk method using Equation 3.2. The approach for determination of band gap energy from specular reflectance spectra is shown in Figure 3.8. The values of E_g determined for PAni and PAni-NiO nanocomposites are summarized in Table 3.2.

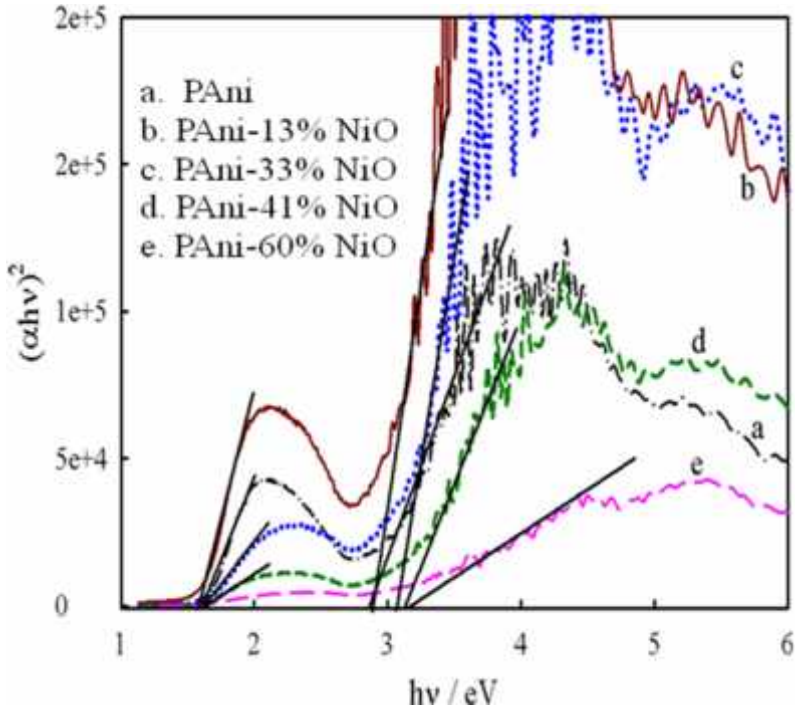

Figure 3.8. Band gap energy from specular reflectance spectra.

The PAni in the emeraldine salt form exhibits three characteristic bands at 239, 447 and above 800 nm. These three bands are attributed to π-π*, polaron-π* and π-polaron

band extending at the near infrared region, respectively as illustrated in Figure 3.7. PAni exhibits polaron-π* band at 2.82 eV corresponding to 447 nm and π-polaron band at 1.50 eV corresponding to ~800 nm [34]. From the Table 3.2 it can be observed that E_g decreases from PAni (2.93 eV) to PN1 (2.82 eV). Besides, E_{g2} is significantly decreased from 1.50 eV in PAni to 1.26 eV in PN1. This finding may be due to increment of number and movement of charge carriers upon incorporation of NiO in PAni of PN1. Similar decrease in E_{g2} values were noticed if the amount of NiO was increased in the composite (see Table 3.2). The adsorbed oxygen in the samples can cause more intense grain boundaries resulting in the chemisorption which results the conduction electrons trapped near the surface of the materials. Thus, transition of electrons from valence band to conduction band facilitates and band gap decreases [35]. This supports the observation of high conductivity of PN1. The decrease in conductivity in the order of PN1 > PN2 > PN3 > PN4 may be consistent since the intensity of the band at 447 nm of PAni, which corresponds to the number of charge carriers due to improvement of crystallinity of PAni-NiO composites, decreases with increasing NiO.

Table 3.2. AC conductivity and band gap energy (E_g) of PAni and PAni-NiO nanocomposites

Sample	Conductivity$\times 10^3$ σ (S cm^{-1})	Band gap E_{g1} (eV)	Band gap E_{g2} (eV)
PAni	0.08	2.93	1.50
PN1	5.6	2.82	1.26
PN2	2.3	2.88	1.02
PN3	2.2	2.84	0.99
PN4	1.1	2.58	0.74

3.3.8. Electrochemical Impedance Spectroscopy

The Nyquist plot derived from the impedance measurements of PAni and PAni-NiO nanocomposites are shown in Figure 3.9. Nyquist plot shows single semicircle in PAni and all PAni-NiO nanocomposites. All the semicircles do not coincide with the real (Z') impedance axis. This may be ascribed to the fact that the bulk resistance may predominate the grain boundary resistance, which is negligibly small [36]. These Nyquist plots were further analyzed to determine conductivity, dielectric properties and specific capacitance of the materials prepared. For determining the respective values, the equivalent circuits shown in Figure 3.10 were considered for simulating the experimental Nyquist plots.

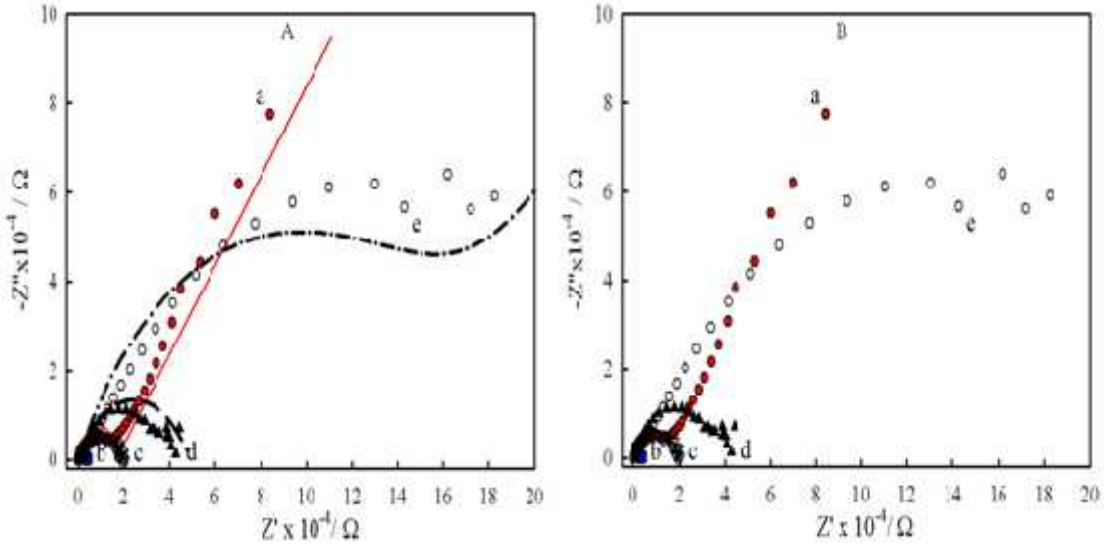

Figure 3.9. Complex impedance diagram (Nyquist plots) and corresponding fitting curves (A and B) (a) PAni, (b) PN1, (c) PN2, (d) PN3 and (e) PN4 at 25 ^{o}C.

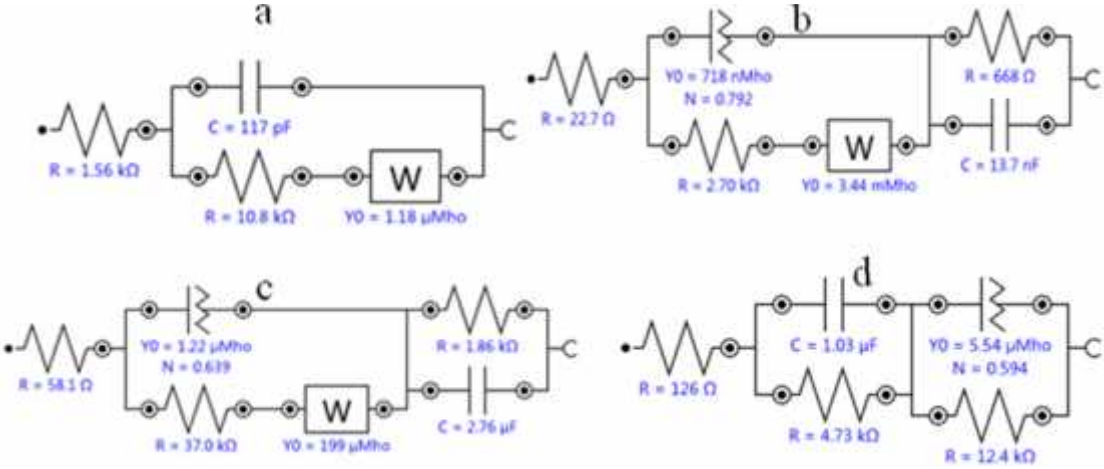

Figure 3.10. Equivalent circuit for (a) PAni, (b) PN1 (c) PN2 and (d) PN4.

3.3.8.1. AC Conductivity of PAni and PAni-NiO Nanocomposites

AC conductivity of PAni and PAni-NiO nanocomposites can be determined from values of real component of impedance (Z') according to equation (3.3) which are presented in Table 3.2. The frequency dependent AC electrical conductivity of PAni and PAni-NiO nanocomposites measured at 25 ^{o}C is shown in Figure 3.11. The AC electrical conductivity of PAni and PAni-NiO nanocomposites is almost constant up to 10^3 Hz and then it continues to increase at higher frequencies. This may be associated with the DC electrical conductivity which is attributed to electronic or ionic charge transport up to a certain frequency and then increases with increasing frequency which is due to AC electrical conductivity [37]. At low frequency up to 10^3

Hz, the dipoles and induced dipoles of PAni-NiO nanocomposites possibly get sufficient time to orient themselves with the applied electric field and thus DC conductivity predominates in the low frequency region. At high frequency range the dipoles or induced dipoles do not have sufficient time to orient themselves against the applied electric field and dispersion of dipoles reduces the extent of polarization and conductivity increases abruptly. Thus, AC electrical conductivity is the combined effect of low and high frequency of the electric field.

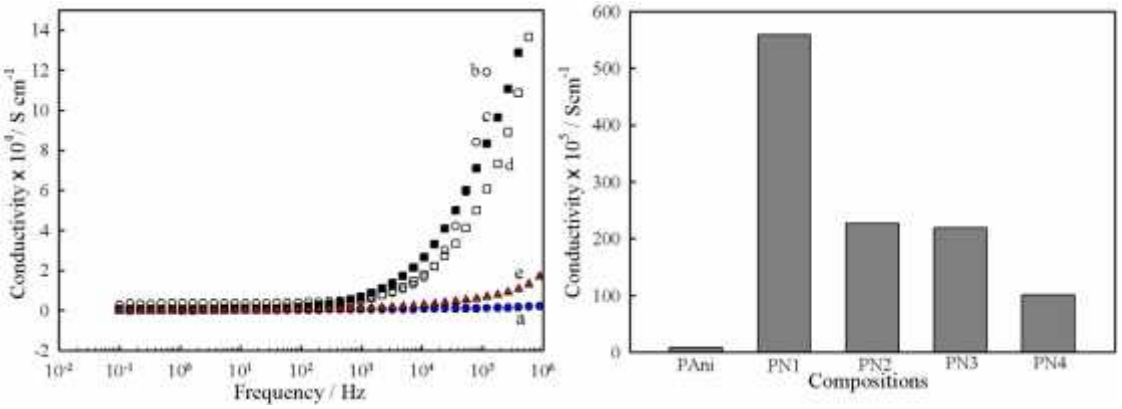

Figure 3.11. Frequency dependent AC conductivity of PAni and PAni-NiO nanocomposites (a) PAni, (b) PN1, (c) PN2, (d) PN3 and (d) PN4 (A), AC conductivity as a function of wt.% of NiO NPs (B).

The AC conductivity of PAni as shown in Figure 3.11 (B) is rather low. The conductivity was however found to abruptly increase by *ca.* 500 times due to the addition of NiO in the composite, PN1. Upon increasing the wt.% NiO in the composite, the conductivity decreased in the order of PN1 > PN2 > PN3 > PN4 (see Table 3.2). First observation might be due to the introduction of interconnected conductive network up through some sort of interactions between PAni chain and NiO NPs in PN1 that would help to augment up the conductivity significantly. The loading of NiO NPs may result in sufficient doping during polymerization through the formation of polaron and bipolarons in the backbone of polymer that creates more charge carriers leading to the higher conductivity than that of PAni. Further increase in NiO NPs may hinder the charge transport due to blockage of some channels among the different conjugated chains of PAni [38].

Alternatively, there might be some sort of interactions between PAni and NiO NPs leading to the decrease of the conjugated lengths in the PAni chains which in turn, may also result in conformational change of PAni structure [39]. This may add to the

lowering of electron transport favorable to the decrease in conductivity. However, the conductivity of all the PAni-NiO nanocomposites was higher than that of PAni.

3.3.8.2. Effect of wt.% NiO NPs on Dielectric Properties

The impedance data can be fitted to the responses of equivalent model circuits whose elements can be correlated with the properties associated with different electric and dielectric components. Figure 3.12 (A) shows the variation of dielectric constant (ε') with frequency for different wt.% of NiO in PAni-NiO nanocomposites at ambient temperature.

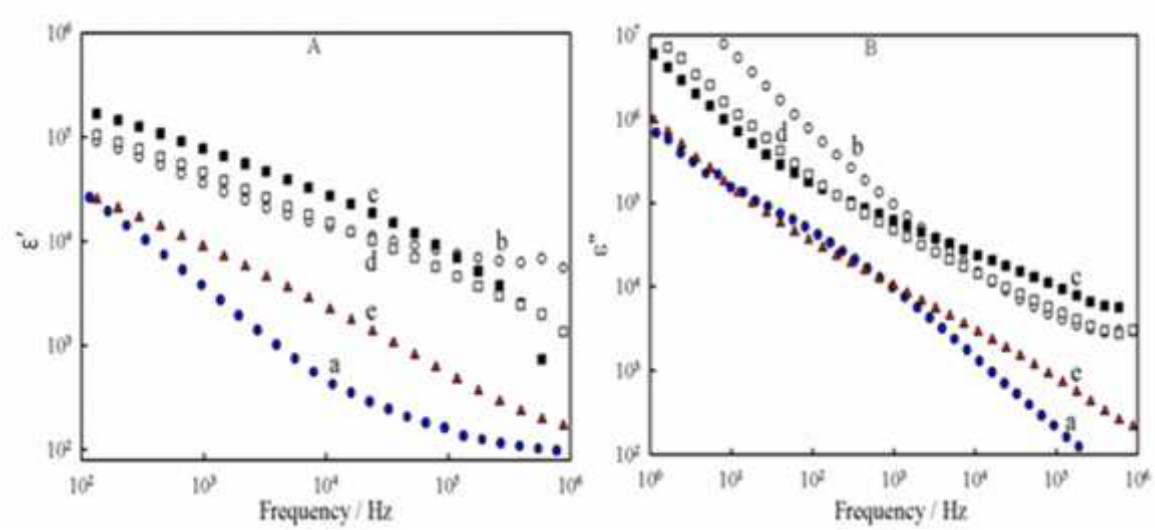

Figure 3.12. Real parts of the permittivity or dielectric constant (ε) (A) and imaginary part of permittivity or loss factor (ε") (B) of (a) PAni, (b) PN1, (c) PN2, (d) PN3 and (e) PN4.

The ε' decreases with increasing frequency. The decrease of ε' with increase in frequency may be attributed to the electrical relaxation processes. The addition of NiO at low wt.% may result in more localization of charge carriers along with polarons causing higher DC conductivity. This may be the reason for higher ε' and strong low frequency dispersion on addition of NiO in PAni [11, 12]. The value of the ε') is very high at lower frequencies and decreases with the increase of frequency. At lower frequencies the grain boundaries are more effective than grains in electrical conduction. It is well known that electric polarization decreases inside the media with the applied frequency. The decrease of polarization of the dielectric constant with increasing frequency is due to the fact that beyond certain frequency of the electric field, the polarons and bipolarons in the composites cannot follow the alternating electric field. An assembly of space charge carriers in a dielectric requires finite time to line up their axes parallel to an alternating electric field. If the frequency of the

field reversal increases, a point will reach when the space charge carriers cannot keep up with the field and the alternation of their direction lags behind the field. As the frequency of the field continues to increase, at some stage the space charge carriers will barely have started to move before the field reverses and make virtually no contribution to the polarization of the dielectric. Therefore, dielectric constant of a material may decrease substantially as the frequency is increased.

The dielectric loss factor (ε") as a function of frequency for all the compositions is depicted in Figure 3.12 (B). The dielectric loss profiles are similar to those of the prifiles for dielectric constant. The increase in hopping of charge carrier in polaron results in a local displacement in the direction of the extent electric field causing an increase in electric polarization which enhances dielectric loss [40].

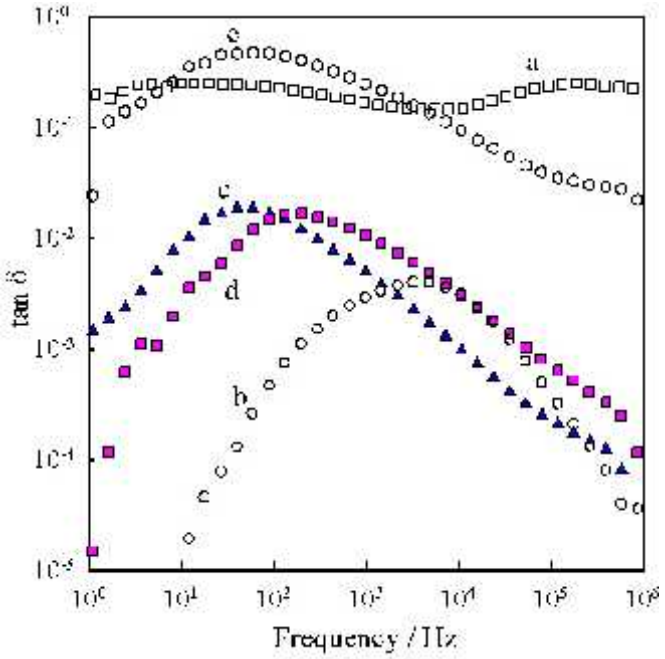

Figure 3.13. Loss factor (tanδ) of (a) PAni (b) PN1 (c) PN2 (d) PN3 and (d) PN4.

The dielectric loss tangent (tanδ) curves exhibit dielectric relaxation peaks which are attributed to the coincidence of the hopping frequency of the charge carriers with that of the external fields. Generally, the electrode processes relax at low frequencies, grain boundaries relax at intermediate frequencies and the relaxation due to the grains of the samples occurs at higher frequencies. The relaxation frequency of PAni is greater than 10^4 Hz which is typical for conducting PAni [41]. The relaxation frequency decreases as the wt.% of NiO NPs increases. This can be explained by the fact that NiO NPs may hinder the movement of polaron and bipolarons as charge

carriers of PAni chain in a certain extent so that they are reluctant to match with the operating frequency.

The loss tangent or tanδ is defined as the ratio of the imaginary part of the dielectric constant to the real part. The dielectric loss factor (tanδ) is shown in Figure 3.13. Large value of tanδ is observed at a minimum frequency, which is ascribed to the fact that at low frequency of the applied AC electric field the hopping between polarons and bipolarons predominates and the charge carriers follow the field and tanδ values reach maximum values [42]. Figure 3.14 (A), (B), (C) and (D) display real Z' and imaginary Z'' impedance spectra *vs.* frequency of PAni, PN1, PN3 and PN4 nanocomposites, respectively at around 25 ^{o}C. All spectra exhibit a single drop in impedance as the frequency increases. This is ascribed to the polarization relaxation, whose frequency range depends on PAni and composition of PAni-NiO nanocomposites . In PAni, the relaxation was observed above 10^4 Hz, which is typical of conducting PAni. In PAni-NiO nanocomposites the relaxation was observed below the corresponding frequency of PAni.

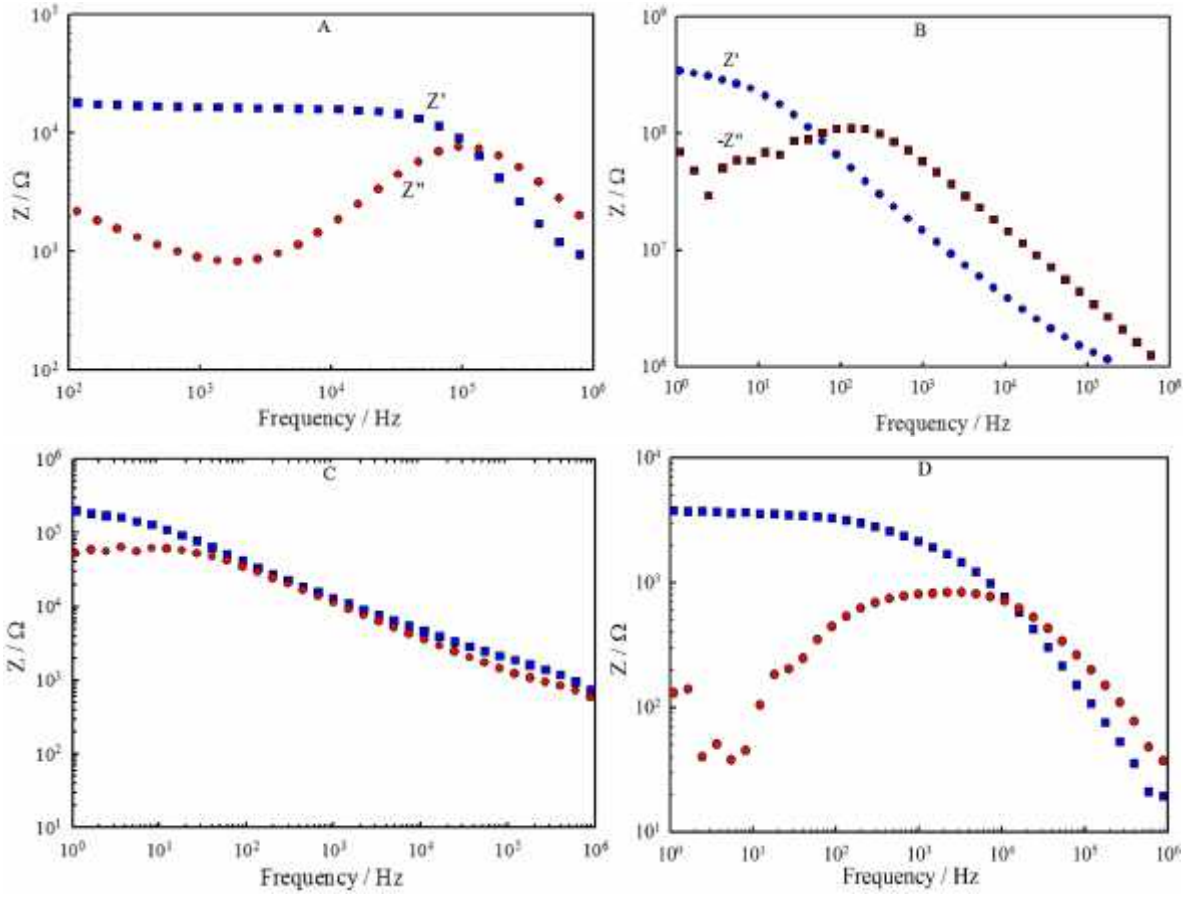

Figure 3.14. Impedance spectra of PAni (A), PN1 (B), PN3 (C) and PN4 (D).

3.3.9. Electrochemical Polymerization of PAni and PAni-NiO composites by Cyclic Voltammetry

Electrodeposition of PAni and PAni-NiO was carried out by cyclic voltammetric technique in the potential range of -0.2-1.2 V and -0.4-1.2 V, respectively, *versus* Ag/AgCl (Sat. KCl) as the reference electrode. Figure 3.15 shows the cyclic voltammograms recorded during the electrodeposition of PAni and PAni-NiO composites. Initially, an oxidation peak was noticed at around -0.10 V for PAni and the oxidation current appeared to be much smaller. This is due to anilinium radical cation in acidic medium. After first few cycles two new anodic peaks corresponding to the cathodic peaks (at 0.51 and 0.95 V) appear. This behavior may be an indication for the initiation of oxidative polymerization of aniline. The peaks at 0.18 V appeared for redox transitions from leucoemeraldine to conducting emeraldine form and the peaks at 0.51 V appeared for redox transitions from emeraldine to pernigraniline form indicating deposition of PAni successfully in the graphite electrode surface [43]. However, the current density increased gradually with successive scans indicating that deposition increased gradually leading to thicker deposit on the graphite electrode surface.

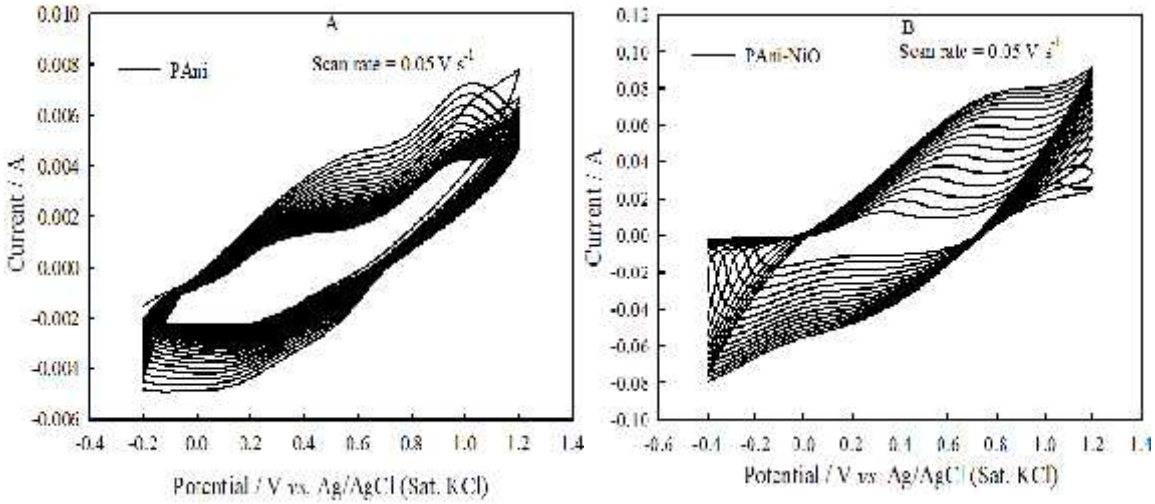

Figure 3.15. Cyclic voltammograms obtained for the electrocodeposition of PAni (A) and PAni-NiO composite (B) on graphite electrode at a scan rate is 0.05 V s^{-1}.

In case of Figure 3.15 (B) PAni-NiO composite shows different redox transitions from that of PAni. It can be seen that NiO was deposited initially and catalyzed the electrodeposition of PAni-NiO composite. Repeating cycle of the potential may result in a progressive increase of the charge included in both the cathodic and anodic peaks

of CV. Two redox peaks appeared at 0.51 and 0.95 V in the CV of PAni (Figure 3.15 (A)) are merged to a broad peak in the wide potential range of -0.40 – 1.20 V probably due to the incorporation of NiO particles in PAni deposited on graphite electrode surface.

After the electrodeposition of PAni and PAni-NiO composites, CVs were taken in 0.5 M H_2SO_4. The CV of PAni clearly show characteristic differences as seen in Figure 3.16 (A and B). In Figure 3.16 (A), the peak at higher scan rates showed the prominence in redox peaks of PAni whereas in case of PAni-NiO composites in Figure 3.16. (B) showed disappearance of redox peaks at the same scan rates which might be an indication of the deposition of PAni and NiO simultaneously. The peak current also increases in case of PAni-NiO composite compared to PAni at the same scan rates. However, in both the CVs oxidation peaks shifts to the +ve potential direction and correnponding redox peaks shift to the –ve potential direction. The peaks at 0.12 V appeared for redox transitions from leucoemeraldine to conducting emeraldine form and the peaks at 0.58 V appeared for redox transitions from emeraldine to pernigraniline form indicating deposition of PAni successfully in the graphite electrode surface.

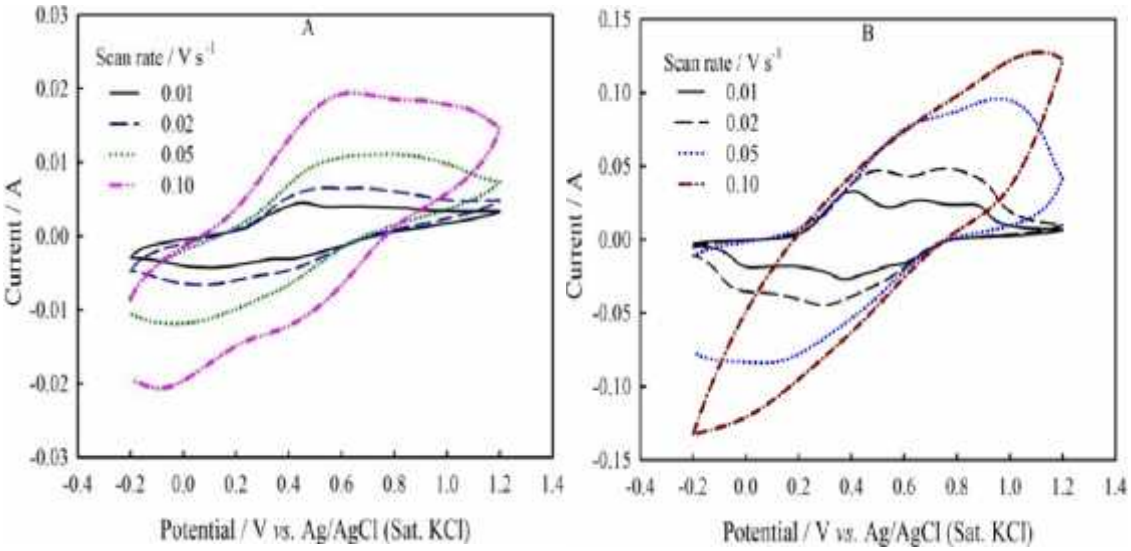

Figure 3.16. CVs for PAni (A) and PAni-NiO composite (B) in 0.5 M H_2SO_4 at different scan rates of 0.01 to 0.10 V s^{-1}.

3.3.9.1. FT-IR Spectra of Electrodeposited PAni and PAni-NiO Composites

FT-IR spectroscopy was employed in order to identify the presence of stretching or bending vibrations in the electrochemically synthesized PAni and PAni–NiO

nanocomposites and hence to confirm formation of the materials. The FT-IR spectra of PAni and PAni-NiO composites prepared electrochemically are shown in Figure 3.17. The absorption bands at 1592 and 1481 cm^{-1} are due to C = N stretching of quinonid and C = C stretching of benzenoid rings, respectively. These two bands for PAni and PAni-NiO composites were shifted to 1599 and 1472 cm^{-1} respectively. This may be attributed due to the H-bonding formation between O-atoms of NiO and H-atoms of pendant H-atom –N-H in the PAni chain. The bands of protonated PAni and PAni –NiO composites appeared at 1127 cm^{-1} and 1164 cm^{-1}, respectively indicating that PAni is in protonated forms in the acidic medium [44]. The band at 589 cm^{-1} can be assigned to -O-H group in hydrated nickel oxide [45].

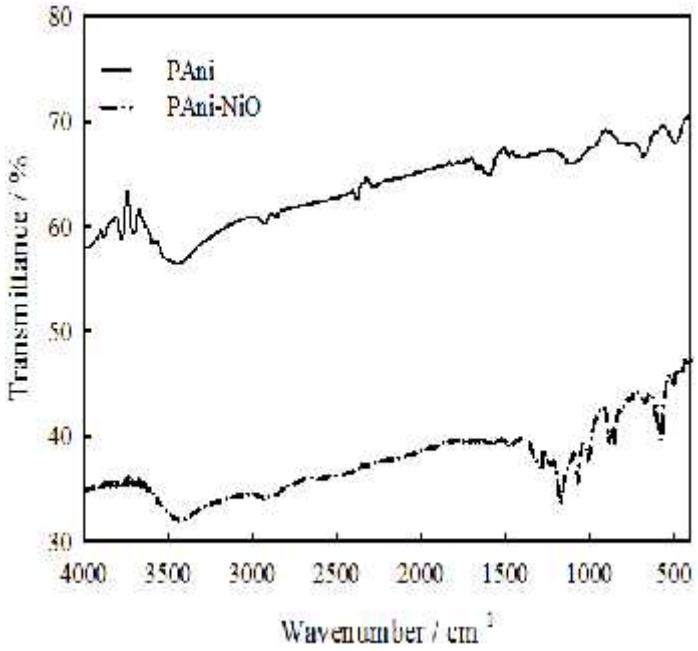

Figure 3.17. FT-IR spectra of electrochemically prepared PAni and PAni-NiO composite.

3.3.10. Chronopotentiometry Analysis

Figure 3.18. illustrates the typical charge–discharge behaviors of the PAni and PAni-NiO modified electrodes recorded in 0.5 M H_2SO_4 aqueous electrolytic solution at current densities 0.25 A g^{-1} to 1.00 A g^{-1}, respectively from (-0.20 to -1.20 V). For both electrodes there is a sharp decrease in voltage at the commencement of discharge. The sharp increase or decrease in voltage at the beginning of charge or discharge is attributed to the effect of internal resistance of the capacitor. The specific capacitance of both electrodes was determined from the chronopotentiometric data Using equation (3.6.A.). Specific capacitance of PAni (233 to 122 F g^{-1}) is higher than

that of PAni-NiO (141 to 89 F g^{-1}) at current densities from 0.25 to 1.00 A g^{-1} (Table 3.3). Specific capacitance of PAni-NiO decreases with incorporation of NiO into PAni which can be explained in the following section.

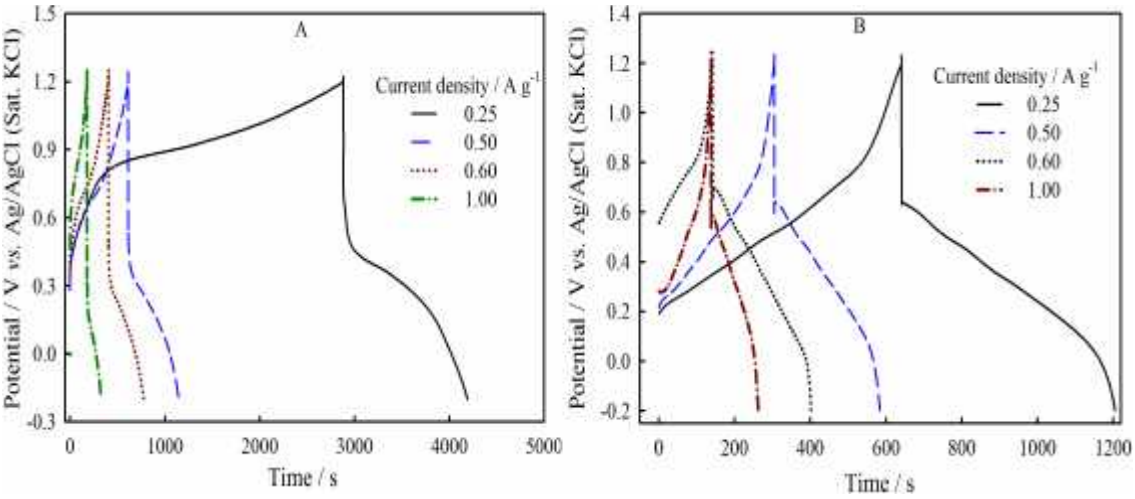

Figure 3.18. Galvanostatic charge-discharge curves of electrochemically prepared PAni (A) and PAni-NiO composite (B) in graphite electrode at current densities from 0.25 to 1.0 A g^{-1}.

Table 3.3. Specific capacitance of electrochemically prepared PAni and PAni-NiO composites

Material	Current density (A g^{-1})	Specific capacitance (F g^{-1})
PAni	0.25	233
	0.50	191
	0.60	162
	1.00	122

Material	Current density (A g^{-1})	Specific capacitance (F g^{-1})
PAni-NiO composite	0.25	141
	0.50	116
	0.60	111
	1.00	89

3.3.11. Electrochemical Impedance Spectroscopy of Electrochemically Prepared PAni and PAni-NiO Composites

Electrochemical impedance measurements were conducted to investigate mechanistic information and reactions occurring at the electrode surface. Electrochemical impedance measurements were performed under different AC potentials of the working electrode (PAni and PAni-NiO deposited electrodes) in an elecytrolytic medium of 0.5 M aquous H_2SO_4. The impedance data of the PAni and PAni-NiO deposited electrodes were recorded in the frequency range of 0.1 to 10^5 Hz with an AC oscillation of 5 mV.

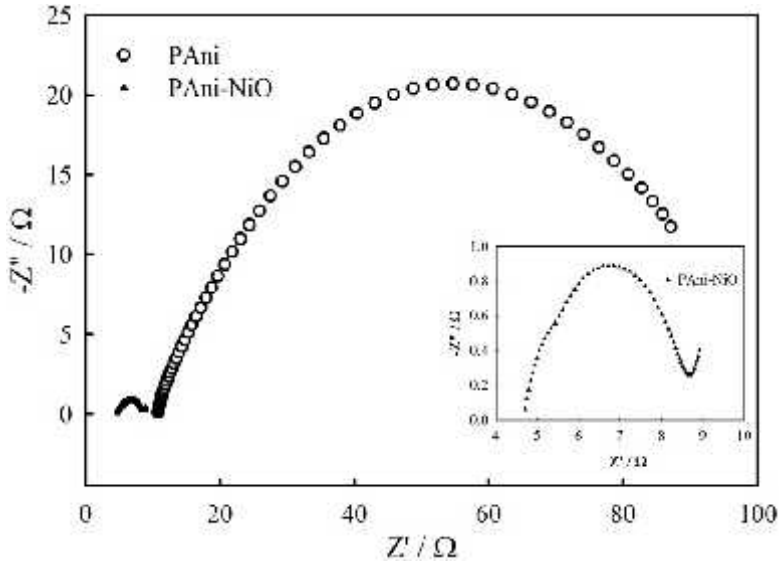

Figure 3.19. Nyquist plots of PAni and PAni-NiO composites at 0.6 V in 0.5 M H_2SO_4 (aq.) on graphite electrodes.

The frequency response analysis of the PAni and Pani-NiO composite deposits on graphite electrodes are shown in Figure 3.19. Both PAni and PAni-NiO composite produced a slightly tilted vertical line at low frequencies on the real axis (x-axis) on the complex impedance plot, a characteristic feature of capacitive behavior. Comparing these two, it is clear that the real component of the impedance of PAni-NiO composite is smaller than that of PAni. The difference can be explained by the fact that after incorporation of NiO particles into the PAni network the charge transfer resistance of the composites become smaller leading to higher conductivity of the composite.

3.3.12. Capacitive Properties of PAni and PAni-NiO Composites

Electrochemical capacitive behavior of PAni and PAni-NiO deposited graphite electrodes used as working electrodes *vs.* Ag/AgCl (Sat. KCl) electrode was studied in 0.5 M aqueous H_2SO_4 medium. From the cyclic voltammograms of PAni and PAni-NiO composites, it can be seen that redox reactions occur on the electrode showing the Faradaic nature or pseudocapacitance. It is evident from the literature that, Faradaic pseudocapacitance is almost 10-100 times larger than that of double layer capacitance. The specific capacitance of PAni and PAni-NiO composites was determined from the charge-discharge curves measured by chronopotentiomery using equation 3.5 which was presented in Table 3.3. It was revealed that specific capacitance of PAni-NiO composite (141 F g^{-1} at 0.25 F g^{-1}) is lower than that of

PAni (233 F g^{-1} at 0.25 F g^{-1}). There might be some reasons behind this finding. Film thickness could not be controlled during electropolymerizations of the materials. Higher thickness of films may lead to the lower specific capacitance in the same electrolytic medium. Morphology of as well as specific surface area of the materials may not be the same leading to anomaly of C_s. Scan rate variation renders different morphology as well as specific surface area of the electroactive materials [46]. Optimization and control during the weight measurement was very difficult because of the absorption of moisture by the electrodes and active materials may pose a problem.

3.3.13. Effect of NiO on Capacitive Properties of PAni-NiO Composites

PAni and PAni-NiO composites exhibit pseudocapitance behavior as evidenced by cyclic votammograms presented in Figure 3.16. Specific capacitance of PAni (233 F g^{-1} at 0.25 F g^{-1}) is higher than that of PAni-NiO (141 F g^{-1} at 0.25 F g^{-1}) composites. Incorporation of NiO into PAni network structure may lead to non-uniformity in the morphology of PAni-NiO composite. Thickness of the PAni-NiO composite during co-deposition may be higher despite same potential cycling of PAni deposition under the same experimental conditions. Different redox behavior of PAni and NiO may pose a problem during co-deposition of PAni-NiO composite arising thicker films than that of PAni. In that case, electrolytic ions may not be accessible into the deep pores or bulk of the composite materials leaving behind the unutilized materials and eventually specific capacitance decreases in the PAni-NiO composite. The decreasing tendency of specific capacitance with thicker films can be explained by the uneven potential distribution across the electrode for unutilization of active materials on the electrode [47]. However, the electrode thickness may be adusted in an efficient means to optimize of the electrochemical performance of the supercapacitor for advanced uses.

3.4. Conclusions

PAni and PAni–NiO nanocomposites could be successfully prepared by chemical oxidative and electrochemical polymerization methods. The thermal stability of the chemically prepared PAni-NiO nanocomposites was higher than that of PAni. The PAni-NiO nanocomposites with low wt.% of NiO NPs offer higher value of conductivity than PAni, but the conductivity decreases at high wt.% of NiO content.

The E_g decreases continuously up to the increased amount of loading of NiO NPs. The values of ε' and ε'' are also very low for the materials. ε' and ε'' of PAni and PAni-NiO nanocomposites may be favorable for application as a promising dielectric materials. The specific capacitances of electrochemically prepared PAni and PAni-NiO composite are as high as 233 F g^{-1} and 141 F g^{-1} at a constant current density of 0.25 F g^{-1} to make them favorable materials for supercapacitor applications.

References

[1] H. Liu, X. B. Hu, J. Y. Wang, and R. I. Boughton, *Structure, conductivity, and thermopower of crystalline polyaniline synthesized by the ultrasonic irradiation polymerization method,* Macromolecules, 2002, 35, 9414–9419.

[2] Y. Xian, Y. Hu, F. Liu, Y. Xian, H. Wang and L. Jin, *Glucose biosensor based on Au nanoparticles–conductive polyaniline nanocomposite,* Biosens. Bioelectron., 2006, 21, 1996–2000.

[3] D. C. Schnitzler, M. S. Meruvia, I. A. Hummelgen and A. J. G. Zarbin, *Preparation and characterization of novel hybrid materials formed from (Ti,Sn)O_2 nanoparticles and polyaniline*, Chem. Mater. 2003, 15, 4658-4665.

[4] A. Houdayer, R. Schneider, D. Billaud, J. Ghanbaja and J. Lambert, *New polyaniline/Ni(0) nanocomposites: Synthesis, characterization and evaluation of their catalytic activity in Heck couplings,* Synth. Met., 2005, 151, 165–174.

[5] S. Radhakrishnana, C. R. Sijua, D. Mahanta, S. Patil and G. Madras, *Conducting polyaniline–nano-TiO_2 composites for smart corrosion resistant coatings,* Electrochim. Acta, 2009, 54, 1249–1254.

[6] F. F. Fang, J. H. Sung and H. J. Choi, *Shear stress and dielectric characteristics of polyaniline/TiO_2 composite-based electrorheological fluid,* J. Macromol. Sci. Phys., 2006, 45, 923–927.

[7] F. F. Fang, J. H. Kim, H. J. Choi and Y. Seo, *Organic/inorganic hybrid of polyaniline/$BaTiO_3$ composites and their electrorheological and dielectric characteristics,* J. Appl. Polym. Sci., 2007, 105, 1853–1860.

[8] S. S. Umarea, B. H. Shambharkar and R. S. Ningthoujam, *Synthesis and characterization of polyaniline–Fe_3O_4 nanocomposite: Electrical conductivity, magnetic, electrochemical studies,* Synth. Met., 2010, 160, 1815–1820.

[9] G. Song, J. Bo and R. Guo, *Synthesis of the composite material of polyaniline/NiO/sodium dodecylbenzenesulfonate in micelles,*Colloid. Polym. Sci., 2005, 283, 677–680.

[10] Y. Qi, J. Zhang, S. Qiu, L. Sun, F. Xu, M. Zhu, L. Ouyang and D. Sun, *Thermal stability, decomposition and glass transition behavior of PANI/NiO composites,* J. Therm. Anal. Calorim., 2009, 98, 533–537.

[11] C. Yang, J. Du, Q. Peng, R. Qiao, W. Chen, C. Xu, Z. Shuai, and M. Gao, *Polyaniline/Fe_3O_4 Nanoparticle Composite: Synthesis and Reaction Mechanism,* J. Phys. Chem. B, 2009, 113, 5052–5058.

[12] J. Zhu, S. Wei, L. Zhang, Y. Mao, J. Ryu, A. B. Karki, D. P. Younge and Z. Guo, *Polyaniline-tungsten oxide metacomposites with tunable electronic properties,* J. Mater. Chem., 2011, 21, 342–348.

[13] P. K. Shen, H. T. Huang, 1 and A. C. C. Tseung, *A study of tungsten trioxide and polyaniline composite films I. electrochemical and electrochromic behavior,* J. Electrochem. Soc., 1992, 139, 1840–1845.

[14] C.-L. Zhu, S.-W. Chou, S.-F. He, W. Liao and C.-C. Chen, *Synthesis of core/shell metal oxide/polyaniline nanocomposites and hollow polyanilinecapsules,* Nanotechnology, 2007, 18, 275604–275610.

[15] K. Karthika, G. K. Selvana, M. Kanagaraj, S. Arumugam and N. V. Jaya, *Particle size effect on the magnetic properties of NiO nanoparticles prepared by a precipitation method,* J. Alloys Compd., 2011, 509, 181–184.

[16] A. G. MacDiarmid, *Synthetic metals: a novel role for organic polymers,* Synth. Met., 2002, 125, 11-22.

[17] S. Butkewitsch and J. Scheinbeim, *Dielectric properties of a hydrated sulfonated poly(styrene–ethylene/butylenes–styrene) triblock copolymer,* Appl. Surf. Sci., 2006, 252, 8277–8286.

[18] D. K. Pradhan, R. N. P. Choudhary and B. K. Samantaray, *Studies of dielectric relaxation and ac conductivity behavior of plasticized polymer nanocomposite electrolytes,* Int. J. Electrochem. Sci., 2008, 3, 597–608.

[19] Q. Li, L. Chen, M. R. Gadinski, S. Zhang, G. Zhang, H. Li, A. Haque, L.-Q. Chen, T. Jackson and Q. Wang, *Flexible high-temperature dielectric materials from polymer nanocomposites*, Nature, 523, 576–579.

[20] C. Bora, A. Kalita, D. Das, S. K. Doluia and P. K. Mukhopadhyay, *Preparation of polyaniline/nickel oxide nanocomposites by liquid/liquid interfacial polymerization and evaluation of their electrical, electrochemical and magnetic properties,* Polym. Int., 2013, 1-8.

[21] B. H. Shambharkar and S. S. Umare, *Synthesis and characterization of Polyaniline/NiO nanocomposite*, J. Appl. Polym. Sci., 2011, 122, 1905–1912.

[22] B. I. Nandapure, S. B. Kondawar, M.Y. Salunkhe and A. I. Nandapure, *Magnetic and transport properties of conducting polyaniline/nickel oxide nanocomposites,* Adv. Mat. Lett. 2013, 4, 134-140.

[23] J. Tauc, R. Grigorovici and A. Vancu, *Optical Properties and electronic structure of amorphous germanium*, Phys. Stat. Sol., 1966, 15, 627-637.

[24] S. Sakthivel, M. C. Hidalgo, D. W. Bahnemann, S.-U. Geissen, V. Murugesan and A. Vogelpohl, *A fine route to tune the photocatalytic activity of TiO_2,* Appl. Catal. B, 2006, 63, 31-40.

[25] J. Wang, L. Wei, L. Zhang, C. Jiang, E. S. Kong and Y. Zhang, *Preparation of high aspect ratio nickel oxide nanowires and their gas sensing devices with fast response and high sensitivity,* J. Mater. Chem., 2012, 22, 8327-8335.

[26] A. Kalam, A. S. Al-Shihri, M. Shakir, A. A. El-Bindary, E. S. S. Yousef, and G. Du, *Spherical NiO nanoparticles (SNPs): synthesis, characterization, and optical properties,* synthesis and reactivity in inorganic, metal-organic, and nano-metal chemistry, 2011, 41, 1324-1330.

[27] K. Anandan and V. Rajendran, *Morphological and size effects of NiO nanoparticles via solvothermal process and their optical properties*, Mater. Sci. Semicond. Process, 2011, 14, 43-47.

[28] B. K. Sharma, A. K. Gupta, N. Khare, S. K. Dhawan and H. C. Gupta, *Synthesis and characterization of polyaniline– ZnO composite and its dielectric behavior,* Synth. Met., 2009, 159, 391–395.

[29] G. K. Paul, A. Bhaumik, A. S. Patra and S. K. Bera, *Enhanced photo-electric response of ZnO/polyaniline layer-by-layer self-assembled films*, Mater. Chem. Phys. 2007, 106, 360–363.

[30] H. A. Gemeay, A. I. Mansour, G. R. El-Sharkawy and B. A. Zaki, *Preparation and characterization of polyaniline/manganese dioxide composites via oxidative polymerization: Effect of acid*s, Eur. Polym. J., 2005, 41, 2575-2583.

[31] S. S. Umare, B. H. Shambharkar and R. S. Ninghthoujam, *Synthesis and characterization of polyaniline–Fe_3O_4 nanocomposite: Electrical conductivity, magnetic, electrochemical studies*, Synth. Met., 2010, 160, 1815-1821.

[32] J. Deng, C. He, Y. Peng, J. Wang, X. Long, P. Li, and A. S. C. Chan, *Magnetic and conductive Fe3O4–polyaniline nanoparticles with core–shell structure,* Synth. Met., 2003, 139, 295–301.

[33] J. Laska, *Conformations of polyaniline in polymer blends,* J. Mol. Struct., 2004, 701, 13–18.

[34] Y. Xia, J. M. Wiesinger, A. G. MacDiarmid and A. J. Epstein, *Camphorsulfonic acid fully doped polyaniline emeraldine salt: conformations in different solvents studied by an ultraviolet/visible/Near-Infrared spectroscopic method,* Chem. Mater. 1995, 7, 443-445.

[35] M. O. Ztas and A. N. Yazici, *The effect of pre-irradiation heat treatment on TL glow curves of ZnS thin film deposited by spray pyrolysis method,* J. Lumin., 2004, 110, 31–37.

[36] F. S. H. Abu-Samaha and M. I. M.Ismail, *AC conductivity of nanoparticles $Co_xFe(1-x)Fe_2O_4$ (x = 0, 0.25 and 1) ferrites,* Mater. Sci. Semicond. Process., 2014, 19, 50–56.

[37] S. Maiti and B. B. Khatua, *Electrochemical and electrical performances of cobalt chloride ($CoCl_2$) doped polyaniline (PANI)/graphene nanoplate (GNP) composite, RSC Adv.*, 2013, 3, 12874-12885.

[38] A. L. Khan and M. Khalid*, Synthesis of nano-sized ZnO and polyaniline-zinc oxide composite: characterization, stability in terms of DC electrical conductivity retention and application in ammonia vapor detection,* J. Appl. Polym. Sci., 2010, 117, 1601–1607.

[39] S.-J. Su and N. Kuramoto, *Processable polyaniline–titanium dioxide nanocomposites: effect of titanium dioxide on the conductivity*, Synth. Met., 2000, 114, 147–153.

[40] I. H. Gul and A. Maqsood, Structural, magnetic and electrical properties of cobalt ferrites prepared by the sol–gel route, J. Alloys Compd., 2008, 465, 227–231.

[41] G. B. Alcantara, L. G. Paterno, F. J. Fonseca, M. A. Pereira-da-Silva, P. C. Morais and M. A. G. Soler, *Dielectric properties of cobalt ferrite nanoparticles in ultrathin nanocomposite films,* Phys. Chem. Chem. Phys., 2013, 15, 19853-19861.

[42] M. L. Dinesha, G. D. Prasanna, C. S. Naveen and H. S. Jayanna, *Structural and dielectric properties of Fe doped ZnO nanoparticles*, Indian J. Phys., 2013, 87, 147–153.

[43] D.-W. Wang, F. Li, J. Zhao, W. Ren, Z.-G. Chen, J. Tan, Z.-S. Wu, I. Gentle, G. Q. Lu, and H.-M. Cheng, *Fabrication of Graphene/Polyaniline composite paper via in situ anodic electropolymerization for high performance flexible electrode*, *ACS Nano*, 2009, *3*, 1745–1752.

[44] X. X. Liu, L. Zhang, Y. B. Li, L. J Bian, Z. Su and L. J. Zhang, *Electropolymerization of aniline in aqueous solutions at pH 2 to 12,* J. Mater Sci. 2005, 40, 4511-4515.

[45] M. A. Ermakova and D. Y. Ermakov, *High-loaded nickel–silica catalysts for hydrogenation, prepared by sol–gel: Route: structure and catalytic behavior,* Appl. Catal. A, 2003, 245, 277-288.

[46] G. K. S. Prakash, P. Suresh, F. Viva and G. A. Olah, *Novel single step electrochemical route to γ-MnO_2 nanoparticle-coated polyaniline nanofibers: Thermal stability and formic acid oxidation on the resulting nanocomposites,* J. Power Sources, 2008, 181, 79–84.

[47] Y. Yin, C. Liu and S. Fan, *Well-constructed CNT Mesh/PANI nanoporous electrode and its thickness effect on the supercapacitor properties,* J. Phys. Chem. C, 2012, 116, 26185−26189.

Abstract

PVA-MnO_2 nanocomposites with different amount of MnO_2 NPs were prepared by introducing preformed MnO_2 NPs in aqueous solution of a non-conducting polymer, PVA. The PVA-MnO_2 nanocomposite films were then prepared by solution casting. The morphology, structure, and thermal stability of the nanocomposites were characterized by SEM, DLS, specular reflectance spectroscopy, FT-IR, XRD and TGA techniques. Composite formation with MnO_2 NPs was revealed from FT-IR spectra in which the bands of -O-H and C=O vibrations of PVA were found to shift and the bands were observed to be less intense. Thermal behavior of PVA-MnO_2 nanocomposite films changes with variation of MnO_2 NPs loading. A complete shielding of UV radiation was found to take place in PVA-MnO_2 nanocomposite films containing greater than 1.0 wt.% of MnO_2 NPs. Supercapacitive performance of PVA-MnO_2 nanocomposites modified graphite electrode with incorporation of an ionic liquid, $[C_2mim][BF_4]$, in 0.5 M aqueous Na_2SO_4 solution was also investigated. PVA-MnO_2 nanocomposite films with greater than 1.0 wt.% MnO_2 could be used as a UV-shielding material in electronic and electrochemical devices. The specific capacitance of PVA-MnO_2 and PVA-MnO_2 nanocomposites incorporated with $[C_2mim][BF_4]$ had prospect for application in supercapacitors.

4.1. Introduction

The development of low-cost, biodegradable and easily processable polymer composites as materials for UV-shielding and electrochemical capacitors is a challenging research task. Polymers as stabilizers prevent agglomeration and precipitation of the reinforcing particles during preparation of nanocomposites [1]. Therefore, polymer nanocomposites have promise as barrier material for electronic devices and as high performance supercapacitor materials. PVA, a non-conducting polymer, has been widely used as a matrix phase for preparing polymer nanocomposites due to its easy processability, non-toxicity for water solubility and high transmittance in film form [2]. PVA films also exhibit excellent oxygen barrier properties (at low relative humidity) [4] and are also a potential material for encapsulation of solar cells [5]. Thermal, mechanical and surface analysis as well as permeability studies has been employed to characterize the PVA-based composite films for their possible application as passivation materials [6].

MnO_2 NPs, on the other hand, are one of the fascinating materials for optical, electronics and catalytic applications. They are non-toxic, low-cost and chemically stabile towards air. They possess outstanding chemical and physical properties suitable for molecular sieves, catalysts, batteries [7], sensors [8], and electrochemical

supercapacitors [9]. PVA has excellent film forming ability and is a promising matrix material due to hydrogen bonding in its surface with MnO_2 NPs [10]. PVA based composites such as, PVA-clay nanocomposites have already been used for the encapsulation of organic solar cells [3]. PVA-reduced graphene oxide, PVA-TiO_2, and PVA-SiO_2 have been used as highly conductive materials for fuel cell application and waste water treatment, respectively. Polymer based composites such as, ZnO-epoxy, acrylic resin-TiO_2, poly(methyl methacrylate) (PMMA)-ZnO, PVA-ZnO have been reported as UV-shielding materials.

PVA-MnO_2 nanocomposite films, in fact, not only eliminate aggregation of MnO_2 NPs but also ensure the compatibility between inorganic MnO_2 NPs and organic PVA matrix. PVA-MnO_2 nanocomposite films have thus been considered for improved performance resulting from synergistic effect of PVA and MnO_2. To the best of our knowledge, it is the first report on PVA-MnO_2 nanocomposite films as UV-shielding material. In addition, the reports on the use of PVA film as supercapacitor material is very rare because of very low capacitance (5.20 nF cm^{-2}) of non-conducting polymer, PVA.

The present work describes the preparation of flexible PVA-MnO_2 nanocomposite films by simple solution casting technique using PVA as the base polymer matrix and MnO_2 NPs as the dispersed phase. The morphology, structure and thermal stability of the nanocomposites were characterized. The shielding of UV with PVA-MnO_2 nanocomposite film was investigated. Supercapacitive performance of PVA-MnO_2 nanocomposite with incorporation of a hydrophilic ionic liquid, [C_2mim][BF_4] in 0.5 M aqueous Na_2SO_4 solution was evaluated by analyzing the specific capacitance.The ultimate goal has been to find the prospect of PVA-MnO_2 nanocomposites as materials for UV-shielding and supercapacitors.

4.2. Experimental

4.2.1. Materials and Methods

All the chemicals used were of analytical grade. PVA (MW 30000, Merck, Germany), potassium permanganate (Merck, India), sodium thiosulfate-5-hydrate (Merck, India) and [C_2mim][BF4] (Sigma-Aldrich, USA) were used as received without any further purifications. All solutions were prepared with deionized water (BOECO, BOE

8082060, Germany). De-ionized water (conductivity: 0.055 μS cm^{-1} at 25.0 °C) from HPLC grade water purification systems (BOECO, Germany) was used throughout the experiments. The optical absorption spectra for PVA and PVA-MnO_2 solution before casting of films were recorded using a double beam Shimadzu UV-Visible spectrophotometer, model UV-1650 PC. Rectangular quartz cells of path length 1 cm were used throughout the investigation. Average particle size and size distribution was measured using Malvern Zetasizer Nano ZS90 with a scattering angle of 90^o. A He-Ne laser beam of 632.8 nm wavelength was used for the measurements. The average diameters were determined from cumulants mean of the intensity average of 50 runs using Stokes–Einstein equation, $R_h = K_B T / 6\pi\eta D_{eff}$, where R_h is the hydrodynamic radius, K_B, the Boltzmann constant, T, the temperature, η, the solvent viscosity, and D_{eff}, the diffusion coefficient. The reproducibility was checked from at least 3 measurements. The temperature of the apparatus was controlled automatically within ±0.01K by a built-in Peltier device.

After casting the films, the specular reflectance spectra and transmission spectra of the samples were recorded on a Shimadzu UV spectrophotometer, model UV-1800. The FTIR spectra were recorded using a Perkin Elmer FT-IR/NIR spectrometer (Frontier) in the spectral range from 4000 to 400 cm^{-1}. The morphological study was performed using JEOL analytical scanning electron microscope, model JSM-6490LA. The films were taken on the carbon coated aluminum stubs for the measurements at an acceleration voltage of 20 kV. Phase analysis and chemical characterization of the samples were carried out using x-ray diffractometer (Philips PW 1724) with x-ray generator using XDC-700 Guinier-Hagg focusing camera with strictly monochromatized Cu Kα radiation (λ=1.540598). Thermal properties were studied by a Hitachi instrument (TG/DTA 7200) in the temperature range of 30–550 ^oC in isothermal condition holding the samples at 550 ^oC for 30 min at a heating rate of 10 $^oC\ min^{-1}$ under nitrogen atmosphere.

Electrochemical characterization of the graphite electrodes fabricated with PVA, PVA-MnO_2 and $[C_2mim][BF_4]$ incorporated PVA-MnO_2 nanocomposites were performed using cyclic voltammetry, chronopotentiometric and electrochemical impedance spectroscopic (EIS) measurements using (CHI 760E) electrochemical workstation. A coiled platinum wire and a saturated Ag/AgCl (Sat. KCl) electrode

were used as counter and reference electrodes, respectively. All the CVs were measured between 0.0 and 1.0 V (*i.e.* operating window of 1.0 V) with respect to the reference electrode at different scan rates (0.01-0.10 V s^{-1}) in 0.5 M aqueous Na_2SO_4 solution. The details about the electrochemical set-up have been described in Section 2.2.3 of Chapter 2.

4.2.2. Synthesis of MnO_2 NPs and PVA-MnO_2 Nanocomposite Films

4.2.2.1. Synthesis of MnO_2 nanoparticles (NPs): In a typical synthesis, 0.0017 g of $KMnO_4$ was dissolved in 10 mL of deionized water and the mixture was sonicated for 30 min. 0.0017 g of sodium thiosulphate was dissolved in 10 mL of deionized water and then it was added drop-wise to the permanganate solution at around 25 °C. The color of the solution changed rapidly from purple to yellow-brown indicating the onset of the formation of MnO_2 NPs and finally appeared dark brown and visibly transparent. Thus, MnO_2 NPs in solution phase was prepared and used for the preparation PVA-MnO_2 nanocomposite films.

4.2.2.2. Preparation of PVA–MnO_2 nanocomposite films: Pristine PVA and PVA-MnO_2 nanocomposite films were prepared by a solution-casting technique. To prepare composite films, 2% (w/w) solution of PVA was prepared in deionized water. The PVA was slowly added to water at 80 °C with continuous stirring for 2 h and subsequently it was cooled down to 25 °C without stirring. PVA-MnO_2 nanocomposite consisting of 0.5, 1.0, 1.5, 2.0 and 4.0 wt.% of MnO_2 NPs in solution was then prepared. Preformed MnO_2 NPs in solution was added drop-wise to the prepared PVA solution with continuous stirring. This solution was placed in magnetic stirrer and heated to 80 °C for volume reduction to a specific value. Then 2.0 mL of above solution was casted in plastic petri dish and kept in oven at 50 °C for 24 h and finally peeled off carefully for characterization. Pristine PVA film was prepared in the same method without adding MnO_2 NPs. Thus, PVA–MnO_2 nanocomposite films with 0.5, 1, 1.5, 2 and 4 wt.% of MnO_2 NPs were prepared. The samples have been labelled as PVA0.5, PVA1, PVA1.5, PVA2 and PVA4, respectively.

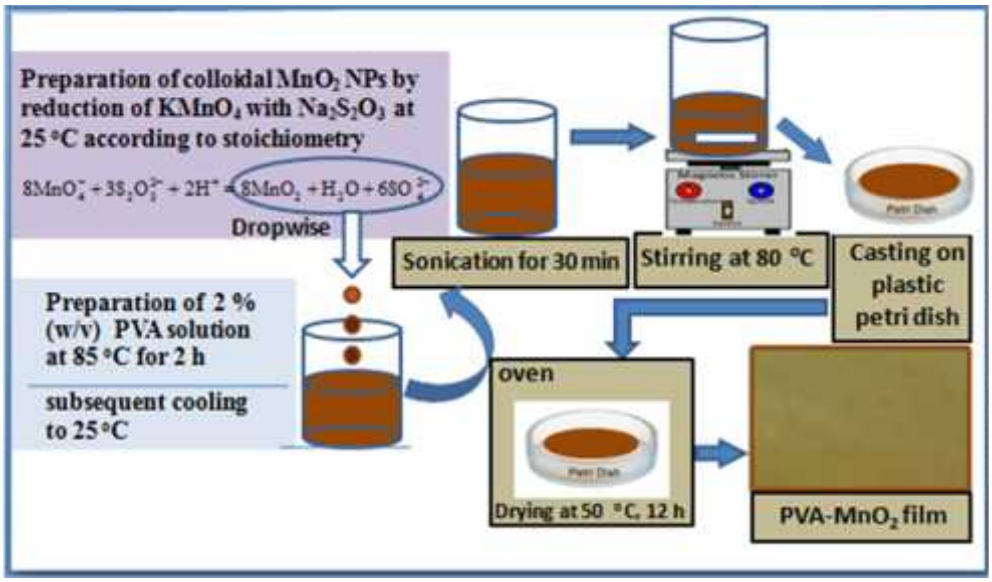

Figure 4.1. Schematic representation of the synthesis of PVA-MnO_2 nanocomposite film.

4.2.3. Preparation of Graphite Electrode Modified with PVA and PVA-MnO_2 Nanocomposite Films

Graphite electrode was mirror polished with a Buehler pad followed by rubbing with offset paper. 10 µL of pristine PVA and PVA-MnO_2 nanocomposite in solution was drop casted onto the graphite electrode surface with a micro-pipette and then dried for 15 h under vacuum. [C_2mim][BF_4] was added to the PVA or PVA-MnO_2 nanocomposite solution so that the weight ratio of [C_2mim][BF_4] were 5, 10 and 20 wt.% PVA-MnO_2 nanocomposites in film form. The total weight of the material in the electrode was usually ~0.3 mg.

4.3. Results and Discussion

4.3.1. UV-visible Spectral Analysis

The representative UV-visible spectra of MnO_2 NPs, PVA and PVA-MnO_2 dispersed in solution are shown in Figure 4.2. Absorption maximum (λ_{max}) of MnO_2 was 352 nm, whereas the λ_{max} of PVA4 was found to be 364 nm. Such a shifting of λ_{max} towards higher wavelength indicates that there could be a strong interaction between MnO_2 NPs and PVA, resulting in the formation of MnO_2 and PVA aggregates. Difference spectrum of PVA4 and MnO_2 shows a hump in the UV region which further supports a strong interaction between PVA and MnO_2 NPs [11].

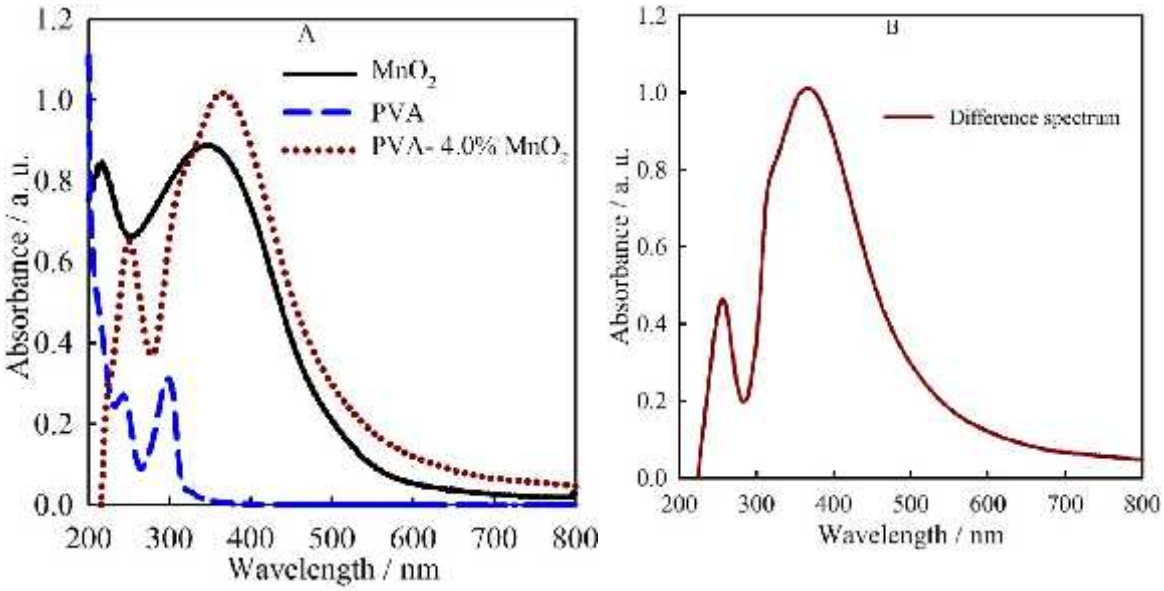

Figure 4.2. UV-vis spectra of MnO_2, PVA and PVA4 (A) and difference spectrum of aqueous solution of PVA and PVA4 (B) solution before film casting.

To justify further, the effect of MnO_2 loading in the composite on the value of λ_{max} was examined. Figure 4.3 demonstrates the effect of MnO_2 NPs loading in the PVA-MnO_2 nanocomposites.

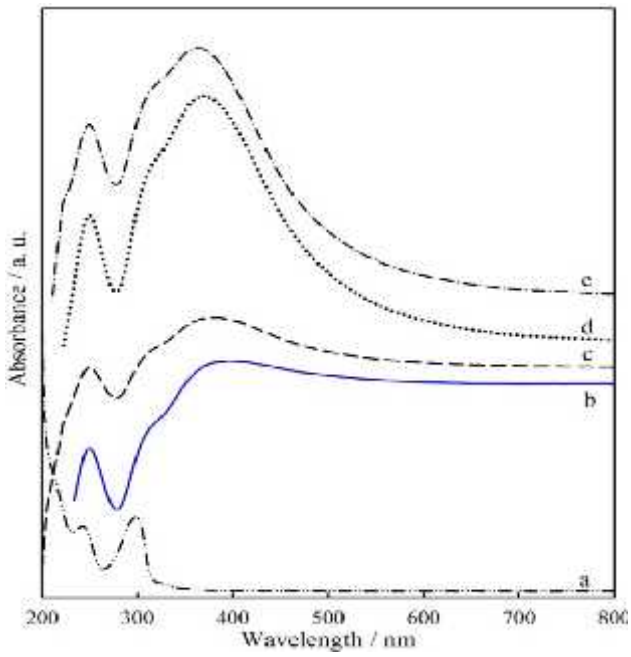

Figure 4.3. UV-vis spectra of (a) PVA, (b) PVA0.5, (c) PVA1, (d) PVA2, and (e) PVA4 solution before film casting.

The λ_{max} increases with respect to wt.% loading of MnO_2 NPs in all of the PVA-MnO_2 nanocomposites. This may be attributed to the fact that donation of non-boding

electrons of PVA to vacant *d*-orbital of Mn facilitating the electronic transition and, as a result, the λ_{max} shifts to higher wavelength [12]. But the shifting of the λ_{max} decreases from PVA0.5 to PVA4 with wt.% of MnO_2 NPs loading in the PVA-MnO_2 nanocomposites. This may be justified by the fact that as the % wt. of MnO_2 increases free volume of polymer decreases thus energy gap between electronic transition becomes higher and λ_{max} shifts to lower wavelength.

4.3.2. Dynamic Light Scattering (DLS) Measurement

DLS measurements were carried out for the aqueous suspension of MnO_2, PVA, and PVA-MnO_2 nanocomposite and the average size distributions are presented in Figure 4.4. Average diameter of MnO_2 NPs, PVA, and PVA4 (PVA-4wt.% MnO_2) nanocomposites are 58, 293 and 93 nm, respectively. DLS usually measures the hydrodynamic diameter of the particles in solution which is based on the Brownian motion of the particles in aqueous solution. Here, the hydrodynamic diameter of the samples is for all molecular size in average that includes PVA and hydration layer of water molecules [13]. The average diameter of PVA-MnO_2 nanocomposites is lower than that of PVA since MnO_2 NPs is encapsulated within the PVA matrix with interactions between MnO_2 NPs and PVA making the particle size smaller.

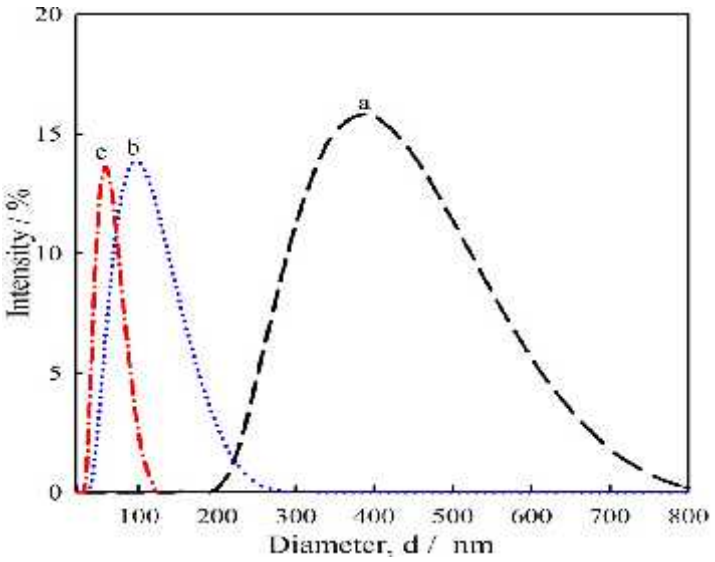

Figure 4.4. Average diameter of (a) PVA (b) PVA4 and (c) MnO_2 NPs from DLS measurements.

4.3.3. FT-IR Spectral Analysis

The FT-IR spectra recorded for the pristine PVA, MnO_2, and PVA-MnO_2 nanocomposite film are shown in Figure 4.5. All characteristic bands corresponding

to pristine PVA film were generally observed in PVA-MnO_2 nanocomposite film including the band of MnO_2. The strong broad at 3339 cm^{-1} of pristine PVA assigned to O-H stretching vibration of hydroxyl group was observed at 3324 cm^{-1} in PVA4 film. The band corresponding to C-H asymmetric stretching vibration occurs at 2942 and 2935 cm^{-1} for the PVA and PVA-MnO_2 nanocomposite film, respectively. This shifting has been considered to be due to the interaction of the hydroxyl group with the positively charged surface of the MnO_2 NPs [14]. This indicates that despite drying this sample may contain trace amount of adsorbed moisture. The band at 1719 cm^{-1} for C=C stretching vibration and 1652 cm^{-1} corresponding to the acetyl C=O group remain the same for PVA-MnO_2 nanocomposite film. The sharp band at 1096 cm^{-1} corresponding to C-O stretching of acetyl groups of PVA backbone becomes broad in PVA-MnO_2, suggesting interaction between PVA and MnO_2 NPs in the composite.

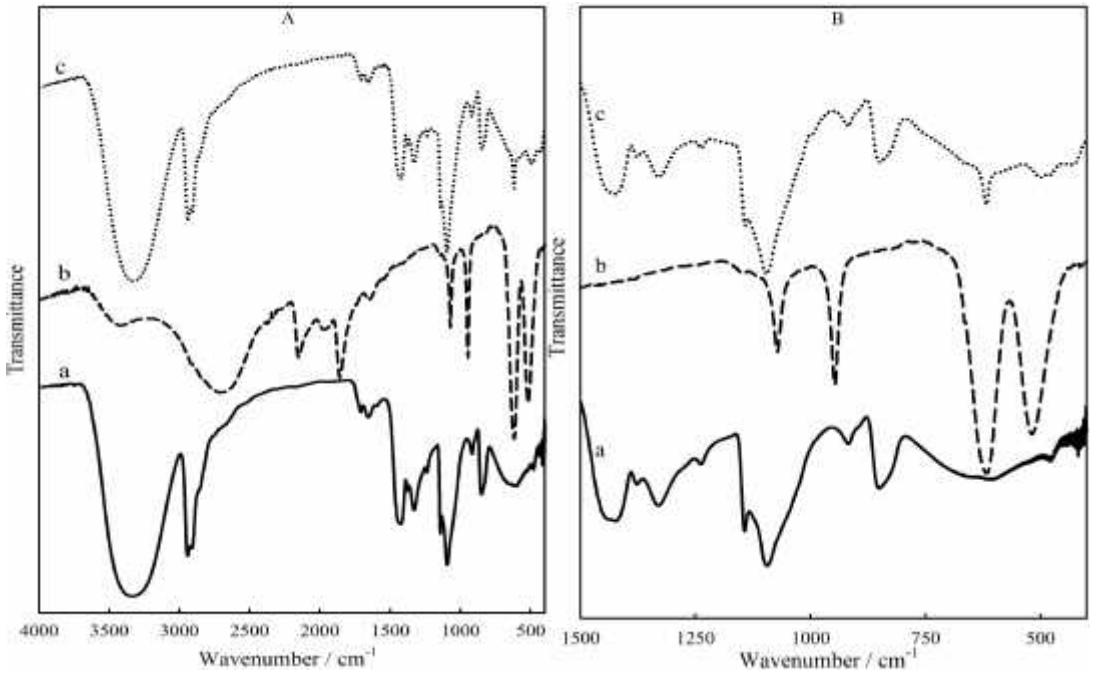

Figure 4.5. FT-IR spectra of (a) PVA, (b) MnO_2 and (c) PVA4 (A-Full scale view and B-small scale view).

4.3.4. Scanning Electron Microscopy

Figure 4.6 shows the photograph and SEM images of PVA-MnO_2 nanocomposite films. The SEM image of PVA film has also been compared in Fig. 4.6. The SEM micrograph of PVA4 nanocomposite film shows spherical MnO_2 NPs are homogeneously dispersed into PVA host matrix. PVA in the PVA film, as evident from Figure 4.6 (B), exists as single phase. The size of the MnO_2 NPs dispersed into the PVA matrix is found to be less than 100 nm.

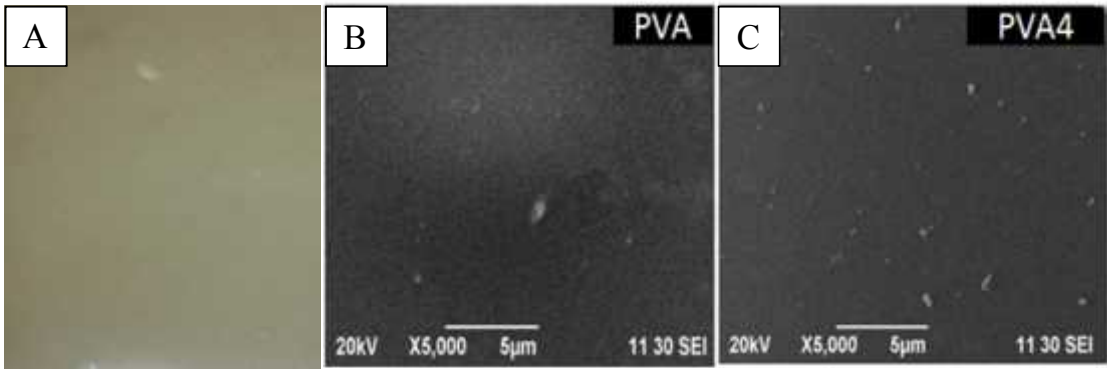

Figure 4.6. Photograph of PVA4 nanocomposite film (A), SEM image of PVA film (B) and SEM image of PVA4 nanocomposite film (C).

4.3.5. Thermogravimetric Analysis

Figure 4.7 shows the TG curves of the pristine PVA and PVA-MnO_2 nanocomposite films. The thermogram of pristine PVA film indicates three major steps of weight loss. In the first step, TGA curve shows gradual weight loss (7%) up to around 110 ^oC due to the removal of absorbed and adsorbed water. In the second step, the PVA film shows a steady weight loss (5%) between 110 and 260 ^oC, which can be attributed to the elimination of pendant -O-H groups and partial degradation of PVA chains [15]. Finally, in the third step, a sharp and gradual weight loss was noticed starting from 260 ^oC onwards for the degradation of the skeletal chain structure of PVA moiety. The hump observed at 430 ^oC in every case is due to formation of an anhydride resulting from the decomposition of PVA [16]. Above 513 ^oC, the results obtained may be associated with the residues of carbonaceous matter only.

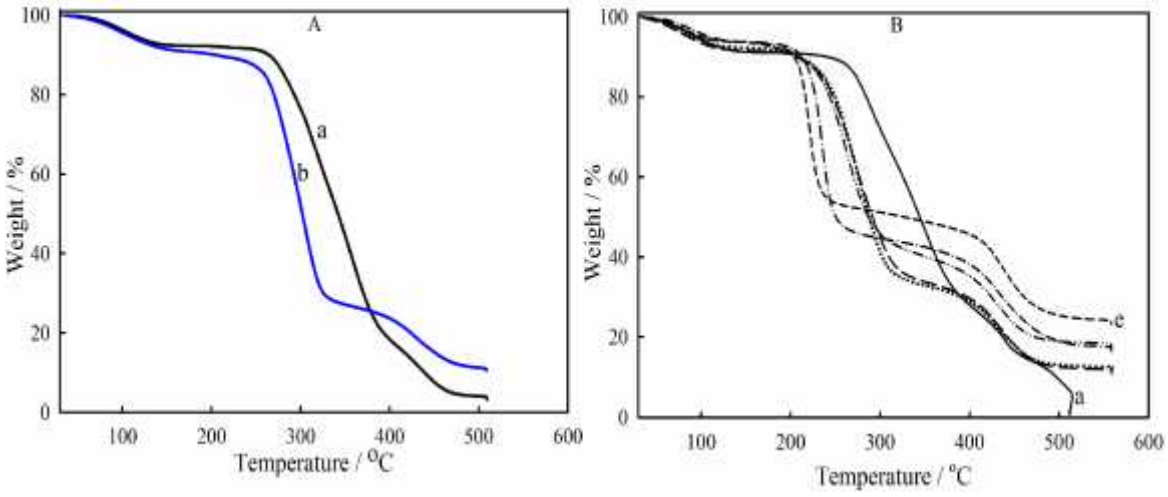

Figure 4.7. TG curves of (a) PVA and (b) PVA0.5 (A) and (a) PVA (b) PVA0.5 (c) PVA1, (d) PVA2, and (e) PVA4 (B).

The thermogram of PVA0.5 film also shows three major steps of weight loss occurring generally at low temperatures compared to pristine PVA (compare curve a with curve b in Figure 4.7). The first event occurring up to 110 ^{o}C is accompanied by a 5% weight loss and is related to the removal of the physically adsorbed water. In the second step 14% weight loss occurs from 110-238 ^{o}C. This step is likely to be due to the decomposition of pendant -O-H groups and partial degradation of PVA chain. A gradual weight loss (46%) occurs in the temperature range of 238-330 ^{o}C, which may correspond to the chain-scission reactions, side-reactions and cyclization reactions. [15]. Finally, the sharp decomposition of PVA occurs after degradation at 330 ^{o}C. The final step occurring in the temperature range of 330-474 ^{o}C with 21% weight loss indicates that total PVA may be removed from the clusters and only MnO_2 NPs and residual carbonaceous particles retain at higher temperature. Careful analyses of thermograms indicate the remarkable change of degradation temperature in PVA-MnO_2 nanocomposites from 260 to 430 ^{o}C with 65% weight loss. Thus, it can be inferred that the thermal stability of PVA0.5 nanocomposites decreases due to the presence of MnO_2 NPs that may initiate the nucleation of degradation process of adhering PVA at low temperature.

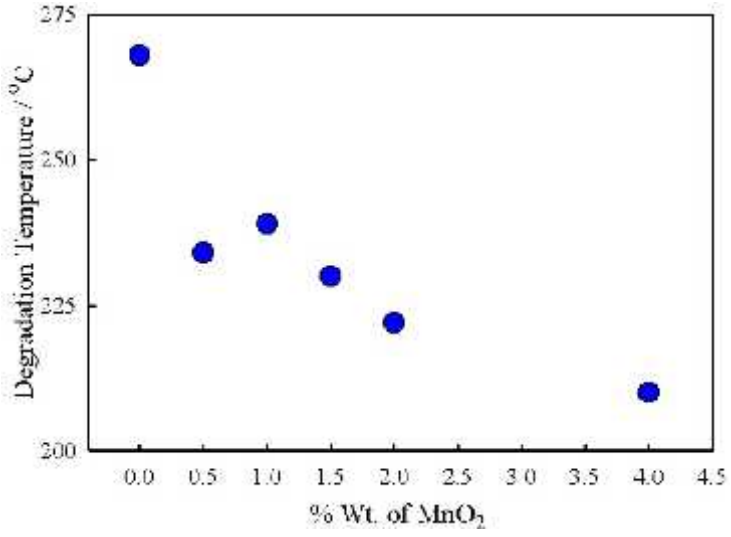

Figure 4.8. Effect of degradation temperature on wt.% of MnO_2.

Figure 4.8 shows the effect of MnO_2 NPs on the thermal degradation of PVA-MnO_2 nanocomposites. From these results, the plot of degradation temperature (t_d) of PVA against wt.% loading of MnO_2 was constructed as presented in Figure 4.8. The t_d generally decreases with increasing MnO_2 NPs in the composite. After addition of 0.5

wt.% of MnO_2 the t_d remains almost constant as MnO_2 NPs occupies the free void interstitial space in the PVA matrix up to 1 wt.% of MnO_2 NPs. With further increase up to 4 wt.% of MnO_2 NPs, free MnO_2 causes the lowering of the t_d for the nanocomposites due to lowering of interfacial interactions. Thus, thermal stability decreases in PVA-MnO_2 nanocomposites may be due to the decreasing tendency of inter chain interactions of PVA as the free volume in PVA decreases at MnO_2 NPs loading. Deformation of PVA chain may take place when MnO_2 NPs are incorporated into the polymer chain which renders the degradation of PVA easily.

4.3.6. XRD Pattern of PVA-MnO_2 Nanocomposite Film

The XRD measurement was performed to examine the crystallinity of the PVA-MnO_2 nanocomposite. Figure 4.9 shows the diffraction pattern of PVA1 nanocomposite film in which broad peaks at 2θ = 19.1, 22.0 and 40.5° were observed. The peaks at 19.1° and 22.0° correspond to the typical reflection of the (101) and (10-1) planes of the semicrystalline PVA, respectively [17]. The peak at 40.5° is assigned to the (220) plane of PVA [18, 19]. However, besides the diffraction peaks of PVA, peaks at 2θ of 30.8° and 44.9° correspond to α-MnO_2 (JCPDS no. 044-0141). It is obvious that there is no significant effect on the general shape of the XRD pattern after incorporation of MnO_2 NPs. The pattern confirms that the MnO_2 NPs are embedded in the PVA matrix.

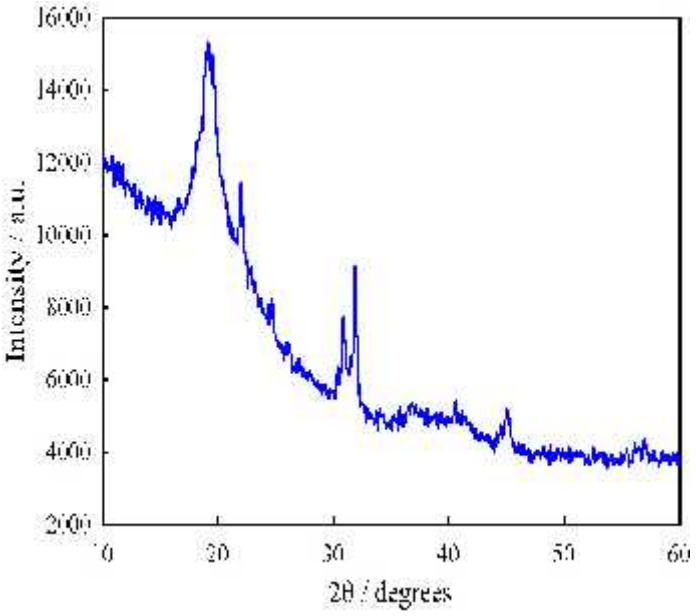

Figure 4.9. XRD pattern of PVA1 nanocomposite film.

4.3.7. Specular Reflectance Spectral Analysis

UV-visible specular reflectance spectra measured for PVA and its MnO_2 composites are shown in Figure 4.10. PVA shows bands at 249 nm for band gap of PVA polymer [20]. Shifting of this band to 254 nm was observed for PVA0.5 nanocomposite film. Shifting in similar trends was noticed for all the nanocomposite films. PVA4 composite film showed no peak at 249 nm and absorption of UV radiation at this wavelength has been unlikely due to complete occupation of MnO_2 NPs in the free void spaces of PVA matrix.

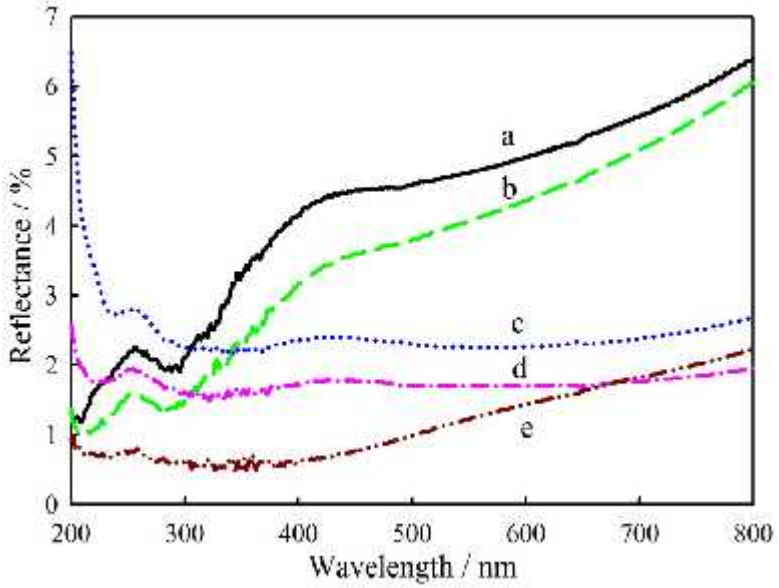

Figure 4.10. Specular reflectance spectra of (a) PVA, (b) PVA0.5, (c) PVA1, (d) PVA2 and (e) PVA4.

4.3.8. Transmittance Spectra of PVA-MnO_2 Nanocomposite Films

UV-visible transmittance spectra of the PVA and PVA-MnO_2 nanocomposite films are shown in Figure 4.11. PVA film is optically transparent in the visible range of 400-800 nm. A decrease in wt.% transmittance is generally evident with incorporation of MnO_2 loading. With increase in loading of MnO_2 NPs, the optical transparency of visible light of the films decreased. The transmittance spectra (Figure 4.11 (A)) reveal that there is a decrease of percentage transmittance in the UV region with the increasing %wt. of MnO_2 NPs into the PVA matrix. This indicates that MnO_2 NPs have the ability to lower the transparency of the PVA-MnO_2 nanocomposite films. Figure 4.11 (B) also compares the transparency in the ultraviolet and visible region which also verifies the same trend in reduction of transparency of light. The PVA-MnO_2 nanocomposite films which contain 1 %wt. or more MnO_2 NPs absorb nearly

hundred percent of UV radiation. Thus, it can be said that MnO_2 NPs impart strong influence on the UV-shielding property of The PVA-MnO_2 nanocomposite films.

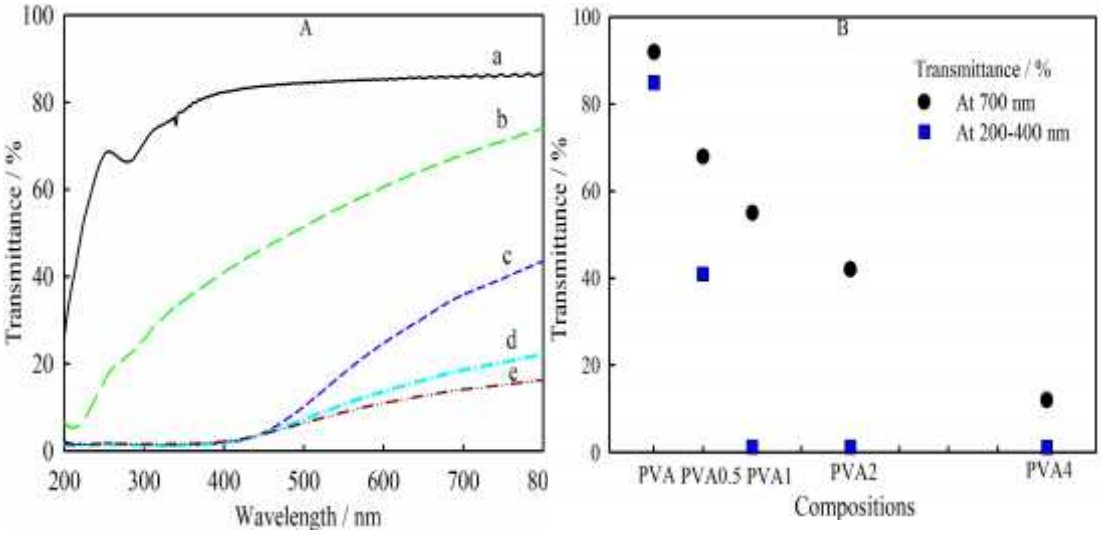

Figure 4.11. Transmittance spectra of (a) PVA , (b) PVA0.5, (c) PVA1, (d) PVA2, and (e) PVA4 (A); transmittance of PVA , PVA0.5, PVA1, PVA2 and PVA4 as a function of wt.% of MnO_2.

Transmittance of different PVA-MnO_2 nanocomposite films at 700 nm is shown in Figure 4.11 (B). At 700 nm, percentage transmittance of PVA film is somewhat lower than that of at 400 nm. With loading of MnO_2 NPs, percentage transmittance of PVA-MnO_2 films begins to decrease. The optical transparency of the films to light is affected by the presence of the MnO_2 NPs [21]. This is due to the fact that as the wt.% loading of MnO_2 NPs increases absorption of UV-visible radiation also increases thereby lowers the transmittance for the nanocomposites. As the MnO_2 NPs greater than 1 wt.%, the nanocomposite films absorbs UV radiation fully and the films might be used as UV-shielding materials.

4.3.9. PVA-MnO_2 Nanocomposite Films as UV-shielding Materials

The UV-shielding property of pristine PVA and PVA-MnO_2 nanocomposite films were evaluated by measuring the transmittance of the film. The UV-vis transmittance spectra of pristine PVA and PVA-MnO_2 nanocomposite films are presented in Figure 4.11. The transmittance spectra showed that pristine PVA film does not markedly absorb in the UV-visible region rather it absorbs a little more and displayed good transparency in the visible region. UV-shielding ability of PVA-MnO_2 nanocomposite films can be explained using the fact that PVA has many free pendant -O-H groups in its chain and acts as the dispersing medium and MnO_2 NPs are suspended in that

medium. Formation of complex by the donation of n-electrons from O atoms to the vacant *d*-orbital of Mn atom may facilitate the absorption of UV radiation rendering PVA-MnO_2 nanocomposite films as UV-shielding material [22].

4.3.10. Electrochemical Characterization of Graphite Electrode-Modified with PVA-MnO_2 Nanocomposite

Cyclic voltammetry and chronopotentiometry or galvanostatic charge-discharge was used to assess the performance of the modified electrode to be used as supercapacitors. Cyclic voltammograms (CVs) were measured in the potential range of 0.0 to 1.0 V *vs.* Ag/AgCl (sat. KCl) at different scan rates of 0.10, 0.02, 0.05 and 0.10 V s^{-1}. Galvanostatic charge-discharge experiments were carried out with PVA and PVA-MnO_2 nanocomposites acting as working electrodes by cycling the voltage from 0 to 1.0 V at different current densities (0.25-1.50 A g^{-1}). Graphite electrode modified with PVA-MnO_2 nanocomposites incorporated with [C_2mim][BF_4] was also characterized with the same experimental methods and conditions described above.

4.3.10.1. Cyclic Voltammetry

Figure 4.12 shows the CVs of PVA and PVA-MnO_2 nanocomposites at different potential scan rates. The CVs in panel (A) show all the CVs other than PVA0.5 exhibit approximately rectangular shapes, at a scan rate of 0.10 V s^{-1}. At low MnO_2 content in the PVA0.5, the material may contribute in transition of oxidation state of MnO_2. This observation indicates capacitive behavior which may originate from the electrical double-layer capacitance of the electrodes. In these CVs, the current passed by the PVA-MnO_2 nanocomposites is higher than that of PVA. This may be ascribed to the synergistic effect from the combined contributions of PVA and MnO_2. The specific capacitance decreases from 25 to 14 F g^{-1} from PVA to PVA4 composite at a scan rate of 0.10 V s^{-1}. The higher CV current densities of PVA-MnO_2 nanocomposites indicate the high conductivity and low internal resistance for the composites as the electrode material. Figure 4.12 (B) shows the CVs of PVA0.5 nanocomposite incorporated with 5 to 20 wt.% [C_2mim][BF_4]. All the CVs are rectangular in shapes indicating the ideal capacitive behavior of the electrodes. The current densities are also higher than those of PVA and PVA0.5 to PVA4 nanocomposites which may be responsible for higher specific capacitance of the composites. The values of specific capacitance evaluated from the CVs are listed in

Table 4.1. The specific capacitance increases from 17 (PVA) to 25 (PVA0.5) F g^{-1} at a scan rate of 0.10 V s^{-1}, then decreases from PVA1 (18 F g^{-1}) to PVA4 (14 F g^{-1}). At low wt.% of MnO_2, Na^+ insertion is favored from 0.5 M Na_2SO_4 electrolytic solution. Partial dissolution of MnO_2 may occur due to the formation of soluble Mn^{2+} ions in solution [23].

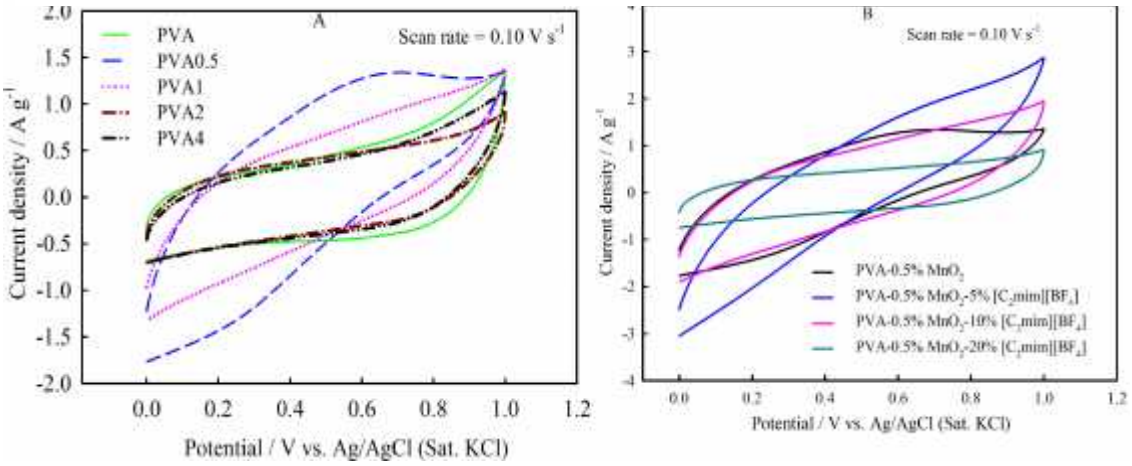

Figure 4.12. CVs of PVA and PVA-MnO_2 Nanocomposites (A) and $[C_2mim][BF_4]$ incorporated PVA0.5 nanocomposite (B) at a scan rate of 0.10 V s^{-1}.

Table 4.1. Specific capacitance of PVA and PVA-MnO_2 nanocomposites (A) and PVA0.5 nanocomposite incorporated with $[C_2mim][BF_4]$ (B) at a scan rate of 0.10 V s^{-1}

Material	MnO_2 content (%)	Specific capacitance (F g^{-1})	Material	$[C_2mim][BF_4]$ content (wt.%)	Specific capacitance (F g^{-1})
PVA	0	17	PVA0.5-5 wt.% $[C_2mim][BF_4]$	5	28
PVA0.5	0.5	25			
PVA1	1	18	PVA0.5-10 wt.% $[C_2mim][BF_4]$	10	26
PVA2	2	14	PVA0.5 20 wt.% $[C_2mim][BF_4]$	20	15
PVA4	4	14			

4.3.10.2. Chronopotentiometry Analysis

Figure 4.13 illustrates the typical charging-discharging behavior of the graphite electrodes modified with PVA and PVA-MnO_2 nanocomposites recorded in 0.5 M Na_2SO_4 aqueous solution at current densities from 0.25 to 1.50 A g^{-1} with the

potential sweep (0.0 to 1.0 V). For both electrodes there is a sharp decrease in voltage at the commencement of discharge followed by linear decrease with time of discharge. The sharp increase or decrease in voltage at the beginning of charge or discharge is attributed to the effect of internal resistance of the capacitor. Linear variation of voltage during charge or discharge is also indicative of the property of a capacitor [24]. From the charge-discharge curves, specific capacitance is determined. The specific capacitance decreases from PVA1 (50 F g^{-1}) to PVA4 (4 F g^{-1}) at current densities from 0.25 to 1.50 A g^{-1}. At lower current density, the charging-discharging process takes longer time which is attributed to the fact that at low current density the active materials on the electrode surface gets sufficient time for the insertion or

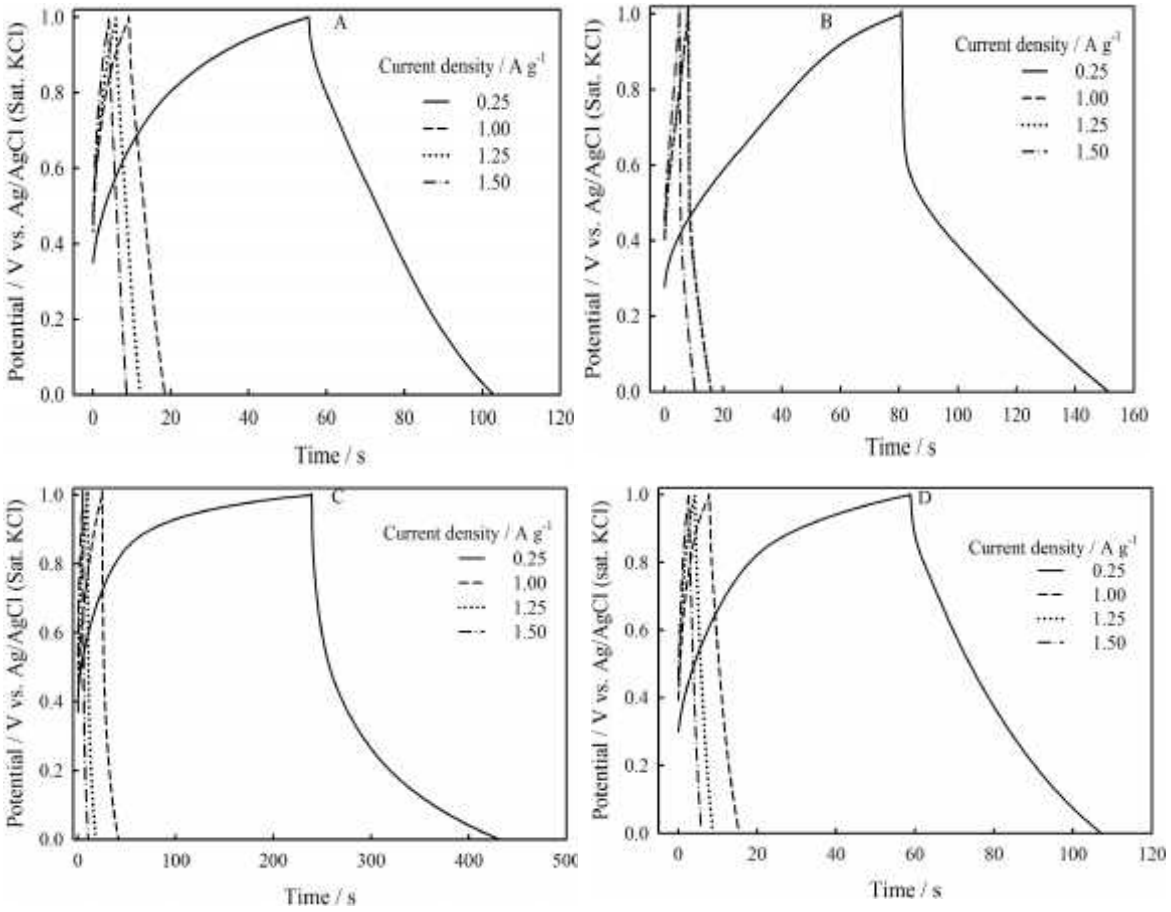

Figure 4.13. Charge-discharge curves of PVA(A) PVA0.5 (B), PVA2 (C) and PVA4 nanocomposites at current densities from 0.25-1.50 A g^{-1}.

release of Na^+ from the electrolytic solution during the charging-discharging process [25, 26]. In case of PVA0.5 nanocomposite incorporated with $[C_2mim][BF_4]$ the specific capacitance decreases from PVA0.5-5% $[C_2mim][BF_4]$ (163 F g^{-1}) to PVA0.5-20% $[C_2mim][BF_4]$ (4 F g^{-1}) at current densities from 0.25 to 1.50 A g^{-1}.

The cycling stability of the fabricated electrodes at a current density of 1.50 A g^{-1} in the potential window 0.0-1.0 V was tested by galvanostatic charge-discharge process up to 1000 cycles.

Table 4.2. Specific capacitance of PVA, PVA-MnO_2 and $[C_2mim][BF_4]$ incorporated PVA0.5 at a current density of 0.25 A g^{-1} from charge-discharge curves

Material	MnO_2 content (%)	Specific capacitance (F g^{-1})	Material	MnO_2 content (%)	Specific capacitance (F g^{-1})
PVA	0	11	PVA0.5-5 wt.% $[C_2mim][BF_4]$	0.5	163
PVA0.5	0.5	17			
PVA1	7	50	PVA0.5-10 wt.% $[C_2mim][BF_4]$	0.5	23
PVA2	20	47	PVA0.5-20 wt.% $[C_2mim][BF_4]$	0.5	11
PVA4	27	12			

4.3.11. Electrochemical Impedance Spectral Analysis

The impedance spectra in the form of Nyquist plots are displayed in Figure 4.14. The impedance spectra are almost similar in form with an arc or depressed semicircle at a higher frequency region and a spike at a lower frequency region.

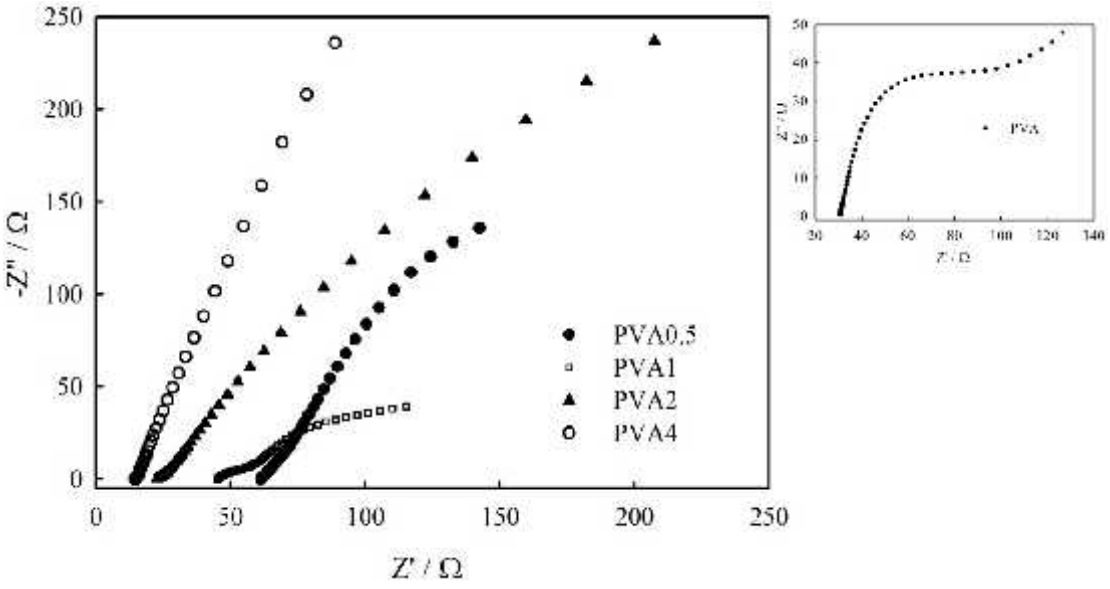

Figure 4.14. Nyquist impedance plot of PVA and PVA-MnO_2 nanocomposites.

The impedance spectra show a major difference in the high-frequency range, which corresponds to the charge transfer resistance (R_{ct}) caused by the Faradaic reactions and the double- layer capacitance (C_{dl}) on the electrode surface fabricated by PVA and PVA-MnO_2 nanocomposites. The tendency of growing semicircle decreases from PVA to PVA4 nanocomposites indicating of more favorable capacitive behavior of the materials.

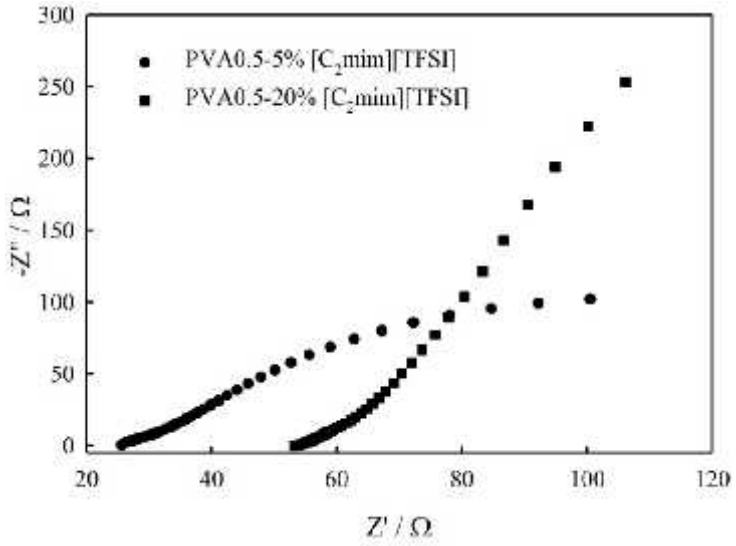

Figure 4.15. Nyquist impedance plot of PVA0.5 nanocomposite incorporated with [C_2mim][BF_4].

From the Nyquist plot in Figure 4.15 it can be assumed that 5 wt.% PVA0.5 nanocomposite incorporated with [C_2mim][BF_4] possesses lower charge transfer resistance indicating higher electrical conductivity than that for incorporation of 20 wt.% [C_2mim][BF_4].

4.3.12. Capacitive Properties of PVA-MnO_2 Nanocomposite Films

Although the capacitance of PVA film is in the order of 5.20 nF cm^{-2}, it is used to fabricate with other inorganic components in many electronic devices as substrate and gate dielectrics in the electronic devices, biomedical devices for clinical and other applications [27]. Capacitive properties of PVA films can be tuned with incorporation of other inorganic components so that the specific capacitance is increased and can thus be used in electronic and biomedical devices efficiently. In Figure 4.16, the specific capacitance of PVA and PVA-MnO_2 nanocomposite films with various wt.% of MnO_2 NPs are presented. For low current densities, the specific capacitance is maximum due to lower electronic and ionic resistance for small potential change

during charge-discharge process which allows to access more electrolytic ions in the electrode surface. The specific capacitance decreases with increasing current densities due to the fact that at higher current densities the Na^+ ions from the 0.5 M Na_2SO_4 electrolytic solution can't access to the deeper pores of the material, rather only able to reach in the outer surface of the materials leading to decrease in specific capacitance [28]. The specific capacitance reaches to a maximum value of 50 F g^{-1} in PVA1 nanocomposite from PVA, then it decreases up to PVA4. This may be due to fact that MnO_2 NPs distributed homogenously into polymeric backbone of PVA at very low wt.% of MnO_2. After that inhomogeneous distribution of MnO_2 NPs may lead to the decrement of specific capacitance. Thus, MnO_2 NPs have a profound effect of tuning the specific capacitance of PVA-MnO_2 nanocomposite films.

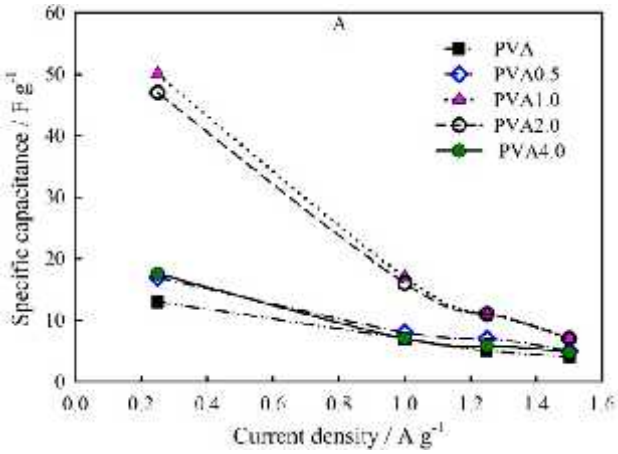

Figure 4.16. Variation of specific capacitance with current densities of PVA and PVA-MnO_2 nanocomposites (A) at current densities from 0.25 to 1.50 A g^{-1}.

4.3.12.1. Capacitive Properties of PVA-MnO_2 Nanocomposite Films Incorporated with [C_2mim][BF_4]

[C_2mim][BF_4] is a hydrophilic IL composed solely of [C_2mim] cation and [BF_4] anions It has high ionic conductivity that makes it possible to be usable in electric, electronic, and electrochemical devices. Although PVA-MnO_2 nanocomposite films possess moderate specific capacitance, their specific capacitance may be increased with incorporation of ionic liquid in the nanocomposites. Figure 4.16 shows the variation of specific capacitance in incorporating [C_2mim][BF_4] on wt.% variation from 5%, 10% and 20% of the weight of PVA0.5 nanocomposite. The specific capacitance reaches to maximum value of 163 F g^{-1} at a current density of 0.25 A g^{-1}.

Then it decreases to 23 and 11 F g^{-1} for 10% and 20% addition of $[C_2mim][BF_4]$ in the material. This may be due to the fact that IL exists as ion aggregates in its pure form but when it is added to other materials it tends to dissociate to some extent [29]. Upon addition of more $[C_2mim][BF_4]$, it can't sufficiently disrupt. Thus insertion of ions from the electrolytic ions into the electrode surface hampers and that is why, specific capacitance decreases.

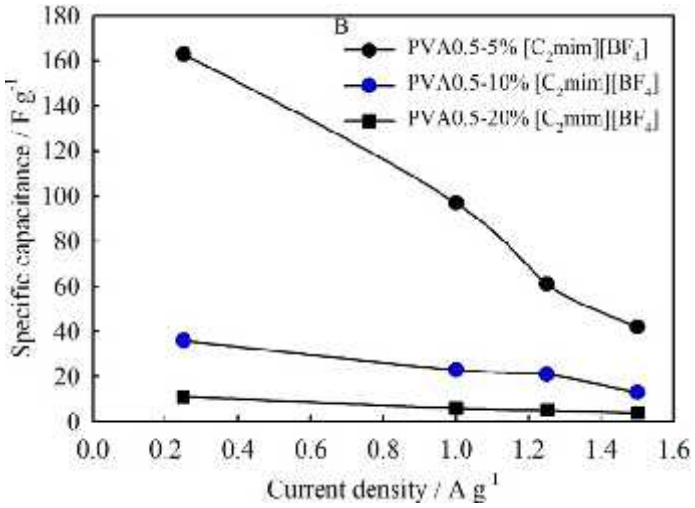

Figure 4.17. Variation of specific capacitance with current densities of PVA0.5 nanocomposite incorporated with $[C_2mim][BF_4]$ incorporated (B) at current densities from 0.25 to 1.50 A g^{-1}.

4.3.12.2. Effect of $[C_2mim][BF_4]$ on Capacitive Properties of PVA-MnO_2 Nanocomposite Films

Capacitive properties of PVA-MnO_2 nanocomposite films incorporated with $[C_2mim][BF_4]$ have been investigated. Figure 4.17 shows the specific capacitance of PVA0.5 nanocomposite with incorporation of various wt.% of $[C_2mim][BF_4]$ at different current densities from 0.25 to 1.50 A g^{-1}. The specific capacitance of PVA-MnO_2 nanocomposite films incorporated with 5 wt.% $[C_2mim][BF_4]$ gave the highest value of 163 F g^{-1}. After that it reduces to a large extent due to the fact that the double layer of IL may provide thick surface at the electrode which is not one layer thick [30, 31]. Due to the formation of thick layer, at higher wt.% of $[C_2mim][BF_4]$, the electrolytic ions may not have the accessibility into the deeper pore of PVA0.5 composite leading to the large decrease of specific capacitance as low as 11 F g^{-1} at a current density of 0.25 A g^{-1}. However, this value is not lower than that of PVA film at the same current density.

4.4. Conclusions

PVA-MnO_2 nanocomposite films with varying compositions of MnO_2 NPs could be prepared through solution casting technique. An ionic liquid, [C_2mim][BF_4] could also be incorporated with these composites. MnO_2 interacts with PVA in the PVA-MnO_2 nanocomposites. The specific capacitance for PVA-MnO_2 nanocomposites modified graphite electrode was as high as 50 F g^{-1} at a charge-discharge current density of 0.25 A g^{-1} in 0.5 M Na_2SO_4 solution. The specific capacitance of graphite electrodes modified with PVA-MnO_2 nanocomposites incorporated with [C_2mim][BF_4] modified decreases from 163 to 11 F g^{-1} at the same current density. The specific capacitance of PVA and PVA0.5 and [C_2mim][BF_4] incorporated PVA0.5 nanocomposites can maintain stability up to 1000 cycles studied. PVA-MnO_2 nanocomposite films with different MnO_2 content could shield UV radiation. The PVA-MnO_2 nanocomposite films are therefore promising for UV-shielding and PVA as well as all the PVA-MnO_2 nanocomposites may be used as materials for supercapacitor application.

References

[1] P.-C. Ma, N. A. Siddiqui, G. Marom, J.-K. Kim, *Dispersion and functionalization of carbon nanotubes for polymer-based nanocomposites: A review,* Composites: Part A, 2010, 41, 1345–1367.

[2] P. K. Khanna, N. Singh, S. Charan, V. V. V. S. Subbarao, R. Gokhale, U. P. Mulik, *Synthesis and characterization of Ag/PVA nanocomposite by chemical reduction method*, Mater. Chem. Phys., 2005, 93, 117–121.

[3] J. Gaume, C. Taviot-Gueho, S. Cros, A. Rivaton, S. Therias and J.-L.Gardette, *Optimization of PVA clay nanocomposite for ultra-barrier multilayer encapsulation of organic solar cells*, Sol. Energy Mater. Sol. Cells, 2012, 99, 240–249.

[4] J. H. Yeun, G. S. Bang, B. J. Park, S. K. Ham and J. H. Chang, *Poly(vinyl alcohol) nanocomposite films: Thermooptical properties, morphology, and gas permeability,* J. Appl. Polym. Sci., 2006, 101, 591–596.

[5] J. Gaume, P. Wong-Wah-Chung, A. Rivaton, S. Therias and J. L. Gardette, *Photochemical behavior of PVA as an oxygen-barrier polymer for solar cell encapsulation*, RSC Adv., 2011, 1, 1471–1481.

[6] S. Gupta, S. Sindhu, K. A. Varman, P. C. Ramamurthy and G. Madras, *Hybrid nanocomposite films of polyvinyl alcohol and ZnO as interactive gas barrier layers for electronics device passivation,* RSC Adv., 2012, 2, 11536–11543.

[7] L. I. Hill, R. Portal, A. Verbaere and D. Guyomard, *One-step electrochemical synthesis of α-MnO2 and α γ-MnO_2 compounds for lithium batteries*, Electrochem. Solid-State Lett., 2001, 4, A180-A183.

[8] X. L. Luo, J. J. Xu, W. Zaho and H. Y. Chen, *Ascorbic acid sensor based on ion-sensitive field-effect transistor modified with MnO_2 nanoparticles,* Anal. Chim. Acta, 2004, 512, 57-61.

[9] J. N. Broughton and M. J. Brett, *Variations in MnO_2 electrodeposition for electrochemical capacitors,* Electrochim. Acta, 2005, 50, 4814-4819.

[10] J. Moon, M. Awano, H. Takagi and Y. Fujishiro, *Synthesis of nanocrystalline manganese oxide powders: Influence of hydrogen peroxide on particle characteristics,* J. Mater. Res., 1999, 14, 4594-4601.

[11] Sreeja, S. Sreedhanya, N. Smijesh, R. Philip and C. I. Muneera, *Organic dye impregnated poly(vinyl alcohol) nanocomposite as an efficient optical limiter: structure, morphology and photophysical properties,* J. Mater. Chem. C, 2013, 1, 3851-3861.

[12] A. M. Atta, G. A. El-Mahdy, H. A. Al-Lohedan, and A. O. Ezzat, *Synthesis and application of hybrid polymer composites based on silver nanoparticles as corrosion protection for line pipe steel,* Molecules, 2014, 19, 6246-6262.

[13] D. G Duff, P. P. Edwards and B. F. G. Johnson, *Formation of a polymer-protected platinum sol: A new understanding of the parameters controlling morphology,* J. Phys. Chem., 1995, 99, 15934-15944.

[14] F. Li, X. Xu, Q. Li, Y. Li, H. Zhang, J. Yu, and A. Cao, *Thermal degradation and their kinetics of biodegradable poly(butylene succinate-co-butylene terephthate) under nitrogen and air atmospheres,* Polym. Degrad. Stab., 2006, 91, 1685-1693.

[15] A. Singhal, M. Kaur, K. A. Dubey, Y. K. Bhardwaj, D. Jain, C. G. S. Pillai and A. K. Tyagi, *Polyvinyl alcohol–In_2O_3 nanocomposite films: synthesis, characterization and gas sensing properties,* RSC Adv., 2012, 2, 7180–7189.

[16] El-Arnaouty, M. B. E. and M. Eid, *Synthesis of grafted hydrogels as mono-divalent cation exchange for drug delivery*, Polym. Plast. Technol. Eng., 2010, 49, 182-190.

[17] M. Watase and K. Nishinari, *Rheological and DSC changes in poly(viny1 alcohol) gels induced by immersion in water,* J. Polym. Sci., Part B: Polym. Phys. Ed., 1985, 23, 1803-1811.

[18] G.-M. Kim, A. S. Asran, G. H. Michler, P. Simon and J. S. Kim, *Electrospun PVA/HAp nanocomposite nanofibers: biomimetics of mineralized hard tissues at a lower level of complexity*, Bioinsp. Biomim., 2008, 3, 1-12.

[19] R. Ricciardi, F. Auriemma, C. D. Rosa and F. Laupretre, *X-ray diffraction analysis of poly(vinyl alcohol) hydrogels, obtained by freezing and thawing techniques,* Macromolecules, 2004, 37, 1921-1927.

[20] A. N. Ananth, S. Umapathy, J. Sophia, T. Mathavan and D. Mangalaraj, *On the optical and thermal properties of in situ/ex situ reduced Ag NP's/PVA composites and its role as a simple SPR-based protein sensor,* Appl. Nanosci., 2011, 1, 87-96.

[21] S. Gupta, S. Sindhu, K. Arul Varman, P. C. Ramamurthy, and G. Madras, *Hybrid nanocomposite films of polyvinyl alcohol and ZnO as interactive gas barrier layers for electronics device passivation*, RSC Adv., 2012, 2, 11536–11543.

[22] M. Sudha, S. Senthilkumar, R. Hariharan, A. Suganthi and M. Rajarajan, *Controlled reduction of the deleterious effects of photocatalytic activity of ZnO nanoparticles by PVA capping,* J. Sol-Gel Sci.Technol., 2012, 61, 14–22.

[23] S. R. Sivakkumar, J. M. Ko, D.Y. Kim, B. C. Kim and G. G. Wallace, *Performance evaluation of CNT/polypyrrole /MnO_2 composite electrodes for electrochemical capacitors,* Electrochim. Acta, 2007, 52, 7377-7385.

[24] E. Frackowiak and F. Beguin, *Electrochemical storage of energy in carbon nanotubes and nanostructured carbons,* Carbon, 2002, 40, 1775 –1787.

[25] R. K. Sharma and L. Zhai, *Multiwall carbon nanotube supported poly(3,4-ethylenedioxythiophene)/manganese oxide nano-composite electrode for super-capacitors,* Electrochim. Acta, 2009, 54, 7148–7155.

[26] W. Sugimoto, H. Iwata, K. Yokoshima, Y. Murakami and Y. Takasu, *Proton and electron conductivity in hydrous ruthenium oxides evaluated by electrochemical impedance spectroscopy: the origin of large capacitance,* J. Phys. Chem. B, 2005, 109, 7330–7338.

[27] C. J. Bettinger and Z. Bao, *Organic Thin-Film Transistors Fabricated on Resorbable Biomaterial Substrates,* Adv. Mater., 2010, 22, 651–655.

[28] C. Portet, P.L. Taberna, P. Simon, E. Flahaut, C. Laberty-Robert, *High power density electrodes for Carbon supercapacitor applications,* Electrochim. Acta, 2005, 50, 4174–4181.

[29] M. A. B. H. Susan, T. Kaneko, A. Noda, and M. Watanabe, *Ion gels prepared by in situ radical polymerization of vinyl monomers in an ionic liquid and their characterization as polymer electrolytes,* J. Am. Chem. Soc., 2005, 127, 4976–4983.

[30] T. Sato, G. Masuda and K. Takagi, *Electrochemical properties of novel ionic liquids for electric double layer capacitor applications,* Electrochim. Acta, 2004, 49, 3603–3611.

[31] M. V. Fedorov, A. A. Kornyshev, *Towards understanding the structure and capacitance of electrical double layer in ionic liquids,* Electrochim. Acta, 2008, 53, 6835–6840.

Abstract

This chapter describes the electrochemical results of composites based on a conducting polymer and a non-conducting polymer using cyclic voltammetric and chronopotentiometric methods. The specific capacitances (C_s) of PAni and PAni-MnO_2 composites at different scan rates and current densities have been compared with those for PVA and PVA-MnO_2 nanocomposites. The capacitative behavior of the composites upon incorporation of two compatible ionic liquids, [C_2mim][TFSI] (for PAni-MnO_2) and [C_2mim][BF_4] (for PVA-MnO_2) have also been examined. The C_s increases from PAni to PAni-MnO_2 composites with increasing of wt.% of MnO_2. PVA and PVA-MnO_2 nanocomposites, on the other hand show different trends. The C_s increases initially up to a certain amount of MnO_2 loading and then it decreases gradually. The difference in the cyclic voltammetric behaviors and charge-discharge curves upon incorporation of the ILs in PAni-MnO_2 and PVA-MnO_2 nanocomposites have been compared and contrasted to explore the potential of the composites for application in supercapacitors.

5.1. Introduction

Polymer composites are combinations of constituents comprising polymers with metal, metal oxides, metal salts *etc.* with a view to having synergistic property in size and morphology, band gap, conductivity, thermal stability, transmittance, dielectric constant and C_s which is not possible for single constituent alone. These composites with synergic effects are often found to exhibit novel functionality for diverse applications [1]. Xu *et al.* showed that polymer composites exhibit synergic properties owing to different types of interactions among the components in their microstructures [2]. Property synergism among the components of the composites or nanocomposites has been interesting for improved mechanical, optoelectronic, thermal and electrochemical properties [3, 4]. The synergistic effect of C_s was found in PAni-graphene oxide composites [5]. Polymers used in composites or nanocomposites serve as good host matrix that prevents agglomeration due to various interactions between dispersed phase and matrix phase whereas metal analogues such as metal or metal oxides act as dispersed or continuous phase that provide improved mechanical, thermal, optoelectronic, electrochemical properties and so on [6].

It may be worth mentioning that nature of conducting and non-conducting polymers have impacts on the C_s and the dispersed phase of metal oxides or metals has also influence on the capacitive nature of composite materials. Dispersibility, porosity,

surface area *etc.* of polymers or metal oxides or metals also influences the C_s [7]. Polymers generally suffer from poor mechanical strength and offer lower C_s as well as less cyclability during charge-discharge and potential cycling due to shrinking and swelling leading to partial degradation. These limitations can be overcome by preparing polymer composites with inorganic components such as metal or metal oxides which offers novel functionality and provides higher specific capacitance than those of polymers. Numerous attempts have been made to investigate the change of the C_s of different polymer composites or nanocomposites by alternating the combinations of polymers and metal oxides with changing electrode materials, electrolytes *etc.* [8]

ILs have been used as alternatives to conventional solvents in green synthesis of polymers and polymer composites, in electrochemical applications such as in capacitors, fuel cells, sensors *etc.* and as additives to tailor the properties of polymer composites [9]. Incorporation of ILs in membrane of polymer composites changes the C_s. ILs have wide electrochemical stability window and most of the ILs are resistant for electrochemical reduction and oxidation up to 5.0 V in different electrodes. They are considered as safe electrolytes for electrochemical devices and used to develop high energy electrochemical supercapacitors. Solid state supercapacitors were designed by polymer gels by incorporating ionic liquid electrolytes for improved performance and cycle life [10]. Supercritical fluid assisted synthesis of MnO_2–graphene composites modified electrode wrapped with an IL have been fabricated for improved supercapacitor performance [11].

In Chapters 3-5, preparation of polymer composites by using conducting and non-conducting polymers as matrix phases has been reported with a view to finding optimum capacitive properties. When ILs are incorporated into the polymer matrix, it is interesting to monitor changes in capacitive behavior depending on the types of interactions between the components of ILs and matrix, and to correlate property changes with the difference in the nature of the polymer matrix.

In spite of a few studies of IL based polymer composites, there have been no reports on the comparative study of the C_s of the conducting and non-conducting polymer based composites with incorporation of ILs of different nature in aqueous electrolytic

solution. To understand the capacitive behavior of conducting and non-conducting polymer based composites with incorporation of ILs depending on the compatibility of mixing with the composites various electrochemical measurements need to be systematically and intensively conducted. In present work, the C_s derived from a conducting polymer based PAni-MnO_2 composites with incorporation of a hydrophobic IL, [C_2mim][TFSI] and that of a non-conducting polymer based PVA-MnO_2 nanocomposites with incorporation of a hydrophilic IL, [C_2mim][BF_4] have been compared. Finally, efforts have been made to develop strategy to optimize conditions for desirable capacitive behavior based on the observations of conducting PAni and non-conducting PVA based composites in absence and presence of ILs.

5.2. Experimental

5.2.1. Materials and Methods

Materials used and methods followed have been described in details in Section 2.2.1 and 4.2.1. Graphite electrode was modified with PAni or PAni-MnO_2 composites with a mixed solution of dimethyl sulfoxide and ethanol by solvent casting method. It was also modified with PVA and PVA-MnO_2 nanocomposites by direct casting of the materials from aqueous solution. ILs were also incorporated into PAni-MnO_2 and PVA-MnO_2 composites. Electrochemical measurements were carried out in a single compartment, three-electrode cell with 0.5 M Na_2SO_4 electrolytic solution.

5.3. Results and Discussion

5.3.1. Capacitive Behavior of Conducting PAni and Non-conducting PVA Based Composites

The cyclic voltammetric and chronopotentiometric results have been analyzed to compare capacitive properties of conducting PAni and non-conducting, PVA. Two different ILs have been chosen ensuring compatibility with the polymers. In fact, hydrophobic [C_2mim][TFSI] and hydrophilic [C_2mim][BF_4] were compatible with PAni and PVA, respectively and could be incorporated into PAni and PVA based composites.

5.3.1.1. From Cyclic Voltammetric Results

Figure 5.1 shows the cyclic voltammograms of PAni (A) and PVA (A1) recorded at different scan rates from 0.01 to 0.10 V s^{-1} in 0.5 M Na_2SO_4 solution. In case of PAni,

two pairs of redox peaks at +0.18 V and 0.72 V correspond to transitions from leucoemeraldine to emeraldine and emeraldine to pernigraniline forms, respectively [12]. The cyclic voltammogramms of PVA (A1) shows no redox peaks indicating absence of Faradaic process and only double layer forms at the interface between electrode and electrolyte. Current density in case of PAni is higher than that of PVA which obviates the more conducting nature of PAni.

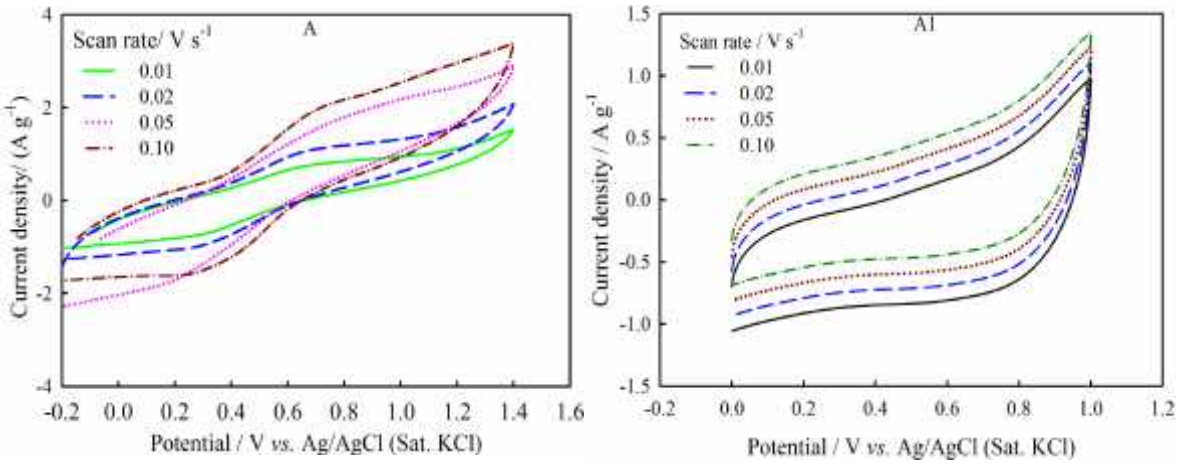

Figure 5.1. Cyclic votammograms of PAni -A and PVA-A1.

From Figure 5.2 (B), the redox peaks appearing for the transition from emeraldine to pernigraniline form of PAni at +0.72 V shifted to a +0.64 V for PM5 composite (PAni-35% MnO_2) indicating interaction between PAni and MnO_2 in the composite. The redox peaks corresponding to the transition from leucoemeraldine to emeraldine also shifted to negative potential. Current densities are also different. The current density is higher in PAni compared to that of PM5 composite. It can be explained by the fact that MnO_2 may block some channels in the PAni network which hinders the electronic movement throughout the material. Figure 5.2 (B1) presents the cyclic voltammograms of PVA with variation of wt.% of MnO_2 NPs at 0.10 V s^{-1} in 0.5 M Na_2SO_4 solution. The cyclic voltammograms in panel (B1) show that all the CVs of materials other than PVA0.5 exhibit approximately rectangular shape, at a scan rate of 0.10 V s^{-1}. This indicates capacitive behavior which may originate from the electrical double-layer capacitance in the electrode surface. In these CVs, the current passed through the PVA-MnO_2 nanocomposites is higher than that of PVA possibly due to the synergistic effect from the combined contributions of PVA and MnO_2.

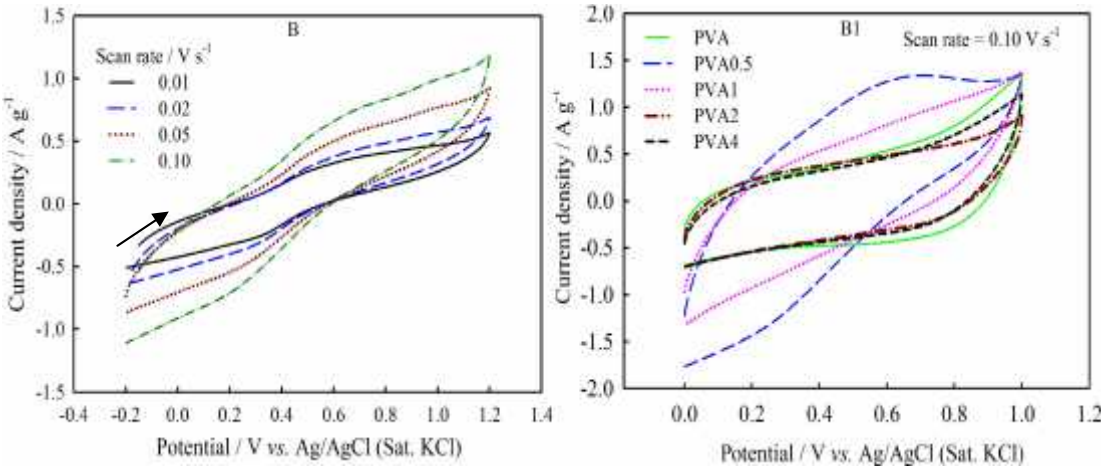

Figure 5.2. CVs of PAni-MnO_2 (PM5)-B and PVA-MnO_2 -B1.

The cyclic voltammetric results show that the C_s decreases from 25 to 14 F g^{-1} from PVA0.5 to PVA4 nanocomposites at a scan rate of 0.10 V s^{-1}. The higher current densities of PVA-MnO_2 nanocomposites at lower wt.% of MnO_2 NPs are also indicative of the high conductivity as well as higher C_s. As the wt.% of MnO_2 NPs increases current density decreases due to blockage of some active sites and C_s decreases in the same manner.

Figure 5.3 shows the CVs of PAni- MnO_2 composite (PM5) incorporated with [C_2mim][TFSI]-C and PVA-MnO_2 nanocomposite (PVA0.5) incorporated with [C_2mim][BF_4])-C1. CVs of Figure 5.3 (C) present similar redox peaks for PM5 composite which disappear gradually as the scan rate increases. This indicates

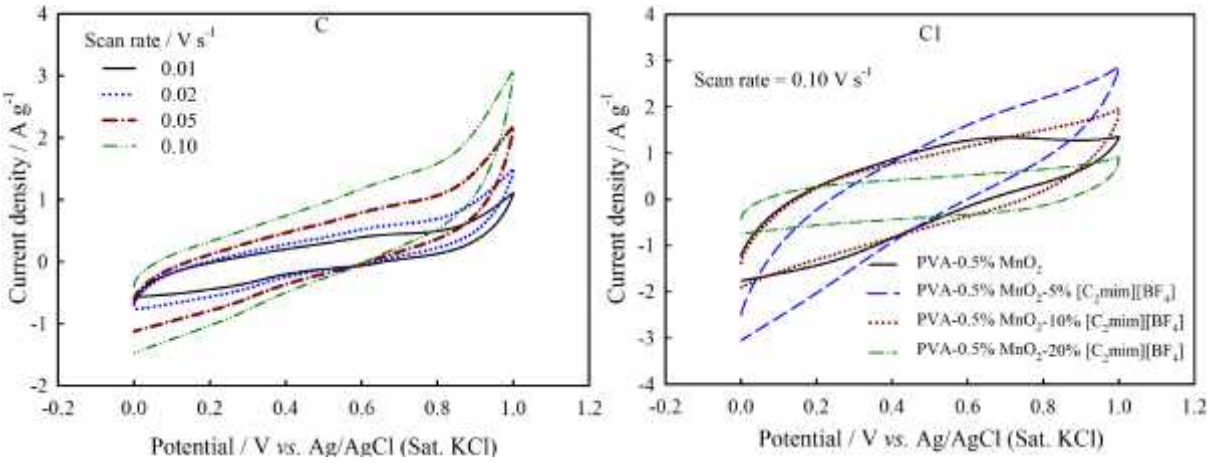

Figure 5.3. CVs of PAni-MnO_2 (PM5)-C incorporated with [C_2mim][TFSI] and PVA-MnO_2 (PVA0.5)- C1 incorporated with [C_2mim][BF_4] .

predominance of double layer upon incorporation of the IL. Double layer capacitance is comparatively low with respect to pseudocapacitance in any electrochemical system, giving rise to relatively low C_s which is consistent with the observation.

In case of CVs of Figure 5.3 (C1), the current density increases with the addition of 0.5 wt.% MnO_2 into PVA. Further increase of current density upon addition of 5 wt.% of $[C_2mim][BF_4]$ is the testimony of augmenting the conductivity. As $[C_2mim][BF_4]$ is added, the current density decreases due to aggregation of ions from $[C_2mim][BF_4]$ causing hindrance of electron transport and thus may have an impact on the decrease of the C_s which finely correlates with the results.

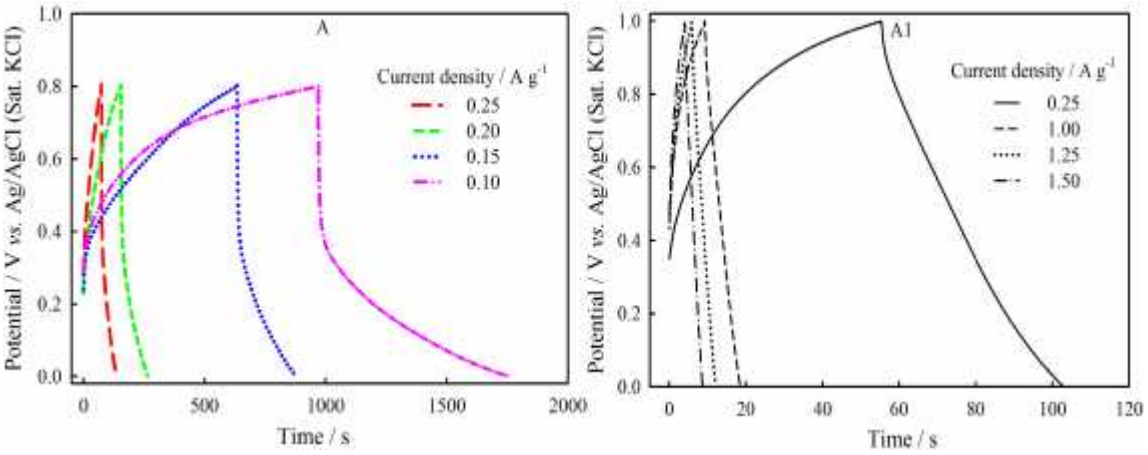

Figure 5.4. Charge-discharge curves of PAni-A and PVA-A1.

Figure 5.4 shows the charge-discharge curves of PAni (A) and PVA (A1) at different current densities. At the same current density of 0.25 A g^{-1} PAni gives higher

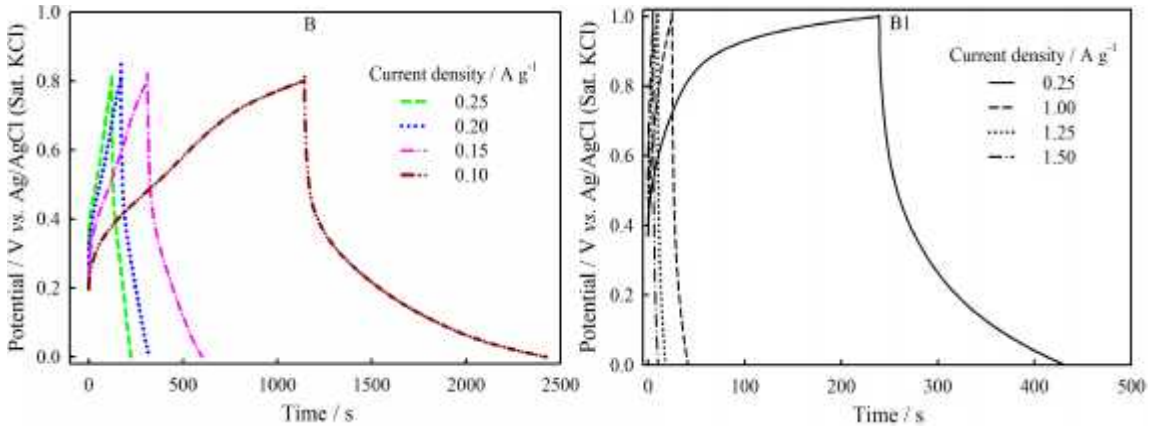

Figure 5.5. Charge-discharge curves of PM1 (PAni-2% MnO_2)-B and PVA2 (PVA-2% MnO_2)-B1 at different current densities.

C_s (19 F g^{-1}) than that of PVA (11 F g^{-1}). This may be attributed to the fact that as PAni contains polarons and bipolarons in its backbone, it is more prone to access more ions from the electrolytic solution during charge-discharge resulting in higher C_s.

5.3.1.2. From Chronopotentiometric Results

Figure 5.5 shows charge-discharge curves of PM1 composite (PAni-2% MnO_2)-B and PVA2 nanocomposite (PVA-2% MnO_2)-B1 at different current densities. 2 wt.% MnO_2 was incorporated in both conducting PAni and non-conducting PVA matrix. The C_s was found to be higher (47 F g^{-1}) in PVA2 than that of PM1 (32 F g^{-1}) at 0.25 A g^{-1} though PVA exhibits lower C_s than that of PAni. In case of PVA-MnO_2 nanocomposite, 2 wt.% MnO_2 NPs was incorporated which renders more specific surface area resulting in more accessible active sites for intercalation or de-intercalation of ions from the electrolyte which may lead to the increased C_s [13].

Table 5.1. Specific capacitance of PAni and PVA at different current densities

Material	Current density (A g^{-1})	Specific capacitance (F g^{-1})	Material	Current density (A g^{-1})	Specific capacitance (F g^{-1})
PAni	0.10	99	PVA	0.25	11
	0.15	45		1.00	9
	0.20	29		1.25	7
	0.25	19		1.50	6

Table 5.2. Specific capacitance of PM1 (PAni-2% MnO_2) and PVA0.5 (PVA-0.5% MnO_2) at different current densities

Material	Current density (A g^{-1})	Specific capacitance (F g^{-1})	Material	Current density (A g^{-1})	Specific capacitance (F g^{-1})
PM1	0.10	160	PVA2	0.25	47
	0.15	54		1.00	16
	0.20	39		1.25	11
	0.25	32		1.50	7

Table 5.3. Specific capacitance of [C_2mim][TFSI] incorporated PM1 (PAni-2% MnO_2) and [C_2mim][BF_4] incorporated PVA0.5 (PVA-0.5% MnO_2) nanocomposites at different current densities

Material	Current density (A g^{-1})	Specific capacitance (F g^{-1})	Material	Current density (A g^{-1})	Specific capacitance (F g^{-1})
	0.10	165		0.25	163
PM1-IL	0.15	83	PVA0.5-IL	1.00	97
	0.20	49		1.25	61
	0.25	45		1.50	42

Figure 5.6 shows charge-discharge curves of PM1(PAni-2% MnO_2)-C incorporated with [C_2mim][TFSI] and PVA0.5 (PVA-0.5% MnO_2)-C1 incorporated with [C_2mim][BF_4] at different current densities. Specific capacitance increases upon incorporation of [C_2mim][TFSI] in PM1 composite (45 F g^{-1}) compared to that of PM1 (32 F g^{-1}). This may be ascribed to the fact that IL helps to achieve intimate contact between PAni and MnO_2 to optimize surface area of electrical double layer and thus the C_s increases [14]. The C_s of PVA0.5 nanocomposite incorporated with [C_2mim][BF_4] (163 F g^{-1}) also increases as compared to that for PVA0.5 (17 F g^{-1}) since to MnO_2 NPs might help to provide by increasing specific surface area on addition of IL to PVA0.5 nanocomposite. Thus, maximum utilization of the electrical double layer of PVA0.5 is achieved by the electrolyte ions [15].

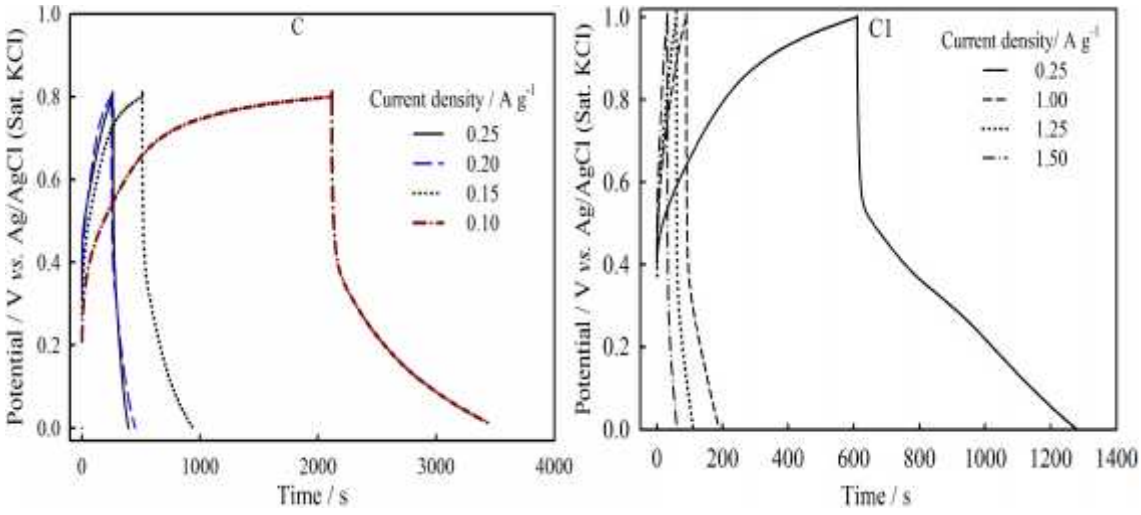

Figure 5.6. Charge-discharge curves of [C_2mim][TFSI] incorporated PM1(PAni-2% MnO_2) - C and [C_2mim][BF_4] incorporated PVA0.5 (PVA-0.5% MnO_2) at different current densities.

5.4. Conclusions

The capacitive behavior of conducting PAni-MnO_2 and non-conducting PVA-MnO_2 composites is found to be influenced by variation of MnO_2 content in the composition and addition of ILs. Redox peaks appear in PAni indicating predominance of pseudocapacitive nature whereas PVA contains no redox peaks specifying dominance of electrical double layer capacitive phenomenon. In PAni-MnO_2 composites both pseudocapacitance and electrical double layer capacitance exist. The C_s decreases from PVA0.5 (25 F g^{-1}) to PVA4 (14 F g^{-1}) at 0.10 V s^{-1}. The current density is almost identical in PM5 incorporated with [C_2mim][TFSI] and PVA0.5 incorporated with [C_2mim][BF_4]. The specific capacitances of PAni, PVA, PM1, PVA2, PM5 incorporated with [C_2mim][TFSI] and PVA0.5 incorporated with [C_2mim][BF_4] is found to be 19, 11, 32, 47, 45 and 163 F g^{-1}, respectively, at a current density of 0.25 F g^{-1}. Thus, variation in composition of the composites and incorporation of ILs has profound influence on the capacitive properties of the composites.

References

[1] M. S. Tamboli, M. V. Kulkarni, R. H. Patil, W. N. Gadec, S. C. Navale and B. B. Kalea, *Nanowires of silver–polyaniline nanocomposite synthesized via* in situ *polymerization and its novel functionality as an antibacterial agent,* Colloids Surf., B: Biointerfaces, 2012, 92, 35-41.

[2] J. Xu, K. Wang, S.-Z. Zu, B.-H. Han and Z. Wei, *Hierarchical nanocomposites of polyaniline nanowire arrays on graphene oxide sheets with synergistic effect for energy storage, ACS Nano*, 2010, 4, 5019–5026.

[3] B. Yuan, C. Bao, X. Qian, S. Jiang, P. Wen, W. Xing, L. Song, K. M. Liew and Y. Hu, *Synergetic dispersion effect of graphene nanohybrid on the thermal stability and mechanical properties of ethylene vinyl acetate copolymer nanocomposite,* Ind. Eng. Chem. Res. 2014, 53, 1143−1149.

[4] Y. Mai, F. Zhang and X. Feng, *Polymer-directed synthesis of metal oxide-containing nanomaterials for electrochemical energy storage,* Nanoscale, 2014, 6, 106-121.

[5] H. Wang, Q. Hao, X. Yang, L. Lu, and X. Wang, *Effect of graphene oxide on the properties of its composite with polyaniline, ACS Appl. Mater. Interfaces*, 2010, *2*, 821–828.

[6] T. Hasell, J. Yang, W. Wang, J. Li, P. D. Brown, M. Poliakoff, E. Lester and S. M. Howdle, *Preparation of polymer–nanoparticle composite beads by a nanoparticle-stabilised suspension polymerization,* J. Mater. Chem., 2007, **17**, 4382-4386.

[7] J. H. Chae, K. C. Nag and G. Z. Chen, *Nanostructured materials for the construction of asymmetrical supercapacitors,* J. Power and Energy, 2010, 224, 479-503.

[8] H. Wang, Q. Hao, X. Yang, L. Lu and X. Wang, *Effect of graphene oxide on the properties of its composite with polyaniline,* ACS Appl. Mater. Interfaces, 2010, 2, 821–828.

[9] D. Wei and A. Ivaska, *Applications of ionic liquids in electrochemical sensors*, Anal. Chim. Acta, 2008, 607, 126–135.

[10] W. Lu, K. Henry, C. Turchi and J. Pellegrino, *Incorporating ionic liquid electrolytes into polymer gels for solid-state ultracapacitors,* J. Electrochem. Soc., 2008, 155, A361-A367.

[11] M.-T. Lee, C.-Y. Fan, Y.-C. Wang, H.-Y. Li, J.-K. Chang and C.-M. Tseng, *Improved supercapacitor performance of MnO_2–graphene composites constructed using a supercritical fluid and wrapped with an ionic liquid,* J. Mater. Chem. A, 2013, 1, 3395-3405.

[12] G. K. S. Prakash, P. Suresh, F. Viva and G. A. Olah, *Novel single step electrochemical route to γ-MnO_2 nanoparticle-coated polyaniline nanofibers: thermal stability and formic acid oxidation on the resulting nanocomposites,* J. Power Sources, 2008, 181, 79–84.

[13] J. Chmiola, G. Yushin, R. Dash and Y. Gogotsi, *Effect of pore size and surface area of carbide derived carbons on specific capacitance,* J. Power Sources, 2006, 158, 765–772.

[14] M.-T. Lee, C.-Y. Fan, Y.-C. Wang, H.-Y. Li, J.-K. Chang and C.-M. Tseng, *Improved supercapacitor performance of MnO_2–graphene composites constructed using a supercritical fluid and wrapped with an ionic liquid,* J. Mater. Chem. A, 2013, 1, 3395-3405.

[15] C. Lian, K. Liu, K. L. Van Aken, Y. Gogotsi, D. J. Wesolowski, H. L. Liu, D. E. Jiang and J. Z. Wu, *Enhancing the capacitive performance of electric double-layer capacitors with ionic liquid mixtures,* ACS Energy Lett. 2016, 1, 21-26.

6.1. General conclusions

Polymer composites, *viz*. PAni-MnO_2, PAni-NiO and PVA-MnO_2 prepared by chemical oxidative polymerization have shown profound influence on property synergism in morphology, thermal stability, conductivity, band gap, dielectric constant and transmittance among their components. PAni shows interconnected network like morphology whereas PAni-MnO_2 composites display compact granular morphology that increases as the amount of MnO_2 increases. PAni shows connected petals of a flower like morphology whereas PAni-NiO composites exhibit spherical bunch-like morphology that increases as the NiO content increases. The size of PAni and PAni-NiO composites falls in the range of 100-200 nm. Average diameter PVA and PVA- MnO_2 nanocomposites are 293 and 93 nm, respectively.

Thermal stability of PAni-NiO is higher than that of PAni, whereas no significant effects of MnO_2 in thermal stability of PAni-MnO_2 are noticed. In case of PVA-MnO_2, thermal stability generally decreases due to incorporation of MnO_2 in PVA. Incorporations of the ionic liquid, [C_2mim][TFSI] into PAni and PAni-MnO_2 are found to further enhance thermal stability.

Conductivity of PAni-NiO nanocomposites initially increases on addition of NiO NPs into PAni and then decreases which is consistent with the results of band gap energy of the materials. Band gap increases initially and then it continuously decreases.

Specific capacitance of PAni-MnO_2 composites prepared chemically is higher than that of PAni with increasing MnO_2 content in the composite. Incorporation of the hydrophobic IL, [C_2mim][TFSI] in PAni-MnO_2 composite is also found to enhance the capacitance value up to certain limit of MnO_2 followed by decrease with further increase in MnO_2 content. PVA-MnO_2 composite prepared chemically results in significant increase in specific capacitance initially up to a loading of a low amount of MnO_2 and then the capacitance decreases on further loading of MnO_2. Incorporation of the hydrophilic IL, [C_2mim][BF_4] into PVA-MnO_2 nanocomposite, specific capacitance dramatically increases by 64 %. Specific capacitance of electrochemically prepared PAni possesses higher value than that of PAni-NiO. The values of specific

capacitance of PAni, PVA and their MnO_2 based composites with incorporation of ILs and PAni-NiO are promising materials for application in supercapacitors.

Transmittance of the PVA-MnO_2 was found to show total absorption of UV-radiation which accounts for the novel functionality of the composites as UV-shielding materials.

Dielectric constant of PAni-NiO nanocomposites are higher than that of PAni and dielectric losses are lower in PAni than the composites which are indicative of promising application as dielectric materials. Thus, property synergism and novel functionality make the composites inevitable for diverse applications.

6.2. Outlook

Synthesis of polymer composite provides an important approach to have synergistic effect through introducing improved properties which *inter alia* include minimizing particle size, preventing particles from agglomeration, expanding active sites of the materials, augmenting conductivity through creating channels for electron and charge transport or conduction, preserving active materials from degradation, improving mechanical strength, extending potential window and cycling stability for electrochemical applications. New functionalities can be achieved by judicious and proper combinations of polymer and inorganic component for versatile applications in multidisciplinary fields. Moreover, polymer nanocomposites are much advantageous in providing more electroactive sites for higher specific surface area and efficient contact of electrolyte ions which give rise to high charge-discharge capacities resulting in higher specific capacitance. Simple methodology has been used to prepare polymer nanocomposites with novel functionality which may be used as UV-shielding and dielectric materials. ILs can be incorporated into the polymer composite to improve the conductivity of the composites which may eventually open new routes for their versatile applicability in thin films, sensors, membranes for fuel cells and in other electronic and electrochemical applications. Biodegradability, biocompatibility, and environment friendly nature of polymer based composites may pave the way for designing green and sustainable energy storage devices to meet the increasing demands of energy crisis. The synthesis strategy in combination with incorporation of ILs can be applied to other conducting and non-conducting polymer based composites to achieve novel functionality for manifold applications.

List of publications

1. **Hemshankar Saha Roy,** M. Yousuf Ali Mollah, Md. Mominul Islam and Md. Abu Bin Hasan Susan, *"Polyaniline-MnO_2 composites with incorporation of hydrophobic ionic liquid for electrochemical supercapacitor",* in preparation.

2. **Hemshankar Saha Roy,** M. Yousuf Ali Mollah, Md. Mominul Islam and Md. Abu Bin Hasan Susan, *"Poly(vinyl alcohol)-MnO_2 nanocomposite films for UV-shielding materials",* in preparation.

3. **Hemshankar Saha Roy,** Md. Mominul Islam, M. Yousuf Ali Mollah and Md. Abu Bin Hasan Susan, *"Hydrophilic ionic liquid incorporated Poly(vinyl alcohol)-MnO_2 nanocomposite films for electrochemical supercapacitor"*, in preparation.

4. **Hemshankar Saha Roy,** Md. Mominul Islam, M. Yousuf Ali Mollah and Md. Abu Bin Hasan Susan, *"Polyaniline-NiO nanocomposites for dielectric materials",* in preparation.

5. **Hemshankar Saha Roy,** M. Yousuf Ali Mollah, Md. Mominul Islam and Md. Abu Bin Hasan Susan, *"Electrochemically prepared Polyaniline-NiO nanocomposites for electrochemical supercapacitor",* in preparation.

List of attended seminars

1. Seminar on Supramolecular systems, organized by the Higher Education Quality Enhancement Project (HEQEP) of the University Grants Commission of Bangladesh, November 15, 2012, Department of Chemistry, University of Dhaka, Bangladesh

2. Bangladesh Chemical Congress, December 07-09, 2012, Dhaka, Bangladesh

3. Seminar on Electrochemistry for Material Science, organized by the Higher Education Quality Enhancement Project (HEQEP) of the University Grants Commission of Bangladesh, December 10, 2012, Department of Chemistry, University of Dhaka, Bangladesh

4. International Bose Conference, February 04, 2013, Dhaka, Bangladesh

5.19th Conference of Islamic World Academy of Sciences, May 06-10, 2013 in Dhaka, Bangladesh

6. Seminar on *Air Quality and Its Consequence: Bangladesh Perspective,* organized by Establishing Air Quality Monitoring Centre (CP-2196), Dhaka, Bangladesh, 28 December, 2013.

7. Seminar on *Tandem Mass Spectrometry and its Application for Analysis of Chemical Contaminats in Food Stuff*, Dhaka, Bangladesh, 02 June, 2015.

8. Seminar on *3D Gel Printer and Future Life Innovation*, organized by the Material Chemistry Research Laboratory, Department of Chemistry, University of Dhaka, Dhaka, 30 August, 2015.

9. Seminar on *New Trophological States of Quantum Matter*, organized by Bose Centre for Advanced Study and Research in Natural Sciences, University of Dhaka, Dhaka, 25 November, 2015.

10. Seminar on *New Insight into the Chemistry on Carbon Nanotubes and Graphene Oxide and Boron Oxide Nanotubes*, organized by Department of Microbiology, University of Dhaka, Dhaka, 10 December, 2015.

List of workshops attended

1. Preparation and Characterization of Novel Functional Materials with Emphasis on Electrochemistry, Dhaka, Bangladesh, 12 February, 2012.

2. Black Carbon Emission from Brick Kilns in Bangladesh, Department of Chemistry, University of Dhaka, 16 November, 2014.

Abstracts published as contribution in the scientific meetings

1. **Hemshankar Saha Roy,** M. Yousuf Ali Mollah, Md. Mominul Islam and Md. Abu Bin Hasan Susan*, "Polyaniline-NiO Nanocomposites for Application as Dielectric Materials",* 1st Symposium on Chemistry For Global Solidarity, Jagannath University, Dhaka, Bangladesh, 14 October, 2016 (Oral presentation)

2. **HemshankarSaha Roy,** M. Yousuf A. Mollah, Md. Mominul Islam and Md. Abu Bin Hasan Susan *"Polyaniline-Nickel Oxide Nanocomposites : Effects of Compositions on Thermal and Electrical Properties",* 16 Asian Chemical Congress, Dhaka, Bangladesh, March 16-19, 2016 (Oral presentation)
3. **HemshankarSaha Roy,** Md. Mominul Islam, M. Yousuf A. Mollah and Md. Abu Bin Hasan Susan *"Synthesis of Metal Oxide-Conducting Polymer Composites",* 2nd International Bose Conference, Dhaka, Bangladesh, December 03-04, 2015 (Oral presentation)

4. **Hemshankar Saha Roy,** Md. Mominul Islam, Md. Abu Bin Hasan Susan and M. Yousuf Ali Mollah *"Fabrication of UV-Shielding Poly(vinyl alcohol)-MnO_2 Nanocomposite thin Films",* 37th Annual Conference 2015, Bangladesh Chemical Society (ACBCS), April 11, 2015, Comilla University, Comilla, Bangladesh (Oral presentation)

5. **Hemshankar Saha Roy,** Md. Mominul Islam, Md. Abu Bin Hasan Susan and M. Yousuf Ali Mollah *"Fabrication of UV-Shielding Poly(vinyl alcohol)-MnO_2 Nanocomposite Films"* 2nd Conference of Bangladesh Crystallographic Association(BCA), 10 January, 2015, Dhaka, Bangladesh (Poster presentation)

6. **Hemshankar Saha Roy,** Md. Mominul Islam, Md. Abu Bin Hasan Susan and M.Yousuf Ali Mollah *"Effect of MnO_2 Nanoparticles on the Properties on Poly(vinyl alcohol)- MnO_2 Nanocomposite Film",* International Conference on Materials Chemistry (ICMC-2014), December 06, 2014, Shahjalal University of Science and Technology, Sylhet, Bangladesh (Oral presentation)

7. **Hemshankar Saha Roy,** M. Yousuf Ali Mollah, Md. Abu Bin Hasan Susan and Md. Mominul Islam *"Preparation, Characterization and Catalytic Application of Polyaniline-manganese Dioxide Composite Modified Carbon Electrode",* 36th Annual Conference of Bangladesh Chemical Society, 01-03 March, 2014, Haji Mohammad Danesh Science and Technology University, Dinajpur, Bangladesh (Oral presentation)

8. **Hemshankar Saha Roy***,* M. Yousuf A. Mollah, Md. Abu bin Hasan Susan and Md. Mominul Islam *"Characterization of Chemically Synthesized Polyaniline-Manganese Dioxide Composite Modified Glassy Carbon Electrode as an Electrochemical Capacitor",* 1st National Conference of Bangladesh Crystallographic Association (BCA), December 05, 2013, Dhaka, Bangladesh (Poster presentation)